WIRELESS CHANNEL MODELING IN THE TVWS BAND BASED ON MEASUREMENTS

A THESIS SUBMITTED TO
THE GRADUATE SCHOOL OF
ENGINEERING AND NATURAL SCIENCES
OF ISTANBUL MEDIPOL UNIVERSITY
IN PARTIAL FULFILLMENT OF THE REQUIREMENTS FOR
THE DEGREE OF
MASTER OF SCIENCE
IN
ELECTRICAL, ELECTRONICS ENGINEERING AND CYBER SYSTEMS

By
Muhammad Hashir Syed
December, 2018

Wireless channel modeling in the TVWS band based on measurements
By Muhammad Hashir Syed
December, 2018

We certify that we have read this thesis and that in our opinion it is fully adequate, in scope and in quality, as a thesis for the degree of Master of Science.

Assist. Prof. Dr. Tunçer Baykaş(Advisor)

Assoc. Prof. Dr. Serhat Erküçük

Assoc. Prof. Dr. M. Kemal Özdemir

Approved by the Graduate School of Engineering and Natural Sciences:

Prof. Dr. Talip Alp
Director of the Graduate School of Engineering and Natural Sciences

I hereby declare that all information in this document has been obtained and presented in accordance with academic rules and ethical conduct. I also declare that, as required by these rules and conduct, I have fully cited and referenced all material and results that are not original to this work.

Name, Last Name: MUHAMMAD HASHIR SYED

Signature :

ABSTRACT

WIRELESS CHANNEL MODELING IN THE TVWS BAND BASED ON MEASUREMENTS

Muhammad Hashir Syed
M.S. in Electrical, Electronics Engineering and Cyber Systems
Advisor: Assist. Prof. Dr. Tunçer Baykaş
December, 2018

In this thesis, we study TV white space (TVWS) bands, which can be used in next generation networks, in indoor-indoor and indoor-outdoor environments. Path loss measurements are taken at the beginning, middle, and at the end of TVWS band. In addition, ray tracing simulation results are obtained in air-ground TVWS channel environment.

Indoor-indoor measurement results are compared with different indoor propagation models in the literature and a new indoor propagation model for TVWS frequencies is proposed, which concatenates the effects of frequency dependent path loss with penetration losses due to floors, walls, and windows. Performance comparison with existing models show that the proposed model achieves superior performance in terms of standard deviation of estimation error (STD).

Similarly, for indoor-outdoor environment, measurements results are fitted to log normal shadowing model. An important observation is that the standard deviation of the shadowing coefficient varies greatly at short and long distances. A distance threshold is determined to differentiate between different short distance and long distance shadowing zones. The results indicate that the shadowing standard deviation is reduced at all transmission frequencies distance zones.

For air-ground channels, ray tracing simulations are performed. Channel parameters are calculated using log normal shadowing model in two different types of scenarios (high rise buildings and sub-urban). It is found that high rise buildings scenario has high shadowing and high path loss coefficient compared to sub-urban which has low shadowing and low path loss coefficient.

Keywords: TV white space, Propagation, Channel Models.

ÖZET

TVBB BANTLARINDA ÖLÇÜME DAYALI KABLOSUZ KANAL MODELLERİNİN ÇIKARIMI

Muhammad Hashir Syed
Elektrik-Elektronik Mühendisliği ve Siber Sistemler, Yüksek Lisans
Tez Danışmanı: Dr. Öğr. Üye. Tunçer Baykaş
Aralık, 2018

Bu tezde, Televizyon beyaz bandlarında binaiçi ve binaiçinden binadışına yapılan kanal ölçüm sonuçları sunulmuştur. Ölçümler TV bandının başında, ortasında ve sonunda bulunan frekanslarda yapılmıştır. Ayrıca hava yer kanalları için ışın takip yöntemi kullanılarak benzetim sonuçları elde edilmiştir.

Binaiçi ölçüm sonuçları literatürde bulunan diğer yol kaybı modelleri ile karşılaştırılmış ve TVWS frekansları için yeni bir model önerilmiştir. Yeni model frekansa bağlı olan yol kaybı değerine ek olarak kapı, pencere ve katlar arasında bulunan kayıpları göz önüne almaktadır. Diğer modellerle karşılaştırıldağında yeni önerdiğimiz modelin daha iyi STD performansına sahip olduğu gözlşenmiştir.

Benzer olarak bina içinden bina dışına olan yol kaybı modeli için log normal gölgeleme modeli seçilmiştir. Kısa ve uzun mesafelerde yapılan ölçümlerde gölgeleme standart sapma değerleri arasında fark olduğu gözlemlenmiştir. Kısa ve uzun mesafe ayrımı için bir eşik değer tanımlanmıştır. Alınan sonuçlar her frekans bandından hata oranının azaldığını göstermiştir.

Hava-yer kanallarında, ışın izleme yöntemi kullanılarak benzetim sonuçları elde edilmiştir. Yüksek katlı binalar ve banliyöler için yapılan çalışmalarda yüksek katlı binalarda hem yol kaybı hem de gölgeleme paramatrelerinin daha yüksek olduğu belirlenmiştir.

Anahtar sözcükler: TV Beyaz Boşlukları, Yayılım, Kanal Modelleri.

Acknowledgement

First of all I would like to acknowledge my supervisor Dr. Tunçer Baykaş for his guidance and support throughout my Master's program. His knowledge and great research experience helped me in completing my degree.

Secondly, I would like to acknowledge my course teachers specially Dr. M. Kemal Ozdemir and Dr Bahadir K. Gunturk for their continuous guidance and support with technical challenges that I faced during my education and research work.

Moreover, I would like to thank my parents and brothers for their moral support to pursue higher education. I would like to thank my lab members and all my colleagues in the university. I would also like to thank Istanbul Medipol University for providing me with the necessary tools and logistics to accomplish my tasks.

Contents

1 Introduction **1**

2 Measurement Setup **5**

3 Indoor to Indoor Wireless Channel Measurements and Modeling **9**

3.1 Measurement Environment 9

3.2 Indoor Channel Models and Results 15

3.3 Proposed Indoor Propagation Channel Model for TVWS Band 26

3.4 Performance Comparisons 29

4 Indoor to Outdoor Wireless Channel Measurements and Modeling **37**

4.1 Measurement Environment 37

4.2 Indoor to Outdoor Channel Model and Results 38

4.3 Proposed Model and Discussion 45

4.4 Performance Comparisons and Results 54

5 Air to Ground Wireless Channel Modeling 57

5.1 Channel parameter estimation 58

5.2 Simulation Results 60

5.2.1 High Rise Building Scenario 61

5.2.2 Sub-urban scenario 74

5.2.3 Modeling Shadowing with Gaussian Mixture Distribution 87

5.3 Comparisons and Discussion 94

6 Conclusion 98

List of Figures

2.1 Measurement setup 6

2.2 Transmitter setup 6

2.3 Receiver setup 6

3.1 3D Model of the university building 10

3.2 2^{nd} Floor plan (Size: 74.1 x 35.75 meters) 11

3.3 3^{rd} Floor plan (Size: 74.1 x 35.75 meters) 12

3.4 Transmitter antenna orientation 13

3.5 Receiver antenna orientations (Left, Up and Right) 14

3.6 Measurement results of received signal strength at the 2^{nd} floor . . 14

3.7 Measurement results of received signal strength with different antenna orientations (see Fig. 3.5) at the 2^{nd} floor 15

3.8 Measurement results compared with estimation results at 480 MHz (log-distance, ITU-R P.1238, LAM) 18

3.9 Measurement results compared with estimation results at 480 MHz (MWF) 18

3.10 Measurement results compared with estimation results at 580 MHz (log-distance, ITU-R P.1238, LAM) 19

3.11 Measurement results compared with estimation results at 580 MHz (MWF) 19

3.12 Measurement results compared with estimation results at 580 MHz (log-distance, ITU-R P.1238, LAM) (3^{rd} floor) 20

3.13 Measurement results compared with estimation results at 580 MHz (MWF) (3^{rd} floor) 21

3.14 Measurement results compared with estimation results at 630 MHz (log-distance, ITU-R P.1238, LAM) 22

3.15 Measurement results compared with estimation results at 630 MHz (MWF) 22

3.16 Measurement results compared with estimation results at 480 MHz (extended LAM) 24

3.17 Measurement results compared with estimation results at 580 MHz (extended LAM) 24

3.18 Measurement results compared with estimation results at 580 MHz (extended LAM)(3^{rd} floor) 25

3.19 Measurement results compared with estimation results at 630 MHz (extended LAM) 25

3.20 Measurement results compared with estimation results at 480 MHz (proposed model) 27

3.21 Measurement results compared with estimation results at 580 MHz (proposed model) 27

3.22 Measurement results compared with estimation results at 580 MHz (proposed model)(3^{rd} floor) 28

3.23 Measurement results compared with estimation results at 630 MHz (proposed model) 28

3.24 Comparison of propagation models on 2^{nd} (a) and 3^{rd} floor (b) . . 30

3.25 Performance comparison of log-distance, ITU-R P.1238 and LAM models at 480 MHz 31

3.26 Performance comparison of the proposed, extended LAM and MWF models at 480 MHz 31

3.27 Performance comparison of log-distance, ITU-R P.1238 and LAM models at 580 MHz 32

3.28 Performance comparison of the proposed, extended LAM and MWF models at 580 MHz 32

3.29 Performance comparison of log-distance, ITU-R P.1238 and LAM models at 580 MHz ($3^{rd}Floor$) 33

3.30 Performance comparison of the proposed, extended LAM and MWF models at 580 MHz ($3^{rd}Floor$) 33

3.31 Performance comparison of log-distance, ITU-R P.1238 and LAM models at 630 MHz 34

3.32 Performance comparison of the proposed, extended LAM and MWF models at 630 MHz 34

4.1 Aerial view of the measurement site. 38

4.2 Measured received power (470 MHz) at different receiver positions (from X until Y in Figure 4.1). 39

4.3 Measured received power (580 MHz) at different receiver positions (from X until Y in Figure 4.1). 40

4.4 Measured received power (670 MHz) at different receiver positions (from X until Y in Figure 4.1). 40

4.5 Measured path loss compared with estimated path loss at 580 MHz. 41

4.6 PDF of X_σ and Gaussian distribution at 580 MHz. 42

4.7 Measured path loss compared with estimated path loss at 470 MHz. 43

4.8 PDF of X_σ and Gaussian distribution at 470 MHz. 43

4.9 Measured path loss compared with estimated path loss at 670 MHz. 44

4.10 PDF of X_σ and Gaussian distribution at 670 MHz. 45

4.11 Concept of Proposed Method. 46

4.12 Absolute standard deviation difference at 470, 580 and 670 MHz . 48

4.13 Measured path loss compared with estimated path loss for short and long distance at 470 MHz. 49

4.14 Measured path loss compared with estimated path loss for short and long distance at 580 MHz. 49

4.15 Measured path loss compared with estimated path loss for short and long distance at 670 MHz. 50

4.16 PDF of X_σ and Gaussian distribution for short distance at 470 MHz. 51

4.17 PDF of X_σ and Gaussian distribution for long distance at 470 MHz. 51

4.18 PDF of X_σ and Gaussian distribution for short distance at 580 MHz. 52

4.19 PDF of X_σ and Gaussian distribution for long distance at 580 MHz. 52

4.20 PDF of X_σ and Gaussian distribution for short distance at 670 MHz. 53

4.21 PDF of X_σ and Gaussian distribution for long distance at 670 MHz. 53

4.22 Shadowing comparison chart at 470 MHz 55

4.23 Shadowing comparison chart at 580 MHz 56

4.24 Shadowing comparison chart at 670 MHz 56

5.1 Channel parameters generation work flow 59

5.2 Ray tracing simulation in Wireless InSite 59

5.3 Corresponding aerial image 60

5.4 Received power color map at 580 MHz and corresponding aerial image(1^{st} Location) 62

5.5 Measured/estimated path loss and measured/ fitted Gaussian PDF of X_σ at 580 MHz (1^{st} Location) 63

5.6 Received power color map at 580 MHz and corresponding aerial image (2^{nd} Location) 64

5.7 Measured/estimated path loss and measured/ fitted Gaussian PDF of X_σ at 580 MHz (2^{nd} Location) 65

5.8 Received power color map at 580 MHz and corresponding aerial image (3^{rd} Location) 66

5.9 Measured/estimated path loss and measured/ fitted Gaussian PDF of X_σ at 580 MHz (3^{rd} Location) 67

5.10 Measured/estimated path loss and measured/ fitted Gaussian PDF of X_σ at 470 MHz (1^{st} Location) 68

5.11 Measured/estimated path loss and measured/ fitted Gaussian PDF of X_σ at 470 MHz (2^{nd} Location) 69

5.12 Measured/estimated path loss and measured/ fitted Gaussian PDF of X_σ at 470 MHz (3^{rd} Location) 70

5.13 Measured/estimated path loss and measured/ fitted Gaussian PDF of X_σ at 670 MHz (1^{st} Location) 71

5.14 Measured/estimated path loss and measured/ fitted Gaussian PDF of X_σ at 670 MHz (2^{nd} Location) 72

5.15 Measured/estimated path loss and measured/ fitted Gaussian PDF of X_σ at 670 MHz (3^{rd} Location) 73

5.16 Received power color map at 580 MHz and corresponding aerial image(1^{st} Location) 75

5.17 Measured/estimated path loss and measured/ fitted Gaussian PDF of X_σ at 580 MHz (1^{st} Location) 76

5.18 Received power color map at 580 MHz and corresponding aerial image (2^{nd} Location) 77

5.19 Measured/estimated path loss and measured/ fitted Gaussian PDF of X_σ at 580 MHz (2^{nd} Location) 78

5.20 Received power color map at 580 MHz and corresponding aerial image (3^{rd} Location) 79

5.21 Measured/estimated path loss and measured/ fitted Gaussian PDF of X_σ at 580 MHz (3^{rd} Location) 80

5.22 Measured/estimated path loss and measured/ fitted Gaussian PDF of X_σ at 470 MHz (1^{st} Location) 81

5.23 Measured/estimated path loss and measured/ fitted Gaussian PDF of X_σ at 470 MHz (2^{nd} Location) 82

5.24 Measured/estimated path loss and measured/ fitted Gaussian PDF of X_σ at 470 MHz (3^{rd} Location) 83

5.25 Measured/estimated path loss and measured/ fitted Gaussian PDF of X_σ at 670 MHz (1^{st} Location) 84

5.26 Measured/estimated path loss and measured/ fitted Gaussian PDF of X_σ at 670 MHz (2^{nd} Location) 85

5.27 Measured/estimated path loss and measured/ fitted Gaussian PDF of X_σ at 670 MHz (3^{rd} Location) 86

5.28 Measured/ fitted GMM PDF and CDF of X_σ at 580 MHz (1^{st} Location) 88

5.29 Measured/ fitted GMM PDF and CDF of X_σ at 580 MHz (2^{nd} Location) 89

5.30 Measured/ fitted GMM PDF and CDF of X_σ at 580 MHz (3^{rd} Location) 90

5.31 Measured/ fitted GMM PDF and CDF of X_σ at 580 MHz (1^{st} Location) 91

5.32 Measured/ fitted GMM PDF and CDF of X_σ at 580 MHz (2^{nd} Location) 92

5.33 Measured/ fitted GMM PDF and CDF of X_σ at 580 MHz (3^{rd} Location) 93

5.34 Comparison of results in high rise and sub-urban scenarios (1^{st} location) 95

List of Tables

2.1 Specifications of USRP B210 5

2.2 Measurement setup parameters 7

3.1 Comparison of propagation models 29

4.1 Comparison of Results 55

5.1 Measurement setup parameters (Wireless InSite) 58

5.2 Comparison of Results 94

5.3 GMM estimated parameters and error metrics 96

Chapter 1

Introduction

During the last decade, the increase in wireless data traffic forced the limits of communication systems in terms of reliability and throughput [1]. One of the solutions is allocating more RF spectrum for data communication purposes in higher frequency bands such as 60 GHz [2] and Tera Hertz (THz) [3] bands. Utilizing such bands result in complex systems due to relatively high path losses and shorter communication ranges. Another solution is utilizing spectrum sharing techniques to increase the efficiency in lower frequency bands [4], which are allocated to other services such as broadcasting. Among these bands, the so called television white space (TVWS) bands have attracted much attention in the last decade. Although it depends on the local regulations, most of the available TVWS bands are between 470 and 700 MHz.

In TVWS bands, regulatory organizations have enabled spectrum sharing [5], where the systems are categorized as primary and secondary systems [6]. Primary systems are the licensed systems. Secondary systems are allowed to operate given that they do not cause harmful interference to the primary users. The efficient and reliable performance of secondary systems becomes more challenging since the available channels for them are limited.

There are multiple standards developed for TVWS bands including IEEE

802.15.4m, 802.11af, 802.22, and 802.19.1 standards, which cover the implementation of systems in these bands for personal, local, and regional area networks as well as for the coexistence of these systems. In [7] and [8], different standards for TVWS are presented. Among them, the standards IEEE 802.11af and IEEE 802.15.4m have use cases for indoor applications. For example, IEEE 802.11af systems can support a local area network, which requires data rates in tens of Mb/s and communication range up to 100 meters. On the other hand, the potential applications of IEEE 802.15.4m standard are low power wireless systems like smart utility networks (SUNs). SUN systems require low data rate (few hundreds of kb/s) and coverage both indoors and outdoors. In addition, TVWS bands can be used in 5G as supplementary channels.

For the spectrum sharing in TVWS band, it is essential to comprehend interference between multiple systems. Therefore, characterization of a wireless channel is a primary factor in estimating interference between coexistence of networks and systems. Thus, detailed channel models are required for network deployments.

There are many propagation models in the literature for TV bands [9], [10]. Most of these models are for outdoor scenarios and for long range systems, such as Okumura–Hata Model [11]. On the other hand the literature for indoor to indoor, indoor to outdoor and air to ground channel scenarios and short range systems in TV bands is limited. Most important channel models for indoor use are the log-distance model [11], Linear Attenuation Model (LAM) [12], ITU-R P.1238 [13], and Multi Wall and Floor Model (MWF) [14]. Indoor to outdoor propagation is also studied in the literature. In [15] researchers proposed frequency dependent indoor to outdoor channel model based on propagation (received power) measurements which were taken on 0.9, 2, 2.5 and 3.5 GHz transmission frequencies and around different residential areas. A model based on ray-tracing simulations is presented in [16]. Authors of [17] propose such a model which evaluates propagation through multiple windows at 0.4-18 GHz frequencies and they also claim that most of the signal leakage from indoor to outdoor is due to installing transmitter close to windows. Similarly in [18], authors addressed propagation through windows including identical structures and used ray tracing and measurements outcomes to propose channel model. In [19, 20, 21], several empirical

path loss based indoor to outdoor channel model were reported where receiver measurements were taken in the neighboring streets. However, these models are not specifically intended for the TVWS band operation. Therefore, more accurate channel models in multiple types of scenarios and environments are needed for TVWS bands.

The design of measurement setup is also another issue due to the fact that synchronization of the devices is a very severe problem in indoor environment. It can be achieved easily by GPS synchronized clock for outdoor applications. Also it is very hard to handle common signal generators and analyzer for extensive measurements. With the advent of software defined radios (SDR) for e.g. USRP [22], the measurement campaign becomes little effortless due to its miniaturized and reconfigurable hardware. Although it does not provide huge bandwidths, it can be used for path loss measurements. For indoor application, synchronization of SDR can be achieved by using certain algorithms and preamble techniques like in [23] where transmitted M-sequence data was captured by USRP and saved in laptop while the synchronization was performed off-line in the software.

Considering aforementioned issues, SDR based measurement setup is designed and propagation characteristics of wireless channel in TVWS band is studied by evaluating path loss measurements in multiple scenarios. Path loss measurements were taken for indoor to indoor and indoor to outdoor environments. In addition, ray tracing simulations were also performed to analyze air to ground channel in TVWS band. New models, methods and channel parameters for TVWS frequency bands are proposed and compared with the existing channel models in the literature.

The rest of this thesis is organized as follows. Chapter II describes the SDR based measurement setup to capture Received Signal Strength (RSS) value and transmitted data. Chapter III presents the measurement results, proposed model, and comparisons between multiple channel models for indoor to indoor environment. Chapter IV proposes the new method to find channel parameters in indoor to outdoor environment and also presents the comparison between the results calculated from new and existing method by using model proposed in the literature.

Chapter V presents the ray tracing simulation results and channel characterization for air to ground channel and Chapter VI concludes the whole thesis.

Chapter 2

Measurement Setup

In this chapter, implementation of a software defined radio based measurement system is discussed which is used to take path loss measurements for indoor to indoor and indoor to outdoor environments which are detailed in following chapters. There are multiple measurement setups proposed in the literature for the path loss measurements. In this work, a cost effective and user friendly measurement system is implemented using USRP. We used USRP B210 from Ettus Research [24] which is controlled by USB 3.0 port on a PC/Laptop. Table 2.1 shows some important specifications of USRP B210.

Table 2.1: Specifications of USRP B210

RF Frequency Range	70 MHz - 6 GHz
Tx Power (max)	+20 dBm
ADC/DAC Resolution	12 bits
ADC/DAC Sample Rate (max)	61.44 MS/s
Bandwidth (max)	Configurable up to 56 MHz
Interface	USB 3.0
Software interface (ettus)	GNU Radio, C++, Python APIs
Weight	350 g

Apart from the software interfaces mentioned from Ettus Research, we also

tested USRP successfully on Matlab [25] and Labview [26] software tools. In order to achieve a good GUI interface for our measurement system, we used Labview software to control USRP. A simple representation of measurement setup is given in Figure 2.1.

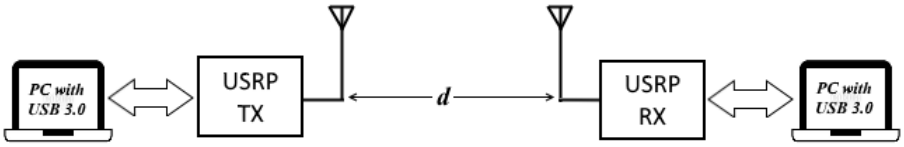

Figure 2.1: Measurement setup

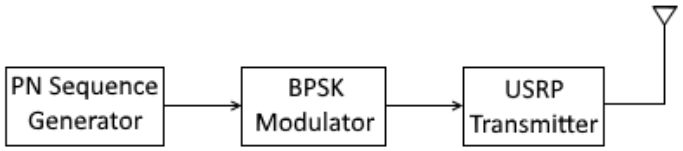

Figure 2.2: Transmitter setup

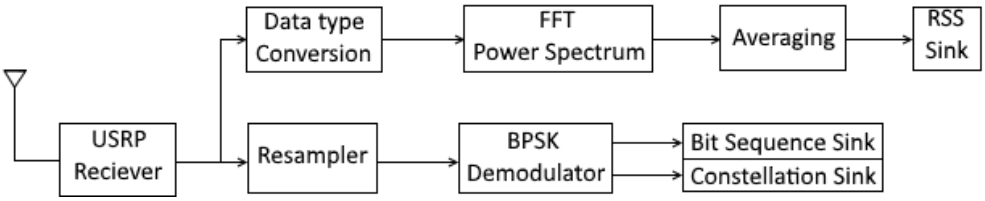

Figure 2.3: Receiver setup

The transmitter (Tx) and receiver (Rx) setups are detailed in Figures 2.2 and 2.3. On the Tx side, PN sequence of level 10 was generated. After that it is passed through a BPSK modulator. There are two operations of this block a) It maps the input bit stream to a complex valued symbol sequence b) It performs pulse shaping filter operation. Finally in the last block it is passed through the RF front end in USRP, which up converts the modulated signal through analog operations and transmit it through antenna (Table 2.2).

On the Rx side in Figure 2.3, signal is picked through antenna and then down converted through RF front end in USRP. Now the block diagram is divided into two branches 1) Received Signal Strength (RSS) detection 2) PN sequence detection and constellation plot.

In the first branch, re-sampler re-samples the acquired signal to multiple of expected symbol rate then signal passes through BPSK demodulator, which has multiple operations here a) filter the received signal phase in order to reduce Inter symbol Interference (ISI) b) extraction of required symbols from oversampled signal c) Frequency offset correction d) Symbol detection and mapping of hard symbols to bit values per the transmitted symbol map. This block is also synchronized for certain symbol map. Finally, we have the received bit sequence and recovered complex waveform for constellation plot.

In the second branch, signal is converted in to Complex Double Waveform Data Type (CDB WDT) then fed to FFT power spectrum block which computes the FFT and forms the power spectrum of the time signal. Now the magnitude values are extracted from the signal and averaging block calculates the RSS by taking mean of 200 magnitude values from left and right of center frequency. This averaging is done in order to reduce the impact of frequency offset and instability in the values. Measurement setup parameters are given in Table 2.2.

Table 2.2: Measurement setup parameters

Center frequency (indoor-indoor)	480, 580, 630 MHz
Center frequency (indoor-outdoor)	470, 580, 670 MHz
Tx Power	16.60 dBm
Antenna polarization	Horizontal
Antenna radiation pattern	Omni-directional
Antenna heights (Tx and Rx)	1.5 m
Transmitted signal	PN sequence
Modulation	BPSK
Sampling rate	300 kHz

Measurements were taken at three different frequencies in TVWS band (start, middle and end of the band). To maximize the measurement area, the transmitter power was set to 16.60 dBm. Receiver antenna height was adjusted to 1.5 meter to model average holding height for a cellular phone. The IQ sampling rate of the receiver was 300 kHz to reduce the posibility of overflow. Antenna polarization and radiation pattern were selected based on the indoor and outdoor environments.

Chapter 3

Indoor to Indoor Wireless Channel Measurements and Modeling

In this chapter, indoor to indoor wireless propagation measurement results and channel models are detailed. In addition, a new channel model for TVWS frequencies and its performance comparisons with other models are also presented.

3.1 Measurement Environment

Measurements were taken on the 2^{nd} and 3^{rd} floor of the C-block building of Istanbul Medipol University, during non-working hours, to reduce interference from human body as much as possible. Figure 3.1 shows the identical 3D model of the university building. Figures 3.2 and 3.3 show the layout of the 2^{nd} and 3^{rd} floor respectively. All indoor walls on the floor maps are wooden material with certain insulation. Some doors are made up of glass and some are wooden, whereas all of the windows of the classrooms, labs and other office area are made of glass. Tx location is marked with black star (cf. south side of the 2^{nd} floor

plan Figure 3.2), whereas Rx positions are marked with red stars in Figures 3.2 and 3.3. Both Tx and Rx antenna heights were kept constant at 1.5 meter during the measurements. Tx system was placed on the 2^{nd} floor while Rx system was placed on a small trolley and RSS values were recorded in a still position at all marked points between Points A and B on 2^{nd} floor, and A and D on 3^{rd} floor.

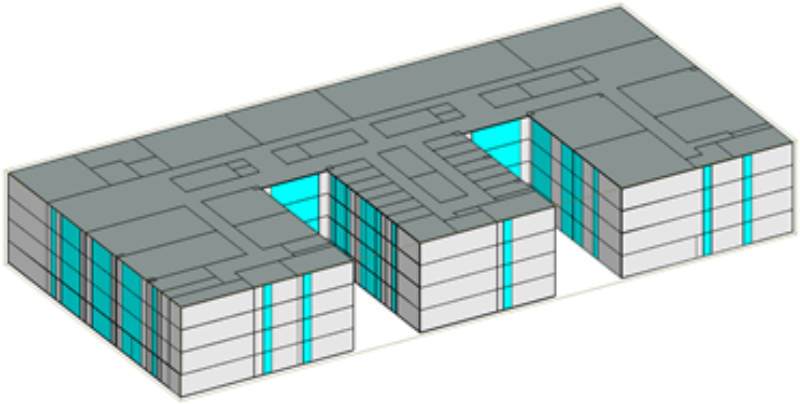

Figure 3.1: 3D Model of the university building

Figure 3.2: 2^{nd} Floor plan (Size: 74.1 x 35.75 meters)

Figure 3.3: 3^{rd} Floor plan (Size: 74.1 x 35.75 meters)

There have been multiple non-LOS (NLOS) paths between Tx and Rx in the measurement setup, which makes it suitable for verifying different models effectively. There were 88 and 63 measurements taken with a separation of approximately 1 meter for 2^{nd} and 3^{rd} floor respectively. In order to mitigate fast fading effects, an average of 10 readings were taken for each location.

Radiation patterns of both Tx and Rx antennas were omni-directional in horizontal axis. The antenna orientation was horizontal for Tx (cf. Figure 3.4). For the Rx, we measured RSS for three different antenna orientations, i.e., up (vertical), left (horizontal) and right (horizontal) (cf. Figure 3.5). Figure 3.6 shows the received signal power at 2^{nd} floor for all 88 locations starting from point A until Point B, when the Rx antenna orientation was vertical (i.e., up), whereas Figure 3.7 presents the results for three different antenna orientations. It was found that all three antenna orientations have similar propagation characteristics. Thus, the rest of the measurements were taken for the vertical antenna orientation.

Figure 3.4: Transmitter antenna orientation

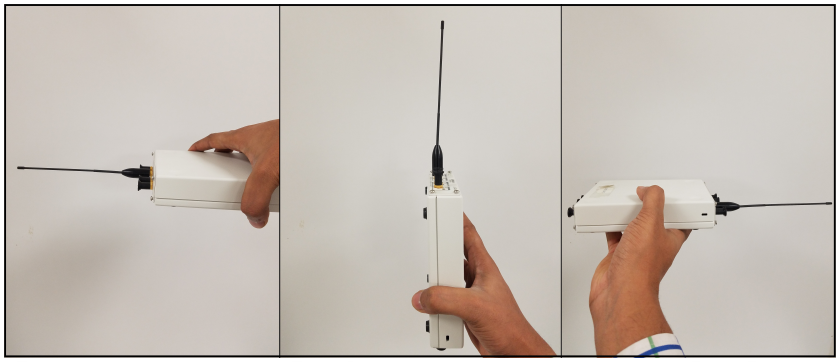

Figure 3.5: Receiver antenna orientations (Left, Up and Right)

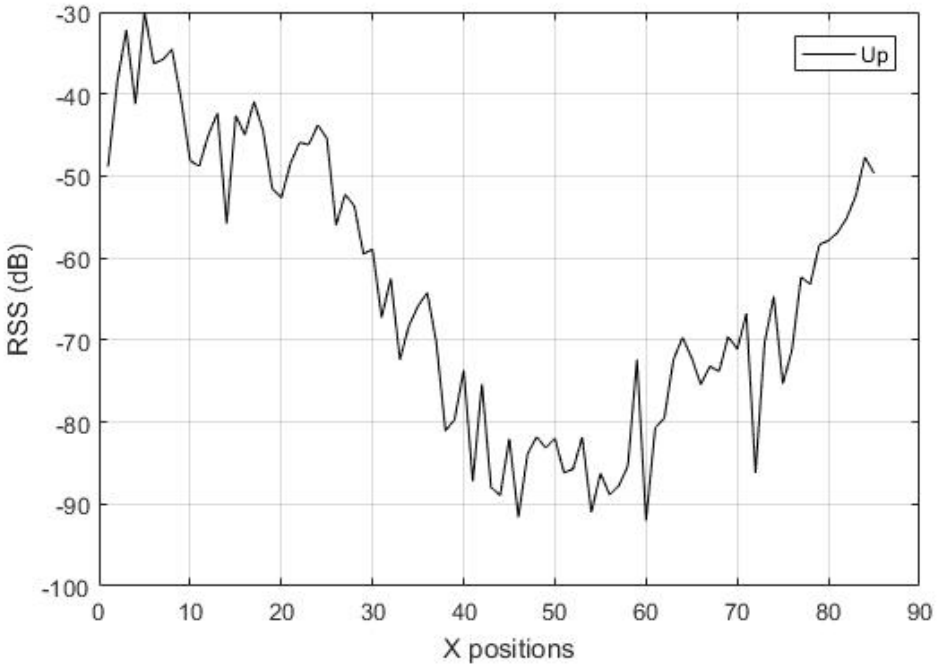

Figure 3.6: Measurement results of received signal strength at the 2^{nd} floor

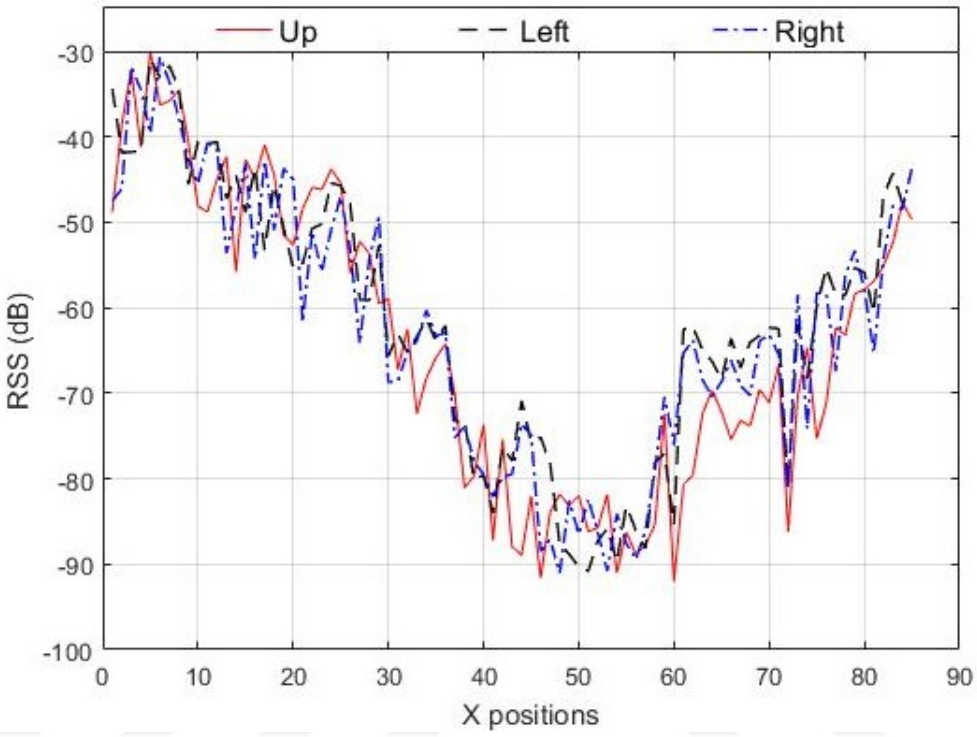

Figure 3.7: Measurement results of received signal strength with different antenna orientations (see Fig. 3.5) at the 2^{nd} floor

3.2 Indoor Channel Models and Results

In this work, a total of 4 indoor path loss models are considered, which take direct path distance in to account when calculating the path loss. These are the log-distance model in which received power of the signal decreases logarithmically with distance [11], Linear Attenuation Model (LAM) which integrates the effect of free space path loss [12], ITU-R P.1238 [13] and Multi Wall and Floor Model (MWF) [14]. Among them, ITU-R P.1238 and MWF models integrate the effect of floors. In addition, the MWF model incorporates the effect of attenuation due to walls. These models are defined as follows:

$$\textbf{Log} - \textbf{distance} : PL = PL(d_0) + 10n \log_{10}\left(\frac{d}{d_0}\right) \tag{3.1}$$

where,

PL = path loss in dB

$PL(d_0)$ = path loss at distance d_0

n = power decay parameter

d_0 = reference distance between Tx and Rx

d = direct path distance between Tx and Rx.

$$\textbf{LAM} : L = L_{FS} + \alpha d \tag{3.2}$$

where,

L = total propagation loss

L_{FS} = free space loss

α = attenuation coefficient

$$\textbf{ITU} - \textbf{RP.1238} \quad : \quad L \quad = \quad 20\log_{10}(f) \; + \; N\log_{10}(d) \; + \; L_f(n) \; - \; 28 \tag{3.3}$$

where,

f = transmission frequency (MHz)

N = distance power loss coefficient

n = total number of floors in between

L_f = attenuation due to floor penetration (dB)

$$\textbf{MWF} \;:\; L_{MWF} \;=\; L_0 \;+\; 10\beta\log(d) \;+\; \sum_{i=1}^{I}\sum_{k=1}^{K_{wi}} L_{wik} \;+\; \sum_{j=1}^{J}\sum_{k=1}^{K_{fj}} L_{fjk} \quad (3.4)$$

where,

L_0 = path loss at 1m distance

β = power delay index

I = number of wall types

J = number of floor types

K_{wi} = number of traversed walls of type i

K_{fj} = number of traversed floors of type j

L_{wik} = attenuation due to wall of type i and k-th traversed wall

L_{fjk} = attenuation due to floor of type j and k-th traversed floor

To assess how the measurements are compared with the models above, initially curve fitting is used to determine the parameters based on the measurements at three different frequencies. Path loss exponent (n) was fitted to the measured data using Matlab's curve fitting tool .

At 480 MHz (2^{nd} floor), parameters after calculations are found to be n = 3.805 for log-distance model, α = 1.45 for LAM, N = 39.2 for ITU-R P.1238 model and β = 1.91 for MWF model. It is to be noted that wooden doors were considered as walls, glass doors were neglected in calculations. The results can be seen in Figures 3.8 and 3.9.

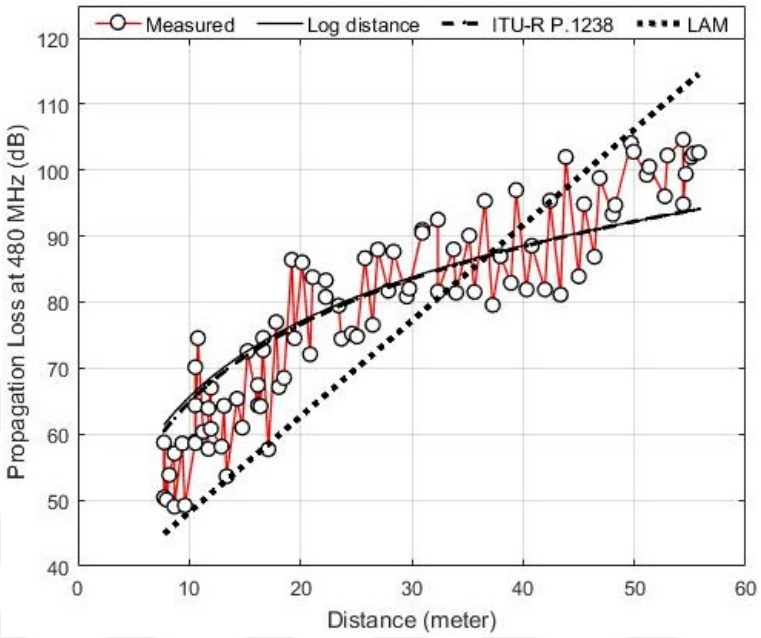

Figure 3.8: Measurement results compared with estimation results at 480 MHz (log-distance, ITU-R P.1238, LAM)

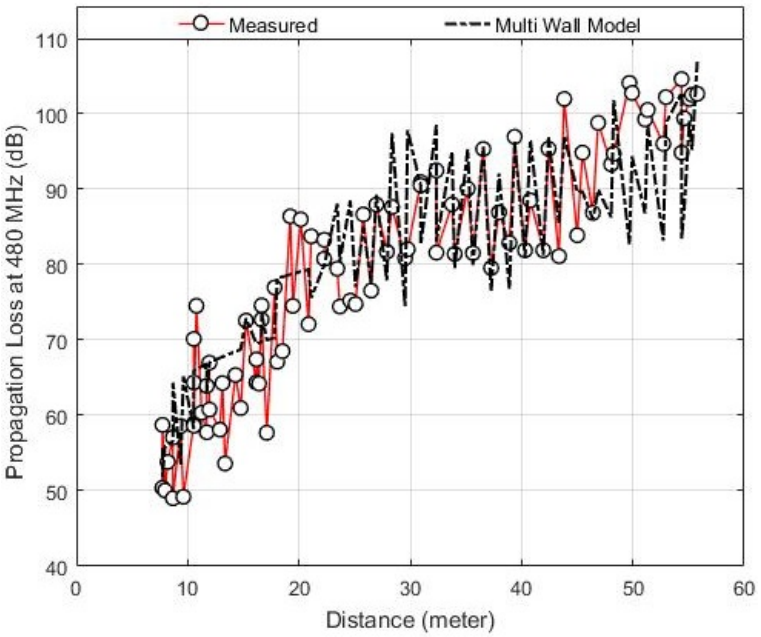

Figure 3.9: Measurement results compared with estimation results at 480 MHz (MWF)

At 580 MHz (2^{nd} floor), parameters after calculations are found to be $n =$

3.558 for log-distance, $\alpha = 1.322$ for LAM, $N = 36.25$ for ITU-R P.1238 and $\beta = 1.663$ for MWF. The results can be seen in Figures 3.10 and 3.11.

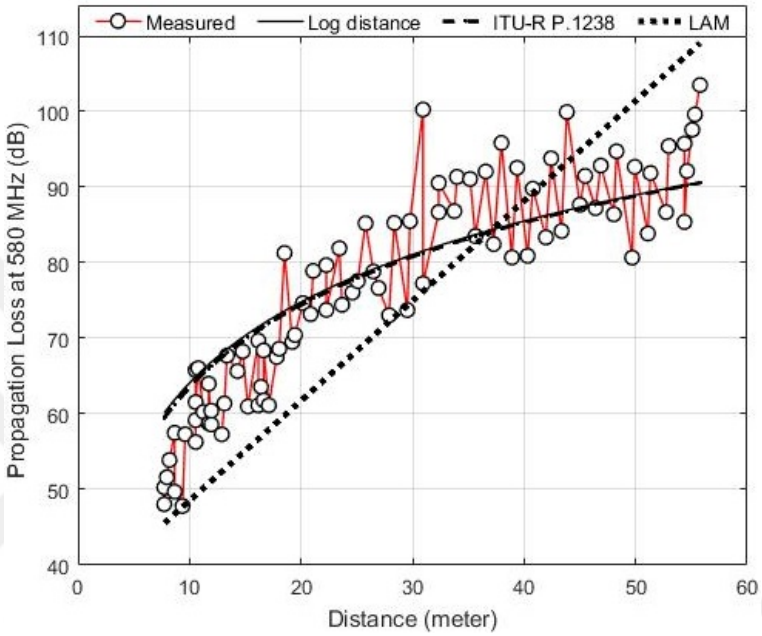

Figure 3.10: Measurement results compared with estimation results at 580 MHz (log-distance, ITU-R P.1238, LAM)

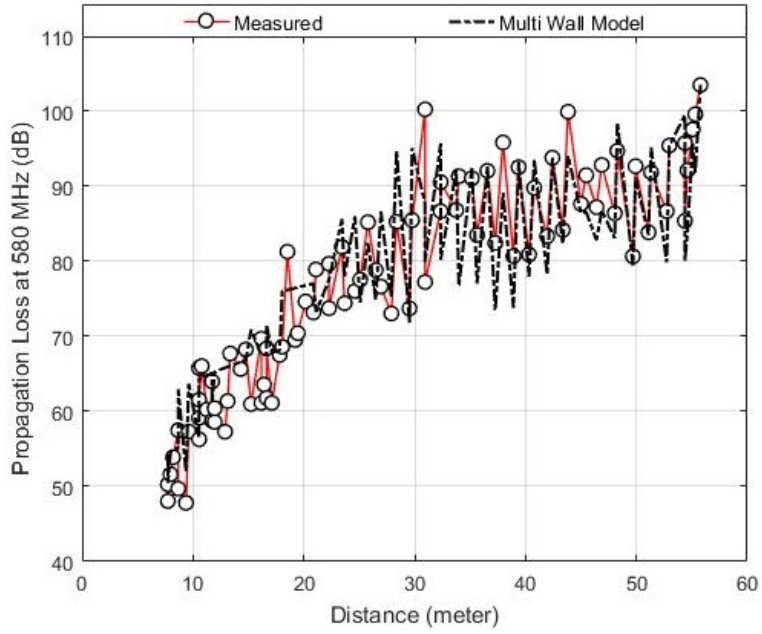

Figure 3.11: Measurement results compared with estimation results at 580 MHz (MWF)

At 580 MHz (3^{rd} floor), parameters after calculations are found to be $n = 3.9$ for log-distance, $\alpha = 1.483$ for LAM, $N = 40.44$ for ITU-R P.1238 and $\beta = 1.501$ for MWF. The results can be seen in Figures 3.12 and 3.13.

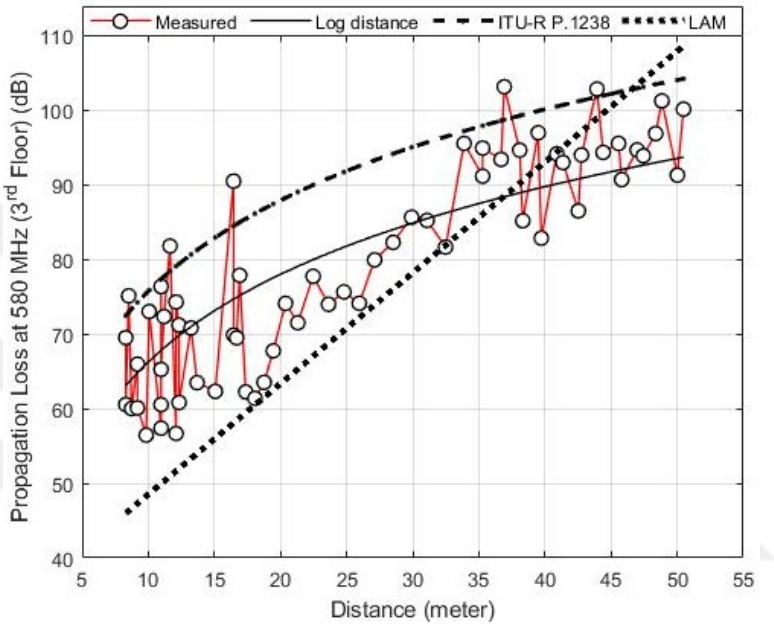

Figure 3.12: Measurement results compared with estimation results at 580 MHz (log-distance, ITU-R P.1238, LAM) (3^{rd} floor)

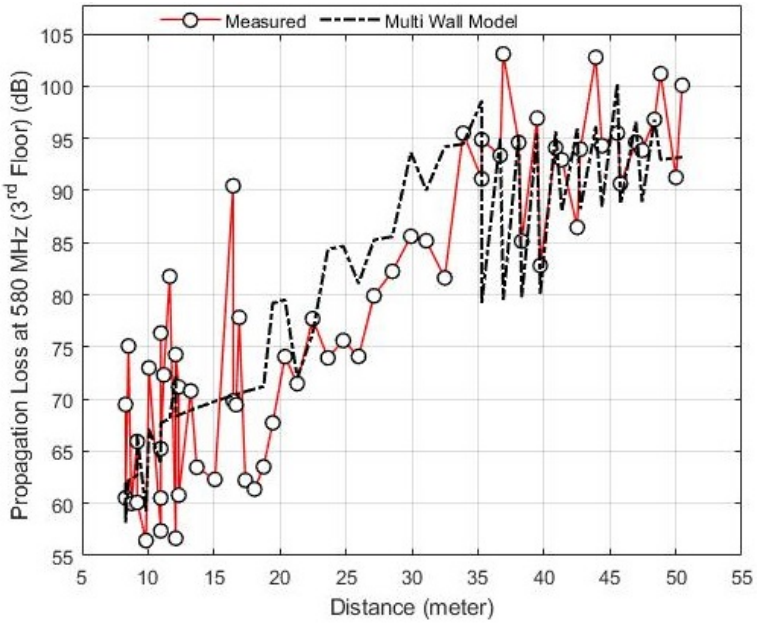

Figure 3.13: Measurement results compared with estimation results at 580 MHz (MWF) (3^{rd} floor)

At 630 MHz (2^{nd} floor), parameters after calculations are found to be n = 3.403 for log-distance, α = 1.255 for LAM, N = 34.63 for ITU-R P.1238 and β = 1.507 for MWF. The results can be seen in Figures 3.14 and 3.15.

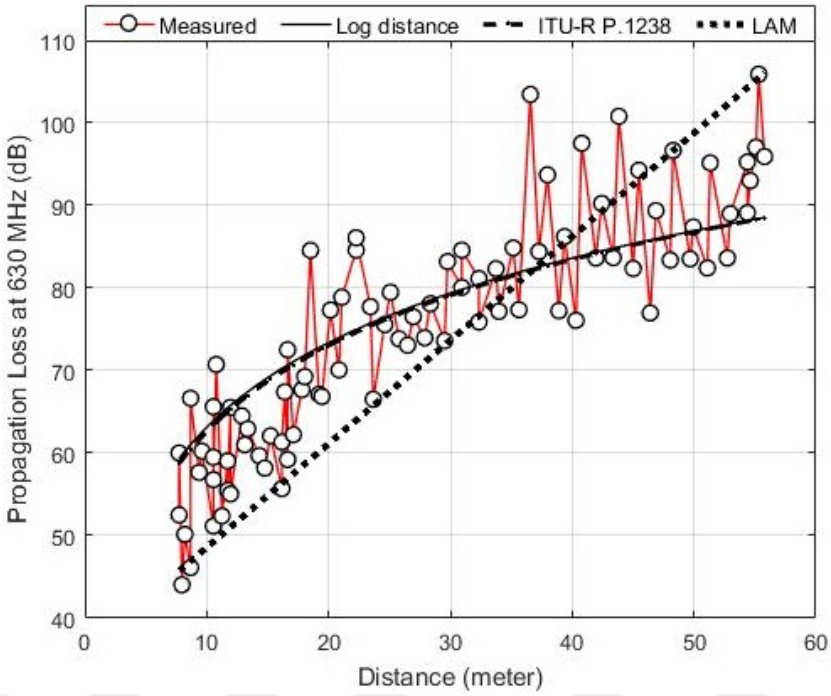

Figure 3.14: Measurement results compared with estimation results at 630 MHz (log-distance, ITU-R P.1238, LAM)

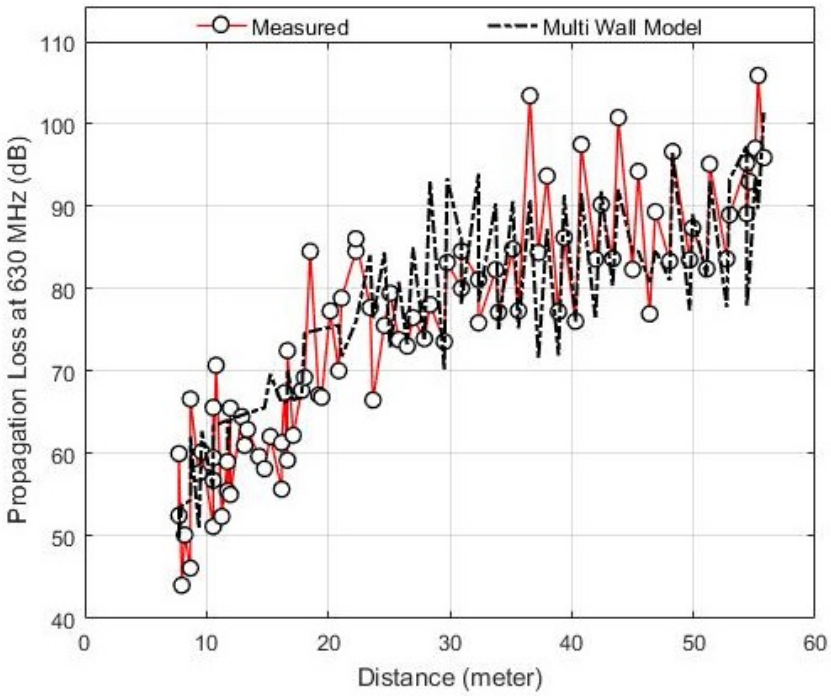

Figure 3.15: Measurement results compared with estimation results at 630 MHz (MWF)

From Figures 3.8-3.15, it can be seen that log-distance and ITU-R P.1238 models have approximately the same results. LAM can only model in a small patch of distance, otherwise, it does not fit the measurement results well. MWF model can represent the measurement results better compared to other three models, as it shows less estimation error throughout the measurement range. This is due to the additional term of propagation loss due to walls in the definition of MWF model. Accordingly, the MWF model seems to be the most suitable model for TVWS frequency bands.

In general, walls, furniture, doors, etc. may be in the direct path distance between Tx and Rx, and cause their own propagation loss. Therefore, it is important to model the loss of these effects to minimize the overall estimation error. On the other hand, the modeling of all these obstacles is not trivial due to their respective positions in an indoor environment. In [27], authors assume that these obstacles are uniformly distributed in the indoor environment and propose another model based on this assumption, which is a variation of the existing LAM model (we have named it extended LAM in this paper). The model is given as:

$$L = L_{FS} + \gamma d + n_w L_w + n_f L_f + C \tag{3.5}$$

In the above equation, γ is the attenuation coefficient, n_w is the number of penetrating walls, n_f is the number of penetrating floors, L_w is the loss of each wall, L_f is the loss of each floor and C is the attenuation constant. We have also performed estimations using this model and compared with measurement results. The comparison at 480, 580 (2^{nd} and 3^{rd} floor) and 630 MHz are plotted in Figure 3.16-3.19.

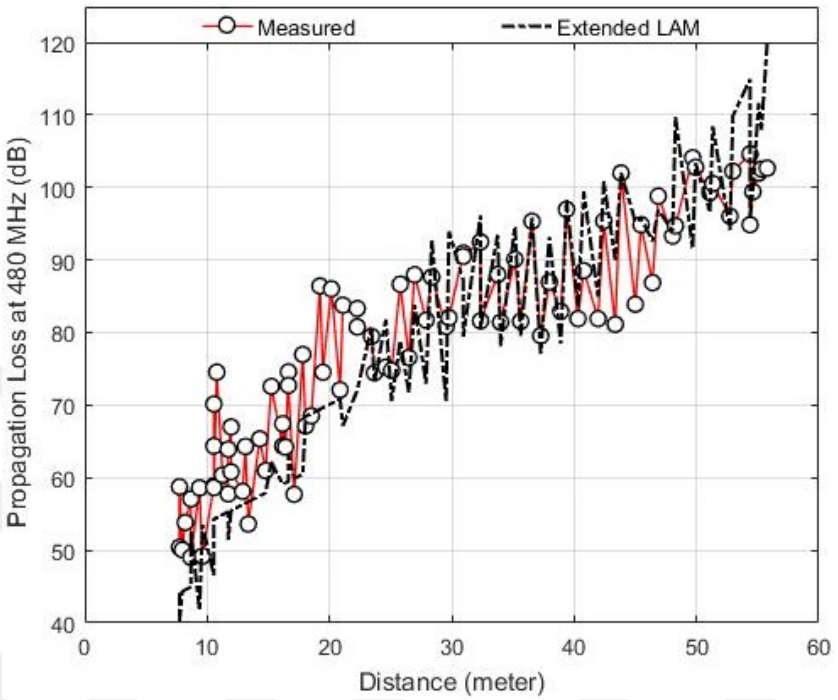

Figure 3.16: Measurement results compared with estimation results at 480 MHz (extended LAM)

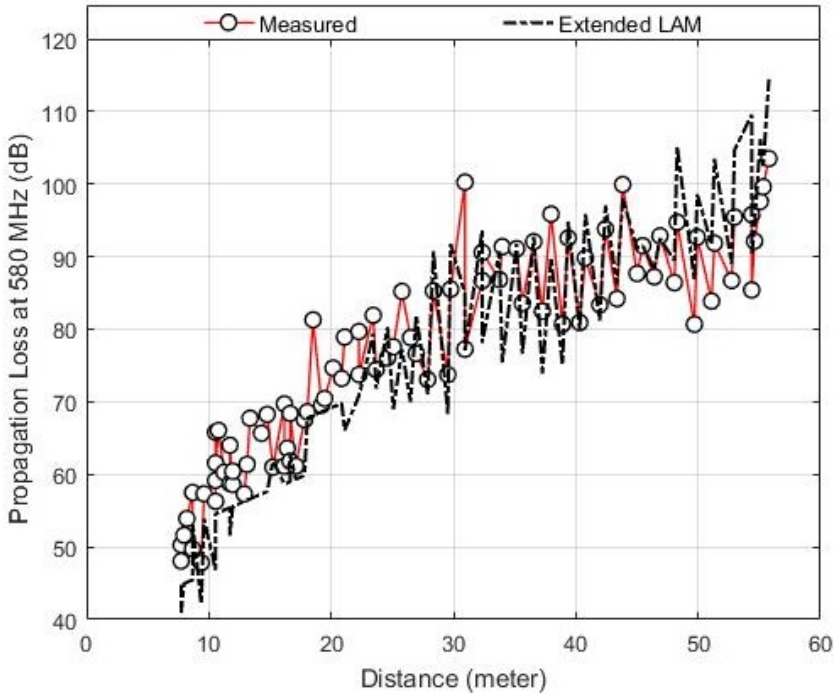

Figure 3.17: Measurement results compared with estimation results at 580 MHz (extended LAM)

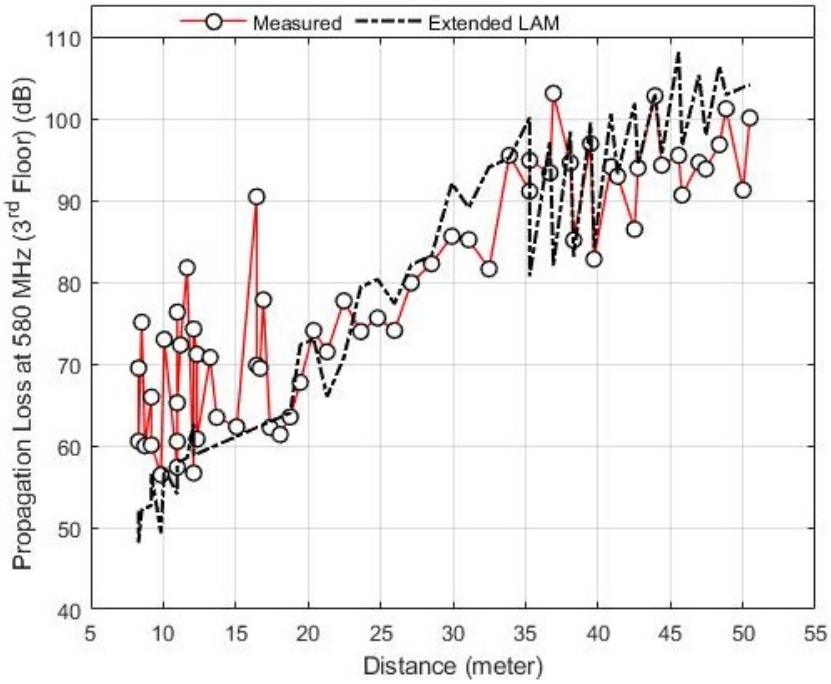

Figure 3.18: Measurement results compared with estimation results at 580 MHz (extended LAM)(3^{rd} floor)

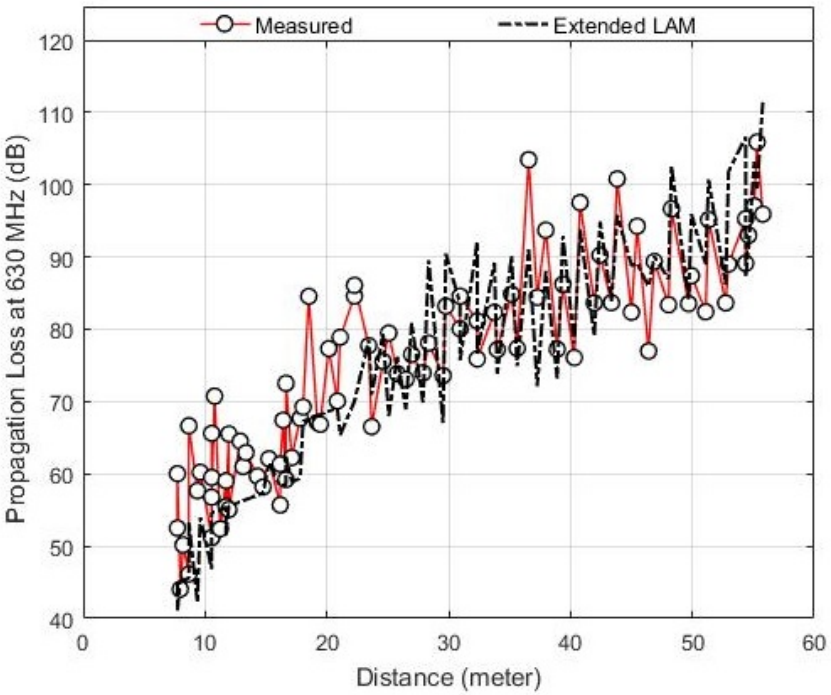

Figure 3.19: Measurement results compared with estimation results at 630 MHz (extended LAM)

In Figures 3.16-3.19, the estimated values of γ are: 0.8521 at 480 MHz, 0.767 at 580 MHz (2^{nd} floor), 0.777 at 580 MHz (3^{rd} floor) and 0.656 at 630 MHz. The extended LAM model can model the measurement results similar to the MWF model and better than the LAM model.

3.3 Proposed Indoor Propagation Channel Model for TVWS Band

None of the channel models considered in the previous section considers the loss due to glass windows and doors. In the literature, it is assumed that glass has slight penetration loss. This assumption can be accepted to some extent, but in cases where there are many glass objects, the effect of glass can be incorporated to minimize the modeling error. Here, we should mention some points on our 2^{nd} floor map with dotted rectangles (c.f. Figure 3.2), where the actual propagation loss is more than the estimated values, calculated from MWF and extended LAM models. Incorporation of loss due to wall does not reduce estimation error at these points. This is because there are less number of walls than the glass windows and glass doors in the direct path. Here, the effects of glass windows and glass doors cannot be neglected on the path loss. Although some of the errors are due to furniture and other obstacles, these objects are harder to model compared to windows and doors. With the addition of these effects, the following equation has been proposed:

$$L = L_{d_0} + 10\zeta \log\left(\frac{d}{d_0}\right) + n_{wl}L_{wl} + n_{wd}L_{wd} + n_dL_d + n_fL_f \tag{3.6}$$

where, L_{d_0} is the path loss at distance d_0, n_{wl} is the number of walls, n_{wd} is the number of windows, n_d is the number of doors, n_f is the number of floors, L_{wl} is the loss of each wall, L_{wd} is the loss of each window, L_d is the loss of each door and L_f is the loss of each floor. The estimated results at 480, 580 (2^{nd} and 3^{rd} floor) and 630 MHz are plotted in Figures 3.20-3.23.

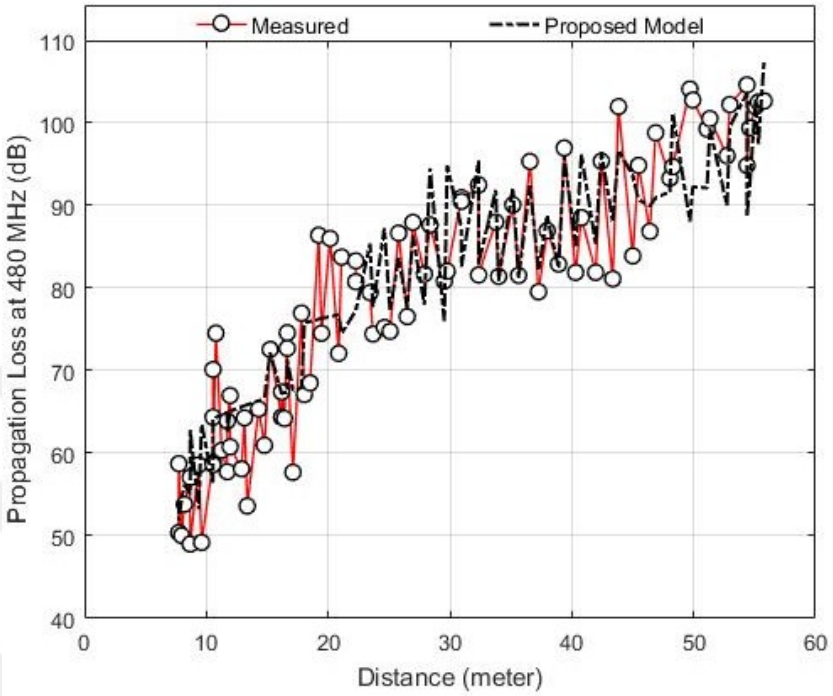

Figure 3.20: Measurement results compared with estimation results at 480 MHz (proposed model)

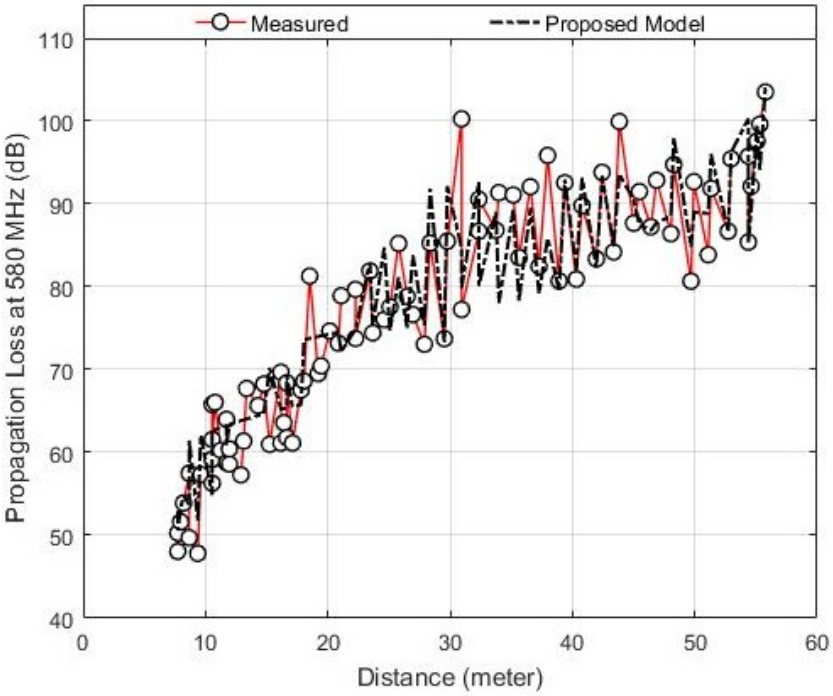

Figure 3.21: Measurement results compared with estimation results at 580 MHz (proposed model)

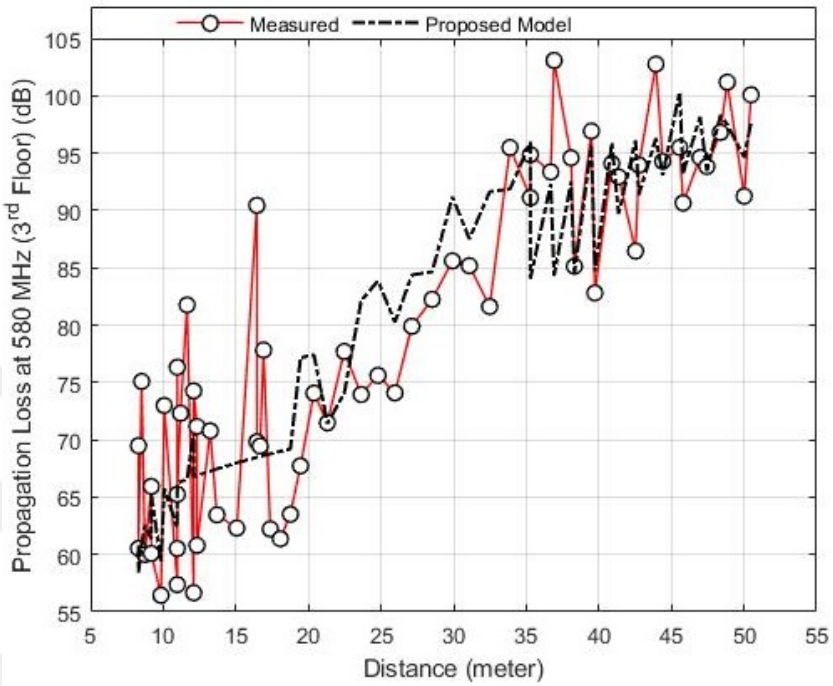

Figure 3.22: Measurement results compared with estimation results at 580 MHz (proposed model)(3^{rd} floor)

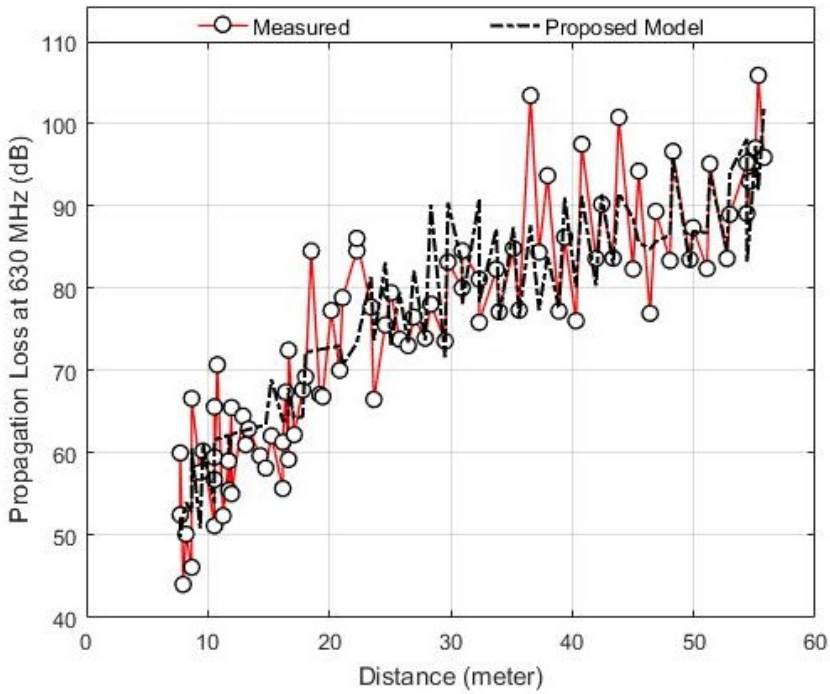

Figure 3.23: Measurement results compared with estimation results at 630 MHz (proposed model)

In our case, windows and most of the sliding doors are made up of glass, where only some of the doors are wooden. Glass doors and windows, wooden doors and walls have approximately same penetration loss which are 1.493 and 3.878 dB, respectively. After calculations ζ was found to be 1.637 at 480 MHz, 1.39 at 580 MHz (2^{nd} floor), 1.276 at 580 MHz (3^{rd} floor), and 1.234 at 630 MHz.

As seen in Figures 3.20-3.23, the difference in measured and estimated path loss values are reduced as compared to Figures 3.9, 3.11, 3.13 and 3.15 (MWF model), since we add the additional loss due to glass windows and doors in the proposed model. In the floor map, total number of wooden doors/walls and glass doors/windows in the direct path ranges from 0 to 10 and 0 to 9, respectively.

3.4 Performance Comparisons

In this section, we compare the accuracy of the proposed model with other models at three different transmission frequencies. The results are given in Table 3.1 and Figure 3.24. The proposed model shows the best performance in terms of the standard deviation of estimation error as compared to other models at all the frequencies. Incorporation of the effect of walls, windows, and doors has reduced the estimation error significantly.

Table 3.1: Comparison of propagation models

Frequency	**Parameter**	**LAM**	**Log-distance**	**ITU-R P.1238**	**Extended LAM**	**MWF**	**Proposed Model**
480 MHz ($2^{nd}Floor$)	STD (dB)	11.22	7.39	7.16	8.60	7.22	6.15
580 MHz ($2^{nd}Floor$)	STD (dB)	10.53	6.73	6.58	7.02	5.56	4.74
630 MHz ($2^{nd}Floor$)	STD (dB)	10.45	7.57	7.46	7.69	6.83	6.04
580 MHz ($3^{rd}Floor$)	STD (dB)	13.01	7.29	12.67	10.09	7.78	7.00

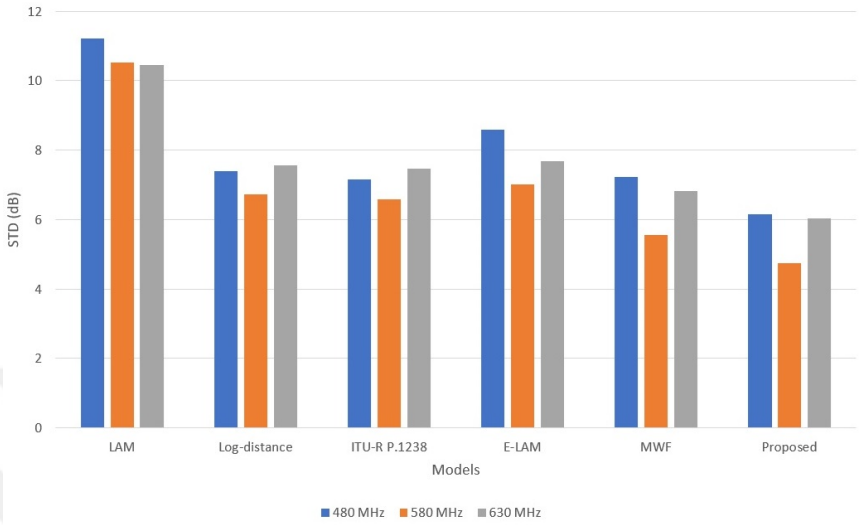

(a)

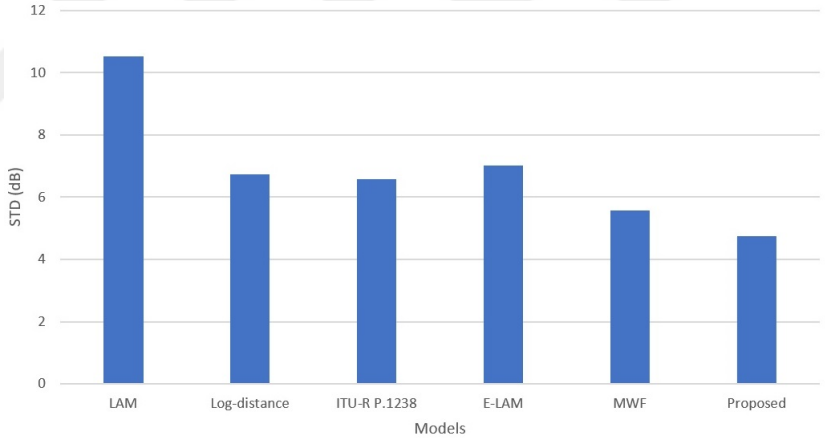

(b)

Figure 3.24: Comparison of propagation models on 2^{nd} (a) and 3^{rd} floor (b)

Finally, Figures 3.25-3.32 present the squared error with respect to direct path distance between Tx and Rx for different propagation models at different frequencies (including $3^{rd}Floor$). It is clear that all of the models have less squared error at 580 MHz ($2^{nd}Floor$) because less interference from other channels was observed only at 580 MHz frequency. So, here only the results at 580 MHz ($2^{nd}Floor$) will be discussed.

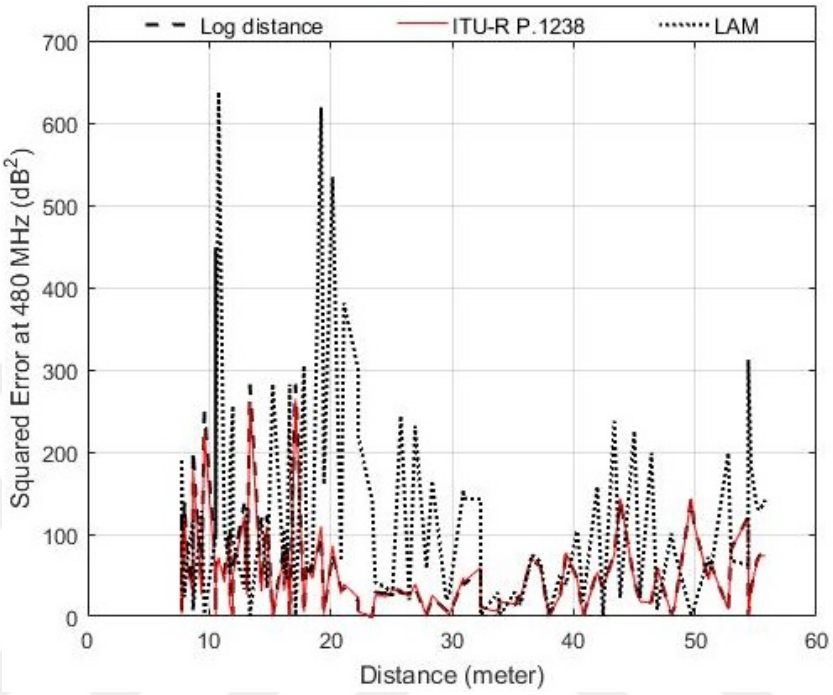

Figure 3.25: Performance comparison of log-distance, ITU-R P.1238 and LAM models at 480 MHz

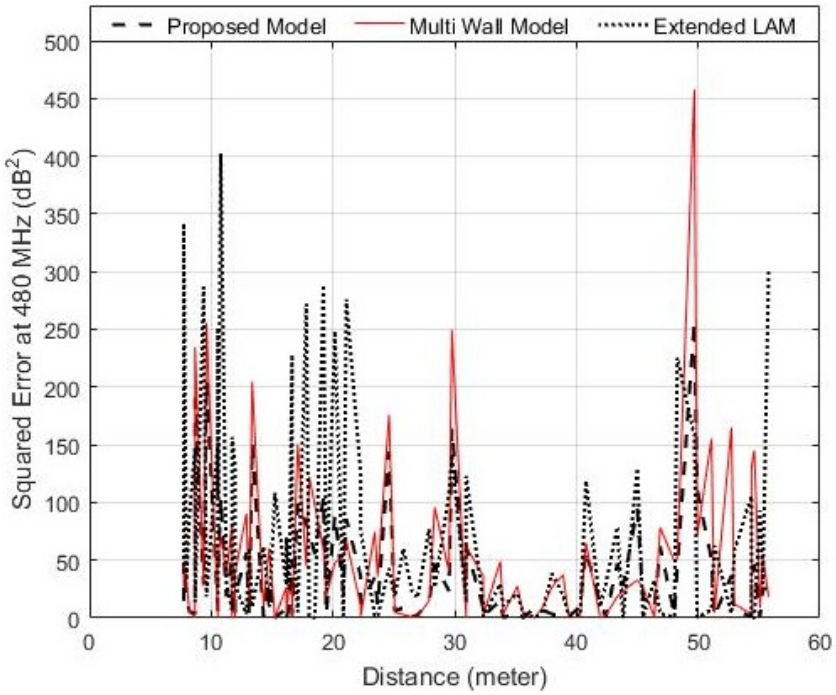

Figure 3.26: Performance comparison of the proposed, extended LAM and MWF models at 480 MHz

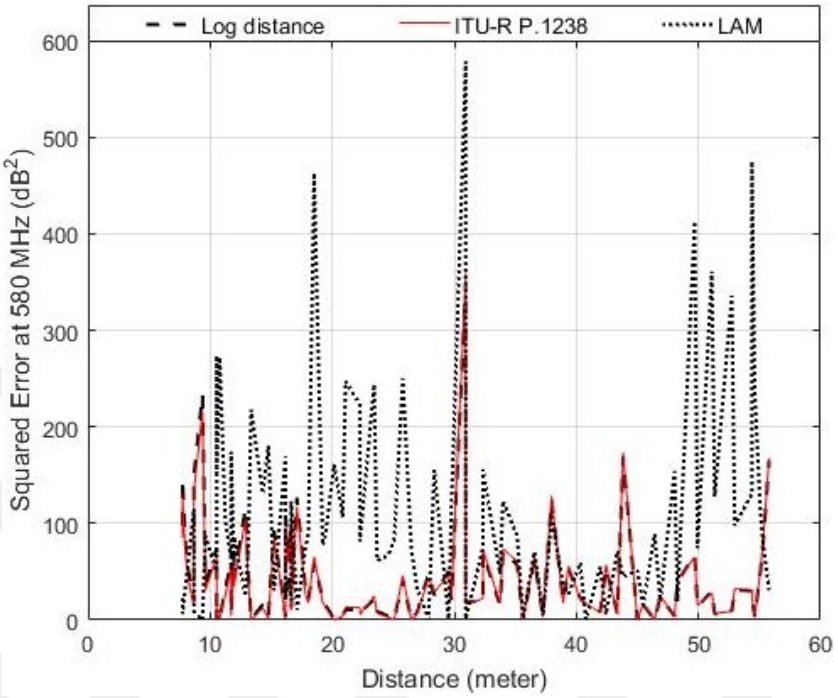

Figure 3.27: Performance comparison of log-distance, ITU-R P.1238 and LAM models at 580 MHz

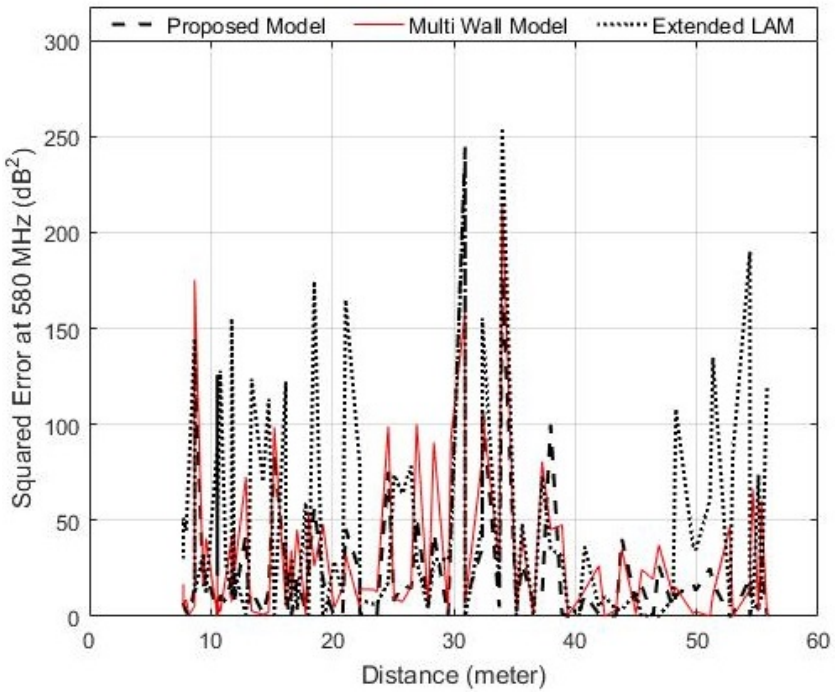

Figure 3.28: Performance comparison of the proposed, extended LAM and MWF models at 580 MHz

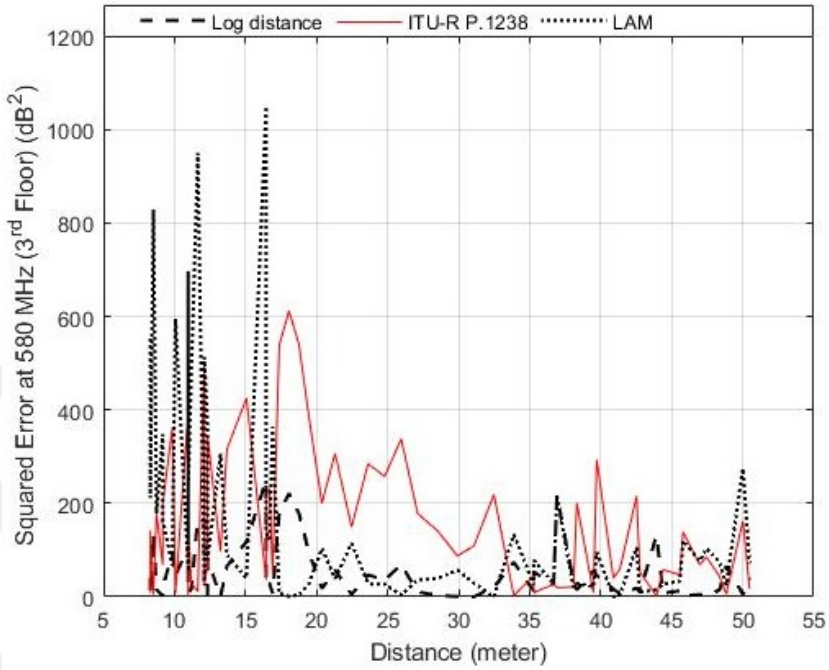

Figure 3.29: Performance comparison of log-distance, ITU-R P.1238 and LAM models at 580 MHz ($3^{rd}Floor$)

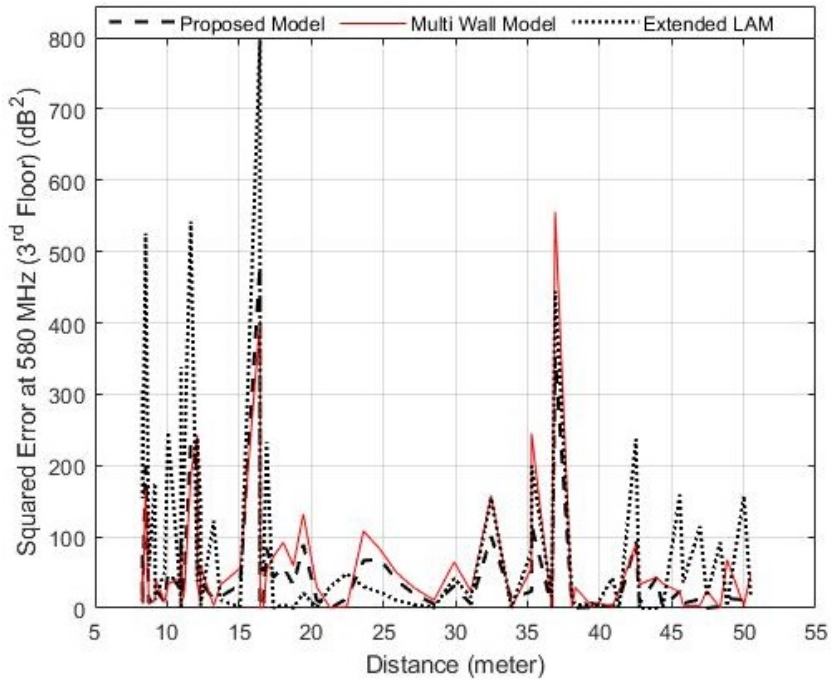

Figure 3.30: Performance comparison of the proposed, extended LAM and MWF models at 580 MHz ($3^{rd}Floor$)

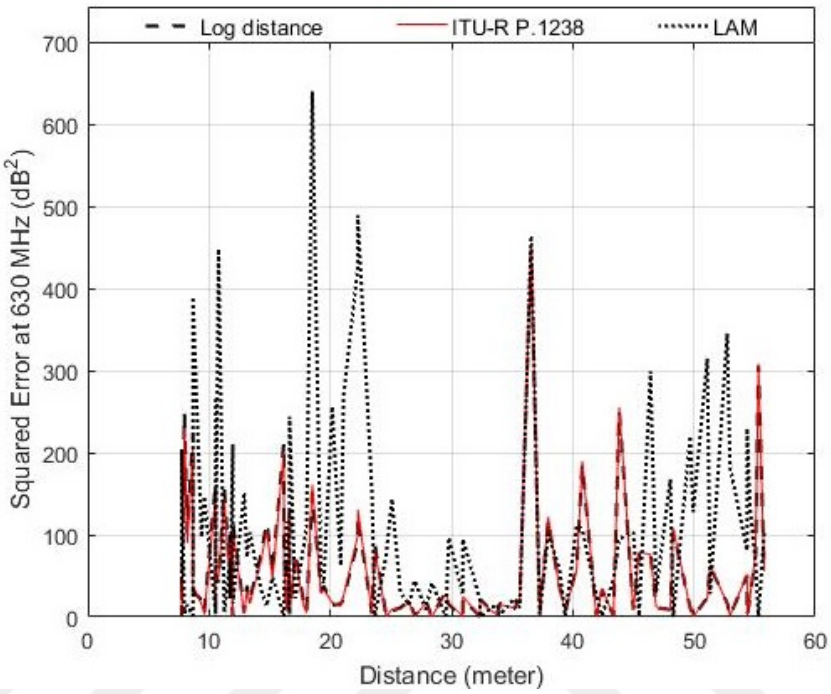

Figure 3.31: Performance comparison of log-distance, ITU-R P.1238 and LAM models at 630 MHz

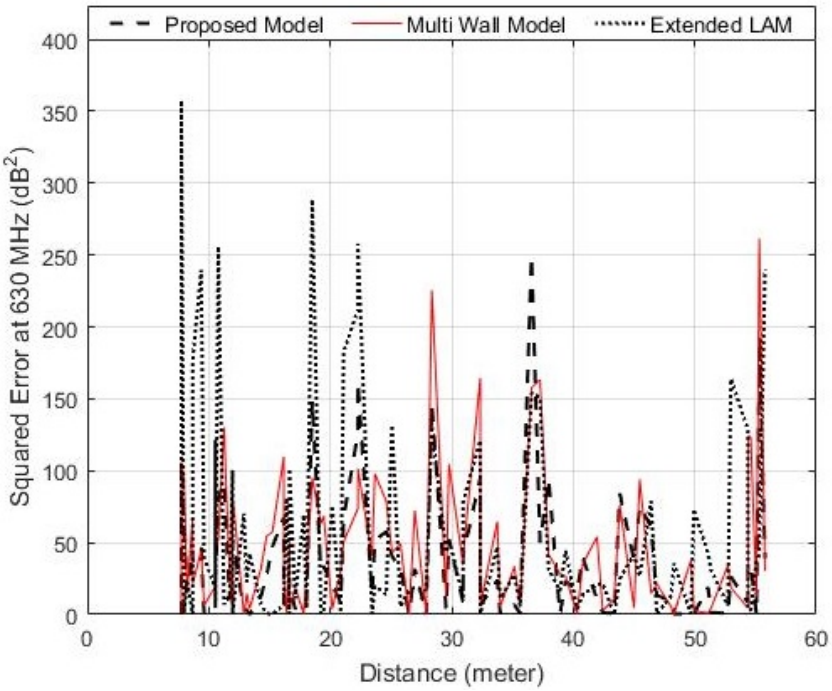

Figure 3.32: Performance comparison of the proposed, extended LAM and MWF models at 630 MHz

In Figure 3.27, LAM model has minimum (0.0130 dB^2) and maximum (578.48 dB^2) squared error at location number 03 and 39 with direct path distance of 9.375 and 30.93 meters respectively. Similarly, ITU-R P.1238 model has minimum (1.38x10^{-4} dB^2) and maximum (521.51 dB^2) squared error at location number 78 and 39 with distance 26.48 and 30.93 meters and Log distance model has minimum (0.039 dB^2) and maximum (350.08 dB^2) squared error at location number 72 and 39 with distance 35.62 and 30.93 meters.

In Figure 3.28, extended LAM model has minimum squared error (2.28x10^{-4} dB^2) at location number 49 and maximum squared error (254.62 dB^2) at location number 73 with a direct path distance of 45.47 and 33.98 meters, respectively. MWF model has minimum squared error (4.45x10^{-6} dB^2) at location number 47 and maximum squared error (215.05 dB^2) at location number 73 with direct path distance of 42.42 and 33.98 meters. Lastly, the proposed model has minimum squared error (0.0014 dB^2) at location number 61 and maximum squared error (244.48 dB^2) at location number 39 with direct path distance of 52.73 and 30.93 meters.

Since the proposed and the MWF models have better performance compared to the other models (c.f. Table 3.1), we only compare their estimation results at specific locations, which are indicated with dotted rectangles in ($2^{nd}Floor$) Map. At location numbers 59, 60 and 61, total number of walls and windows in the direct path are 5, 4, 4 and 6, 6, 7 and the distance in meters are 54.61, 54.37 and 52.73, respectively. According to our theory, increasing the number of windows should increase the error of the MWF model. The squared error values calculated from MWF model are 66.09 dB^2, 28.11 dB^2, 46.61 dB^2, whereas the proposed model has the error values of 8.26 dB^2, 0.0018 dB^2, 0.0014 dB^2. As a result, we can conclude that observations support our theory and the proposed model improves estimation performance.

If the direct path distance is long and there are many obstructions, both proposed model and MWF model have higher error values. However, the error of the proposed model is still lower than the MWF model. For example, at location number 57, the direct distance is 55.31 meters. RSS at this location is -83.02

dB. Measured path loss is 99.62 dB. MWF model and proposed model path loss estimations are 91.85 and 94.10 dB. The error of the proposed model is smaller but still high. However, overall results show that the proposed model is effective in indoor environments.

Chapter 4

Indoor to Outdoor Wireless Channel Measurements and Modeling

In this chapter, propagation characteristics in TVWS frequency bands are presented by capturing path loss values at multiple locations in indoor to outdoor environment and validated with log normal shadowing model. Further, a new model is proposed to find channel parameters for the mentioned environment. The goal of the model is to improve shadowing coefficient estimation.

4.1 Measurement Environment

During the measurement campaign, a BPSK modulated PN sequence is transmitted using USRP at TVWS frequencies which was placed inside the building. Transmitted signal is captured by another USRP outside the building. Proper spectrum scanning was performed before the measurement campaign to make sure that the frequencies of interest were vacant during transmission. Normally TVWS bands are defined between 470 to 700 MHz. We took measurements at

the center frequencies 470, 580 and 670 MHz.

Figure 4.1 shows indoor to outdoor measurement environment. Transmitter location is marked with yellow thumb pin (cf. west side of Figure 4.1). It is to be noted that terrain is not flat on the measurement site. The building with transmitter has multiple types of materials in the indoor environment (i.e. glass, wood, concrete, iron, and metal) which can reflect, diffract and, scatter the propagating signal.

Measurements were taken at 188 locations with a separation of 1 meter outside the university building i.e. from X (start) till Y (end) (cf. south and north-east side of Figure 4.1 respectively). For each location, an average of 10 readings were taken to mitigate fast fading effects.

Figure 4.1: Aerial view of the measurement site.

4.2 Indoor to Outdoor Channel Model and Results

There are multiple channel models available in the literature where the effect of direct path distance is incorporated into the path loss. We have used log normal

shadowing channel model (LNSM) in this work [11]. This model is defined by 4.1.

$$PL_{dB} = PL(d_0) + 10n \log_{10}\left(\frac{d}{d_0}\right) + X_\sigma \tag{4.1}$$

Where, $PL(d_0)$ is the path loss in dB at a reference distance $d_0 = 4.2$ meters which was found to be 38.9 dB at 470 MHz and 41.9 dB at 580 and 670 MHz, d is the direct distance between transmitter and receiver, n is the path loss exponent and X_σ is shadowing random variable with a zero mean and standard deviation of σ. Figures 4.2-4.4 show the received power versus distance results at 470, 580 and 670 MHz respectively.

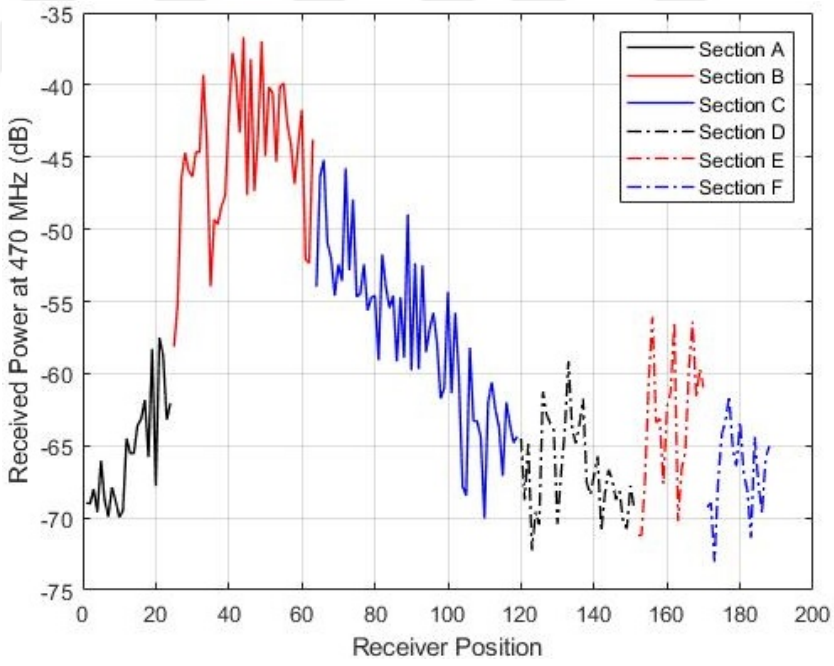

Figure 4.2: Measured received power (470 MHz) at different receiver positions (from X until Y in Figure 4.1).

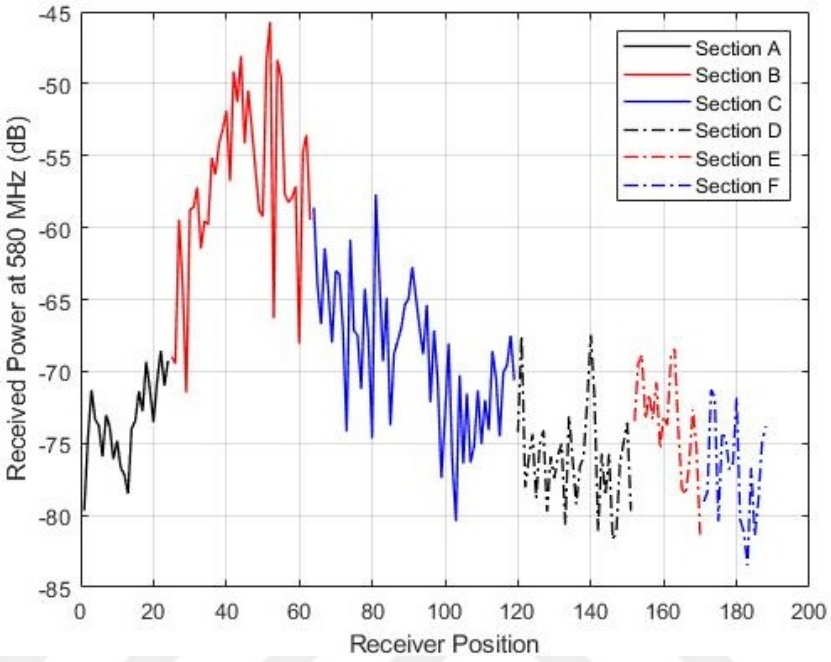

Figure 4.3: Measured received power (580 MHz) at different receiver positions (from X until Y in Figure 4.1).

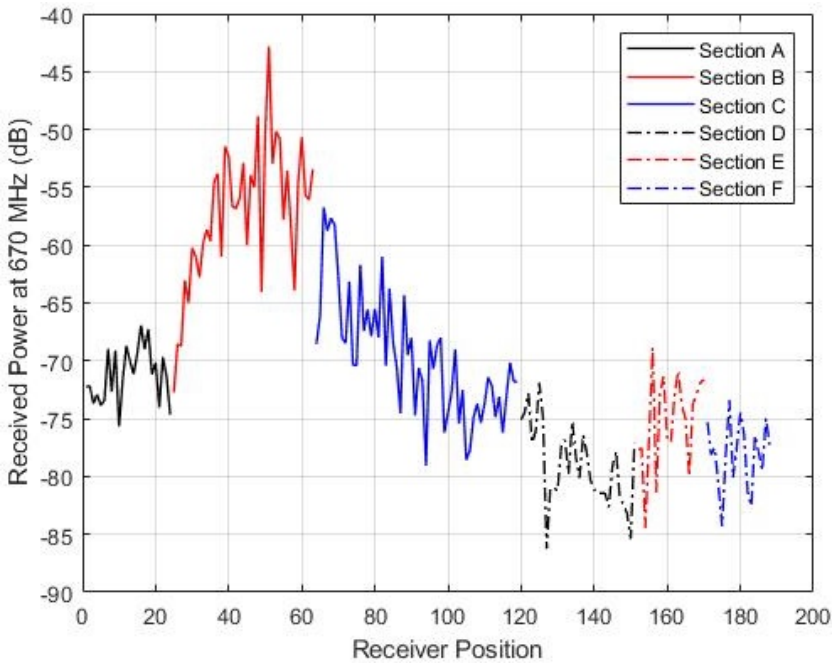

Figure 4.4: Measured received power (670 MHz) at different receiver positions (from X until Y in Figure 4.1).

Figure 4.5 shows the measured path loss and estimated path loss which is calculated from log normal shadowing channel model at 580 MHz frequency. Channel parameters are found to be $n = 3.9185$ and $\sigma = 8.4240$ dB. We fitted path loss exponent (n) to our data using Matlab's curve fitting tool .

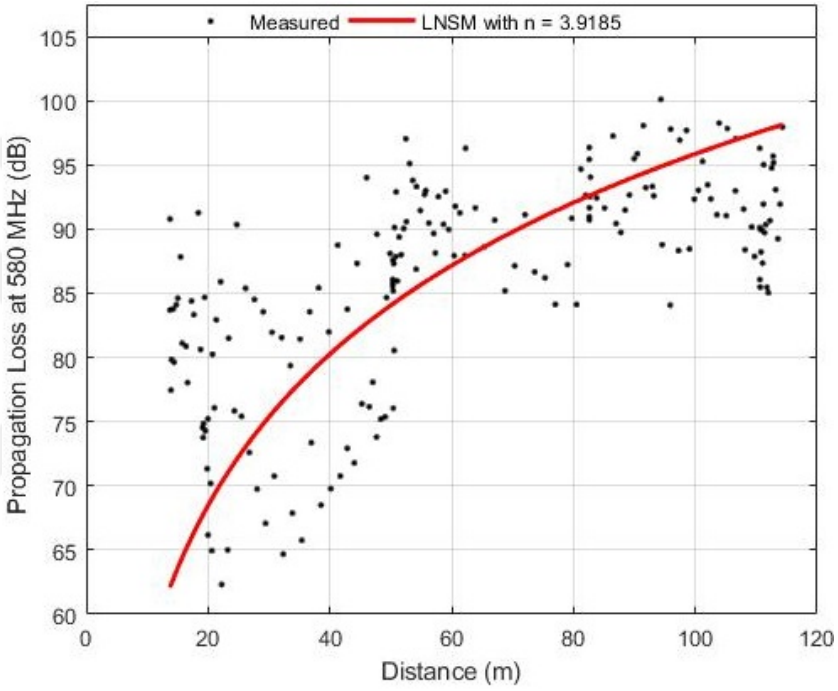

Figure 4.5: Measured path loss compared with estimated path loss at 580 MHz.

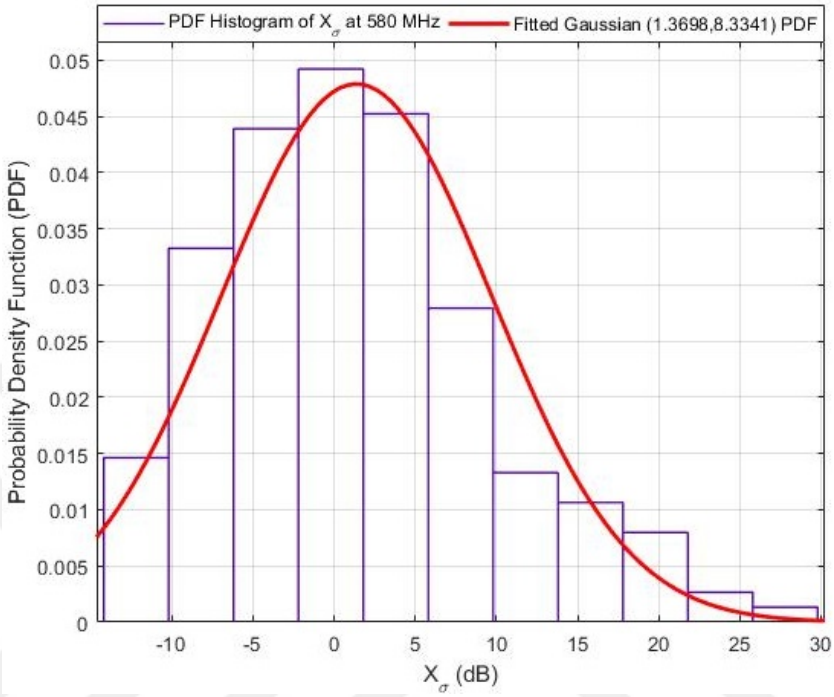

Figure 4.6: PDF of X_σ and Gaussian distribution at 580 MHz.

Figure 4.6 shows the measured probability density function (PDF) of X_σ. It includes Gaussian PDF with $\mu = 1.3698$ dB and $\sigma = 8.3341$ dB. We fitted Gaussian PDF on my measured results and found μ and σ by using Log likelihood method in Matlab's distribution fitter tool.

For 470 MHz frequency, Figure 4.7 shows the measured and estimated path loss with channel parameters $n = 3.2951$ and $\sigma = 6.9988$ dB and Figure 4.8 shows the measured PDF of X_σ and fitted Gaussian PDF with $\mu = 0.6242$ dB and $\sigma = 6.9895$ dB. These results show similarity with the results of 580 MHz frequency except the fact that overall path loss is less here.

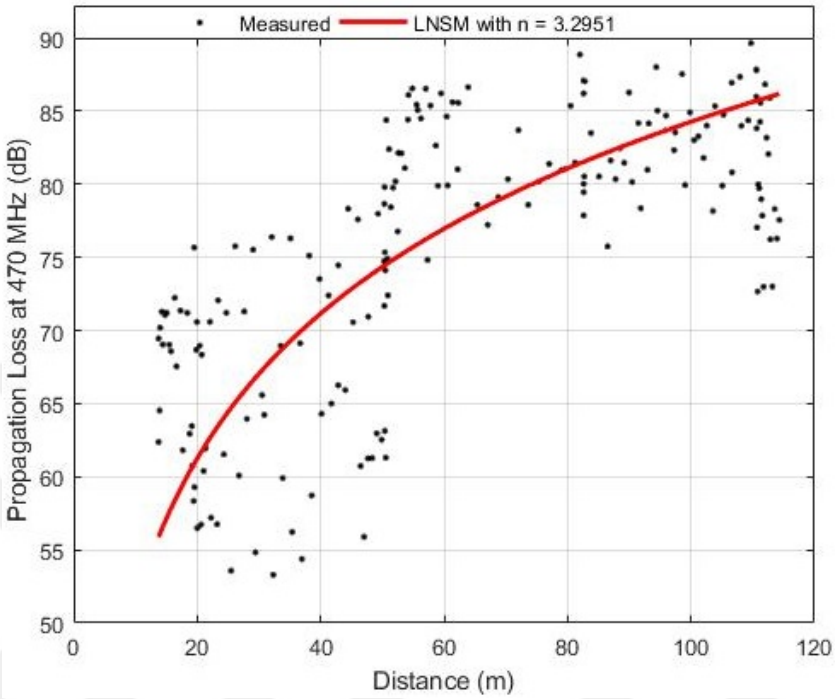

Figure 4.7: Measured path loss compared with estimated path loss at 470 MHz.

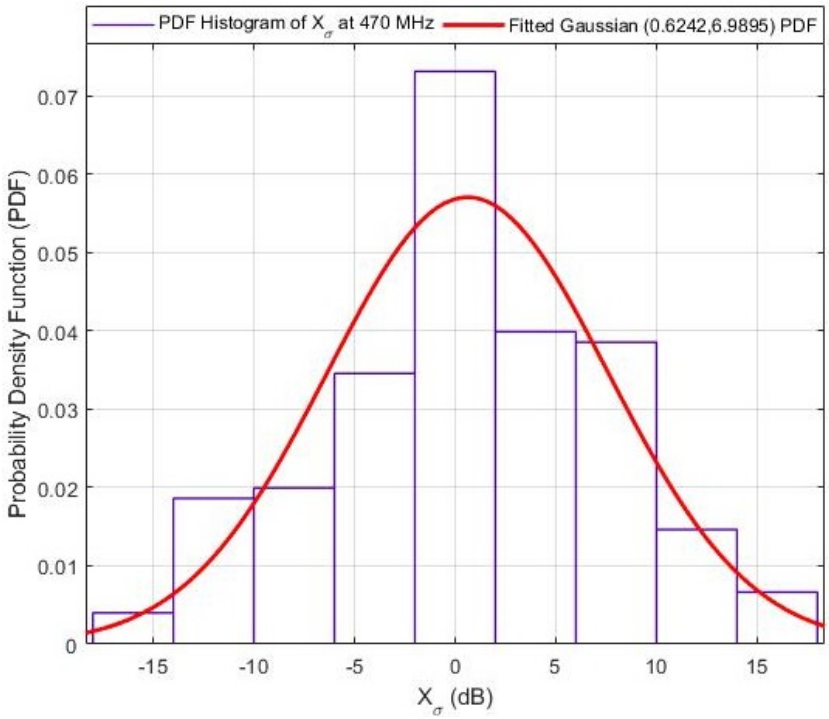

Figure 4.8: PDF of X_σ and Gaussian distribution at 470 MHz.

Figures 4.9 and 4.10 show the measured and estimated path loss with channel parameters $n = 4.0055$ and $\sigma = 7.6879$ dB, and measured PDF of X_σ and fitted Gaussian PDF with $\mu = 1.1715$ dB and $\sigma = 7.6185$ dB at 670 MHz frequency respectively.

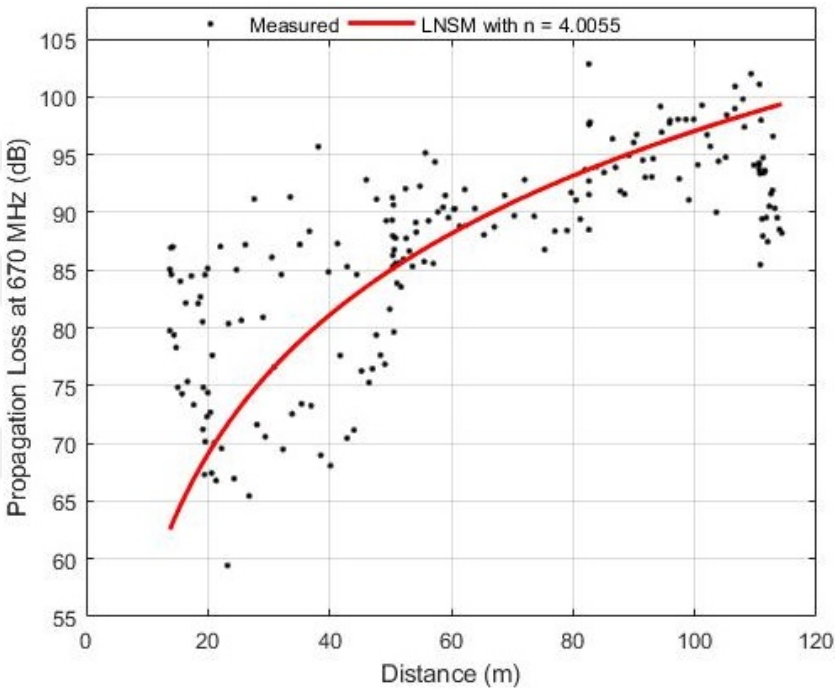

Figure 4.9: Measured path loss compared with estimated path loss at 670 MHz.

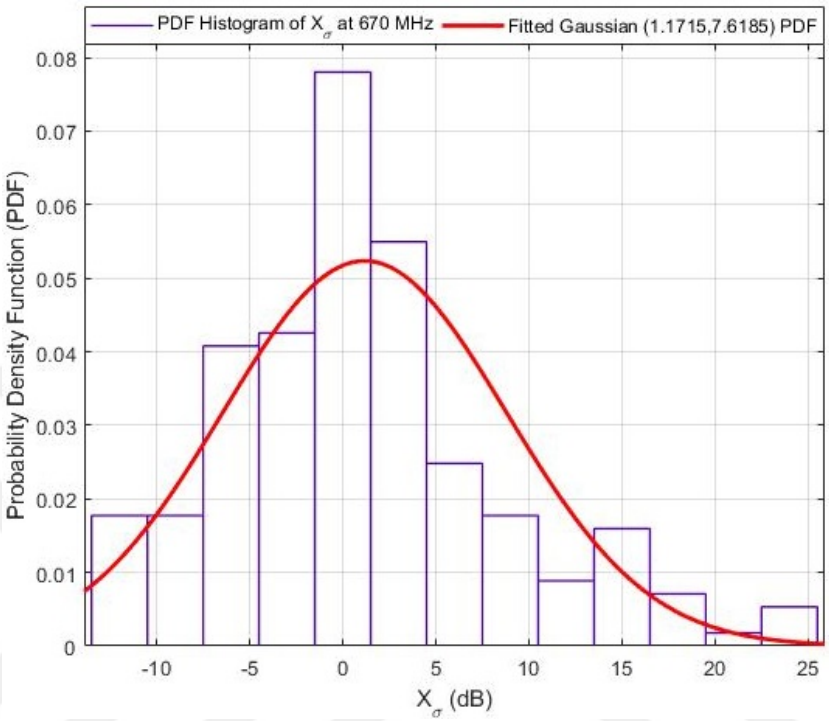

Figure 4.10: PDF of X_σ and Gaussian distribution at 670 MHz.

According to the path loss and shadowing results at 470, 580 and 670 MHz frequencies. We found, for short distances shadowing dominates the path loss value with its large standard deviation. After fitting Gaussian PDF on top of PDF of X_σ, it can be said that Gaussian distribution holds in indoor to outdoor environment.

4.3 Proposed Model and Discussion

From the results of previous section, it can be deduced that, for receiver positions which are close to the transmitter undergoes more shadowing effect than far ones due to strong multi-path reflections. If we model the shadowing of a wireless channel with single value for mentioned environment then it will not correctly model the shadowing for long distance locations because the short distance shadowing has a dominant effect on the overall shadowing value. Therefore, a new

model is proposed which divides measurements for short distance (sd) and long distance (ld) readings based on channel properties. This concept can also be seen in Figure 4.11. For dividing the readings to short-distance and long-distance, an algorithm is proposed (Algorithm 1). The goal of the algorithm is to maximize the difference of shadowing standard deviation between two reading groups. Mathematical representation of the concept is given in 4.2.

$$Divisiondistance = max \mid \sigma_{sd} - \sigma_{ld} \mid \tag{4.2}$$

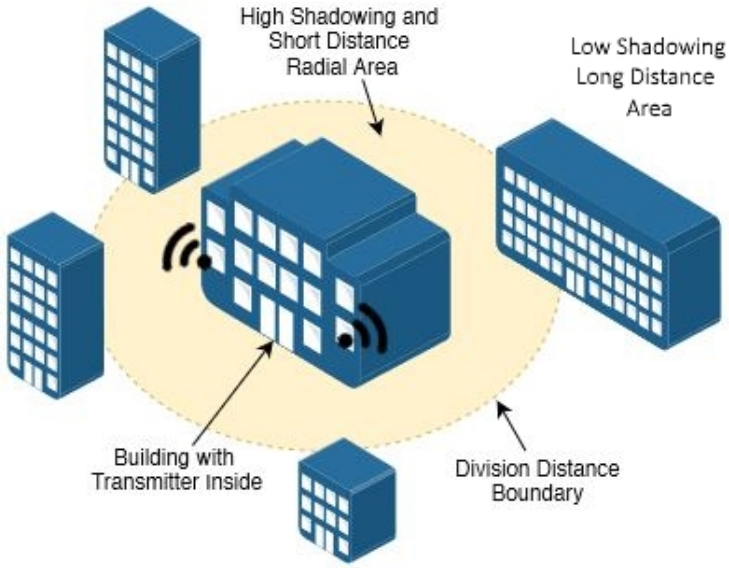

Figure 4.11: Concept of Proposed Method.

In Algorithm 1, start and end values are selected in such a way that the parameters estimations are unbiased. The division distance was found to be 63.89 meters at 470 MHz and 49.1 meters at 580 and 670 MHz frequencies.

Figure 4.12 shows the absolute standard deviation difference with respect to division distances between short and long distance readings at 470, 580 and 670 MHz frequencies.

Algorithm 1 Matlab Algorithm to find division point

1: $X = load('Distance.mat')$
2: $PL = load('Pathloss.mat')$
3: $start = 30$
4: $end = 158$
5: **for** $j = start : 1 : end$
6: $X_{sd} = X(1 : j)$
7: $X_{ld} = X(j + 1 : 188)$ ▷ 188: total no. of readings
8: $PL_{sd} = PL(1 : j)$
9: $PL_{ld} = PL(j + 1 : 188)$
10: $n_1 = CurveFit(X_{sd}, PL_{sd})$
11: $n_2 = CurveFit(X_{ld}, PL_{ld})$
12: $PLE_{sd} = PL_{d_0} + 10 * n_1 * log10(X_{sd}/d_0)$
13: $PLE_{ld} = PL_{d0} + 10 * n_2 * log10(X_{ld}/d_0)$
14: $SE_{sd} = (PL_{sd} - PLE_{sd}).^2$
15: $SE_{ld} = (PL_{ld} - PLE_{ld}).^2$
16: $STD_{sd}(j - low + 1) = sqrt(sum(SE_{sd})/size(X_{sd}))$
17: $STD_{ld}(j - low + 1) = sqrt(sum(SE_{ld})/size(X_{ld}))$
18: $clearall - except, n_{sd}, n_{ld}, STD_{sd}, STD_{ld}, start, end$
$, X, PL$
19: **end**
20: $STD_{diff} = abs(STD_{sd} - STD_{ld})$
21: $[STD_{Maxdiff}, indice] = max(STD_{diff})$
22: **Division** $= X(start + indice)$

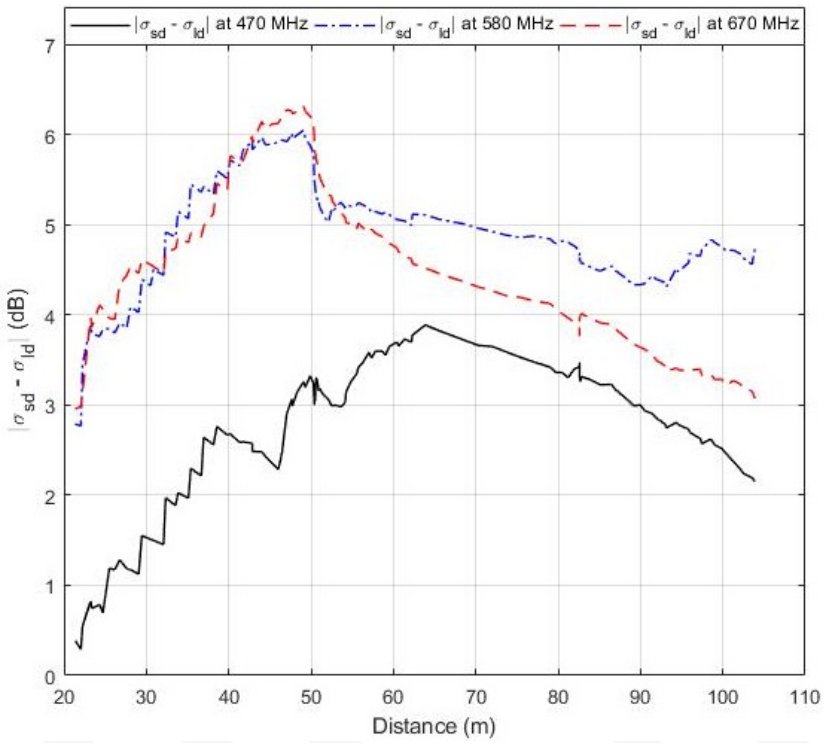

Figure 4.12: Absolute standard deviation difference at 470, 580 and 670 MHz

Following, channel parameters are calculated for short and long distance cases separately. Figures 4.13-4.15 show the measured path loss and estimated path loss for 470, 580 and 670 MHz frequencies respectively.

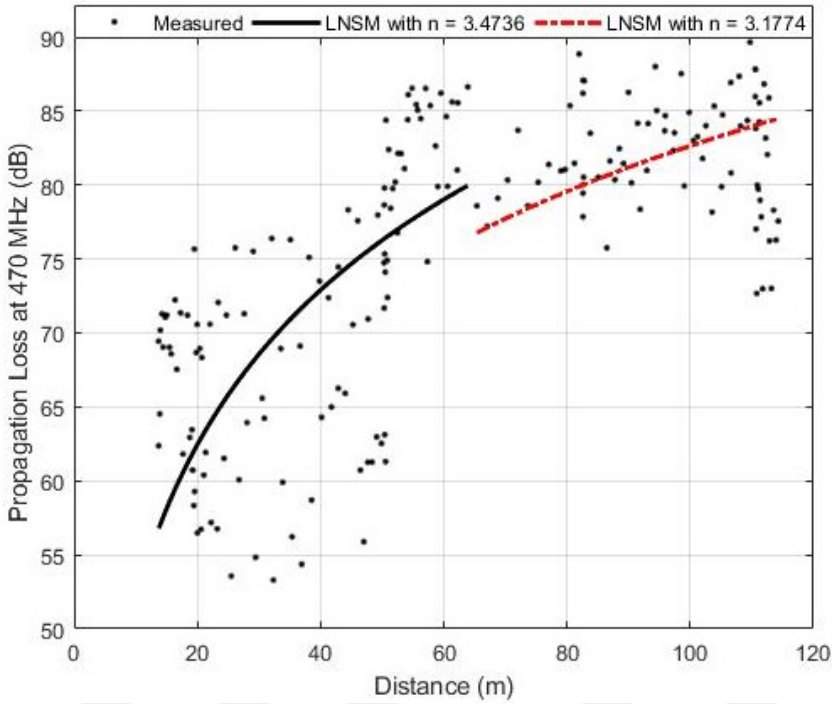

Figure 4.13: Measured path loss compared with estimated path loss for short and long distance at 470 MHz.

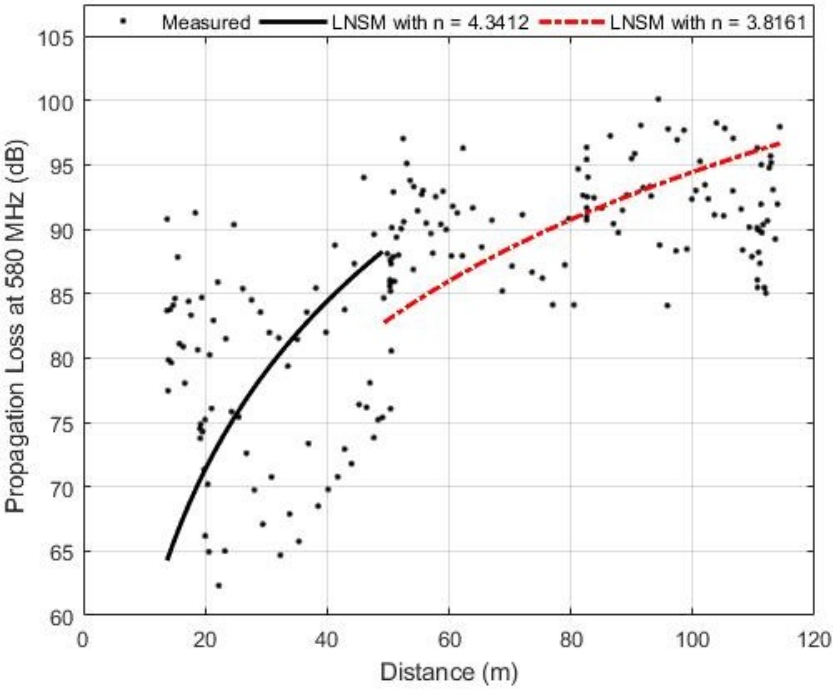

Figure 4.14: Measured path loss compared with estimated path loss for short and long distance at 580 MHz.

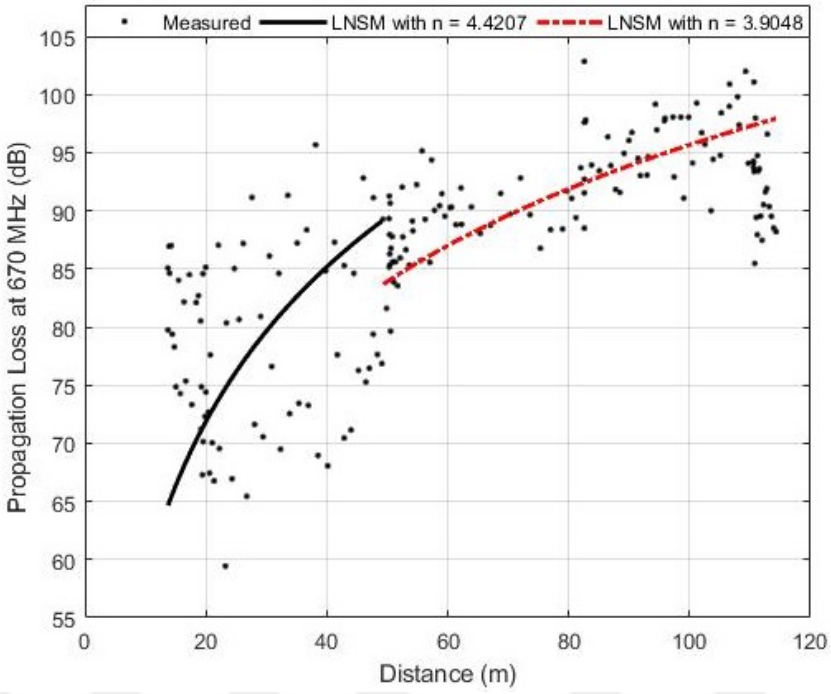

Figure 4.15: Measured path loss compared with estimated path loss for short and long distance at 670 MHz.

In Figures 4.13-4.15, channel parameters at 470 MHz for short and long distance are n = 3.4736, σ = 8.1433 dB and n = 3.1774, σ = 4.2569 dB, respectively. In the same way, at 580 MHz for short distance n = 4.3412 σ = 11.3042 dB and for long distance n = 3.8186 σ = 5.2589 dB and at 670 MHz for short distance n = 4.4207 σ = 10.5940 dB and for long distance n = 3.9048 σ = 4.2834 dB.

Figures 4.16-4.21 show the measured PDF of X_σ and fitted Gaussian PDF for short and long distances at 470, 580 and, 670 MHz frequencies, respectively.

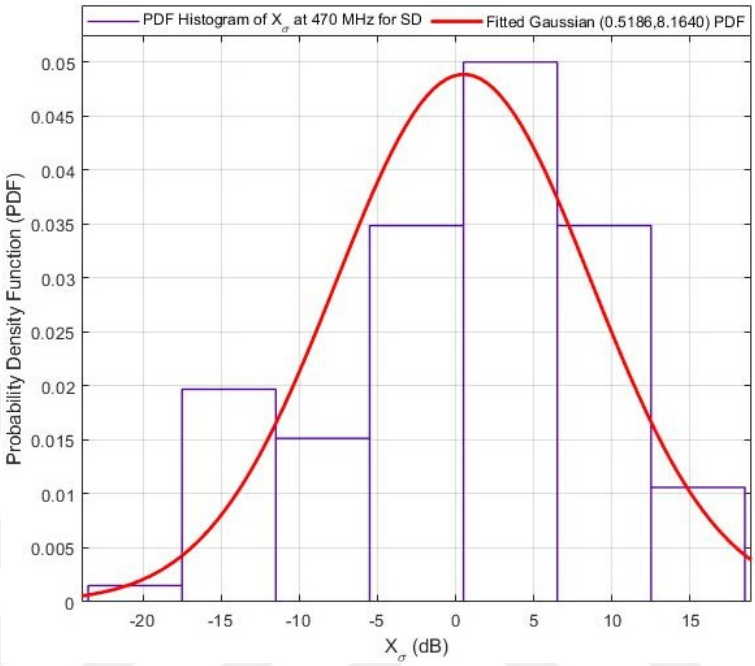

Figure 4.16: PDF of X_σ and Gaussian distribution for short distance at 470 MHz.

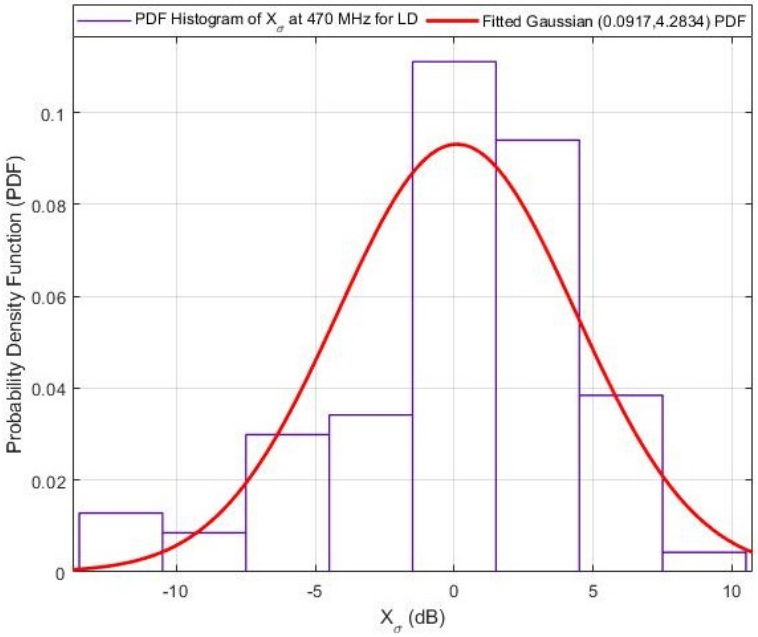

Figure 4.17: PDF of X_σ and Gaussian distribution for long distance at 470 MHz.

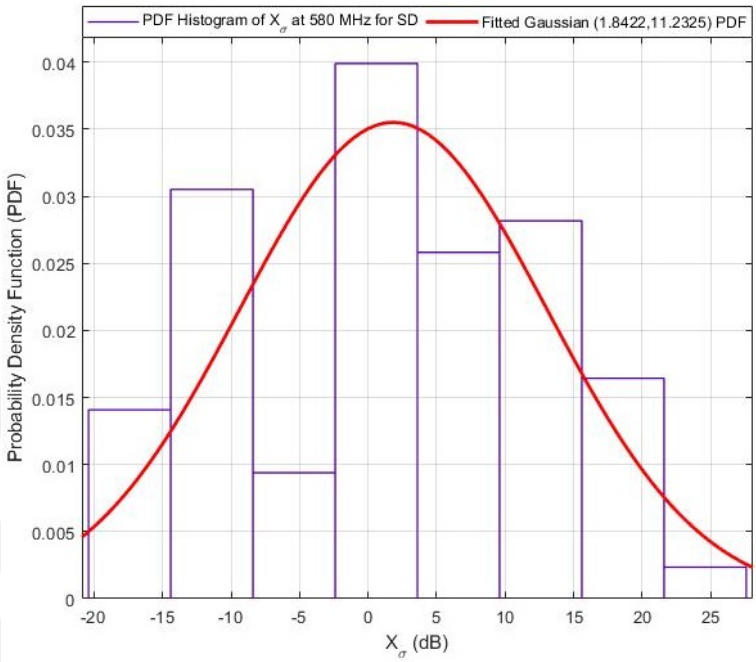

Figure 4.18: PDF of X_σ and Gaussian distribution for short distance at 580 MHz.

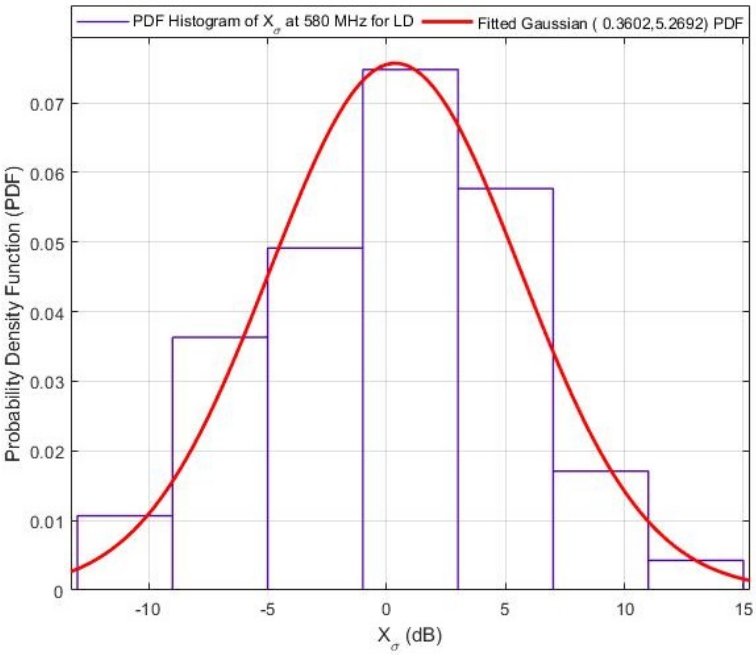

Figure 4.19: PDF of X_σ and Gaussian distribution for long distance at 580 MHz.

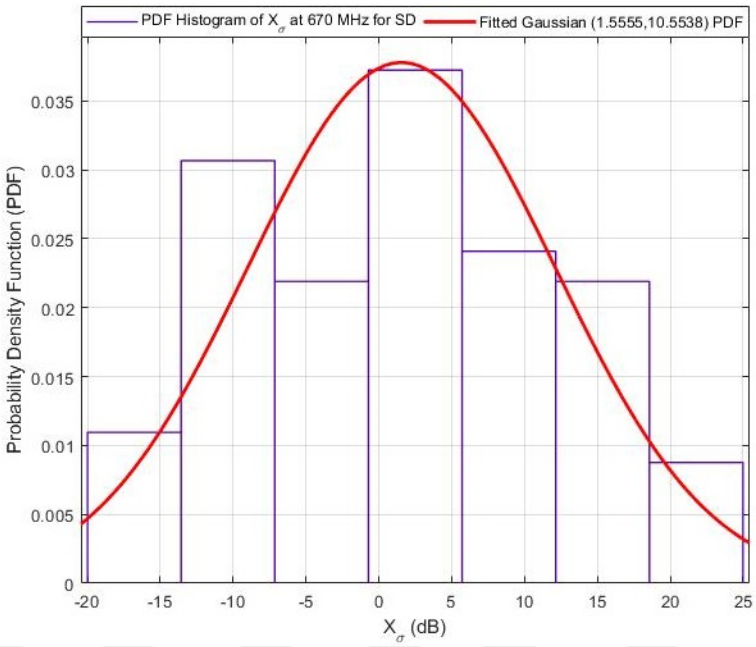

Figure 4.20: PDF of X_σ and Gaussian distribution for short distance at 670 MHz.

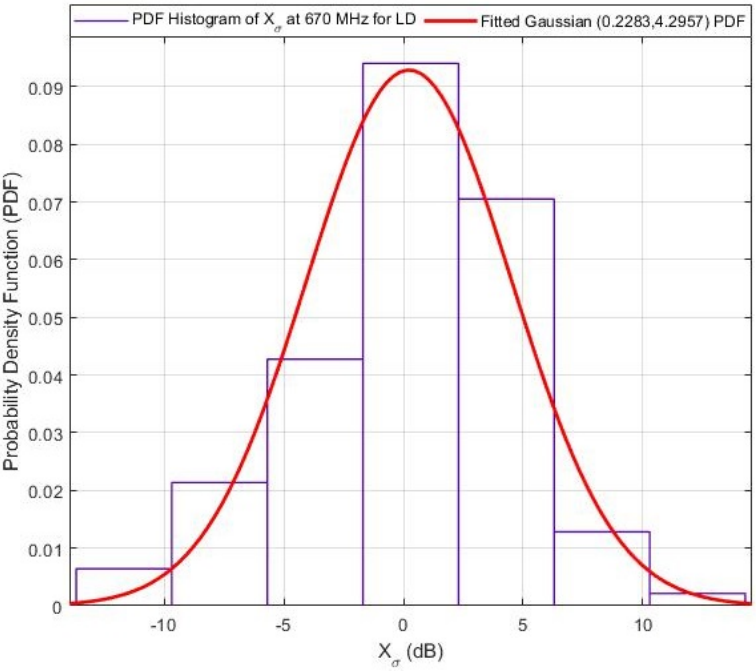

Figure 4.21: PDF of X_σ and Gaussian distribution for long distance at 670 MHz.

In the above results, fitted Gaussian distribution parameters at 470 MHz for short and long distance are $\mu = 0.5186$ dB, $\sigma = 8.1640$ dB and $\mu = 0.0917$ dB, σ

= 4.2834 dB respectively. Similarly, at 580 MHz, for short distance $\mu = 1.8422$ dB, $\sigma = 11.2325$ dB and for long distance $\mu = 0.3602$ dB, $\sigma = 5.2692$ dB and at 670 MHz, for short distance $\mu = 1.5555$ dB $\sigma = 10.5538$ dB and for long distance $\mu = 0.2283$ dB $\sigma = 4.2957$ dB.

It can be seen from the results of this section that after applying proposed method, there is a significant difference in shadowing parameters as compared to those which were calculated in previous section by using log normal channel model. Short distance measurements have more shadowing than long one's and Gaussian distribution holds after the division of data set for mentioned environment .

4.4 Performance Comparisons and Results

In this sections, results are presented to show the accuracy of log normal shadowing and proposed model for indoor to outdoor environment. Here, we compare the results achieved from log normal and proposed models based on statistical parameters. Table 4.1 shows the comparison of results while Figures 4.22-4.24 show the bar chart comparison of shadowing standard deviation values at all transmission frequencies.

Table 4.1: Comparison of Results

Model	Frequency (MHz)	n	$\sigma(dB)$	Fitted Gaussian	
				$\mu(dB)$	$\sigma(dB)$
Log-normal	**470**	3.2951	6.9988	0.6242	6.9895
	580	3.9185	8.4240	1.3698	8.3341
	670	4.0055	7.6879	1.1715	7.6185
Log-normal (short distance)	**470**	3.2951	8.3101	2.1332	8.0684
	580	3.9185	11.8107	5.1852	10.6871
	670	4.0055	11.1144	4.8392	10.0768
Proposed (short distance)	**470**	3.4736	8.1433	0.5186	8.1640
	580	4.3412	11.3042	1.8422	11.2325
	670	4.4207	10.5940	1.5555	10.5538
Log-normal (long distance)	**470**	3.2951	4.5468	-1.5038	4.3186
	580	3.9185	5.4202	-0.9454	5.3601
	670	4.0055	4.4732	-1.0541	4.3659
Proposed (long distance)	**470**	3.1774	4.2569	0.0917	4.2834
	580	3.8161	5.2589	0.3602	5.2692
	670	4.4207	4.2834	0.2283	4.2957

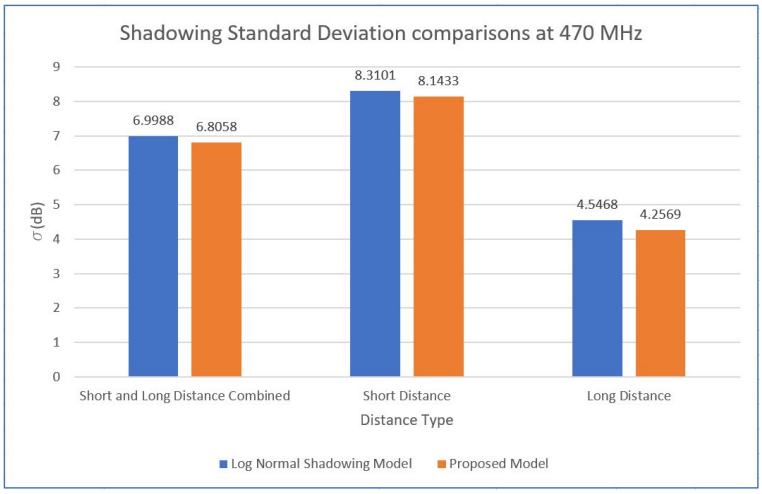

Figure 4.22: Shadowing comparison chart at 470 MHz

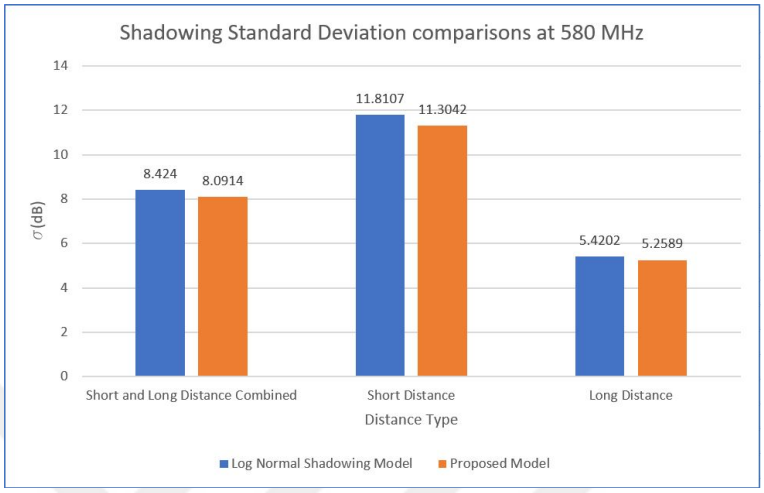

Figure 4.23: Shadowing comparison chart at 580 MHz

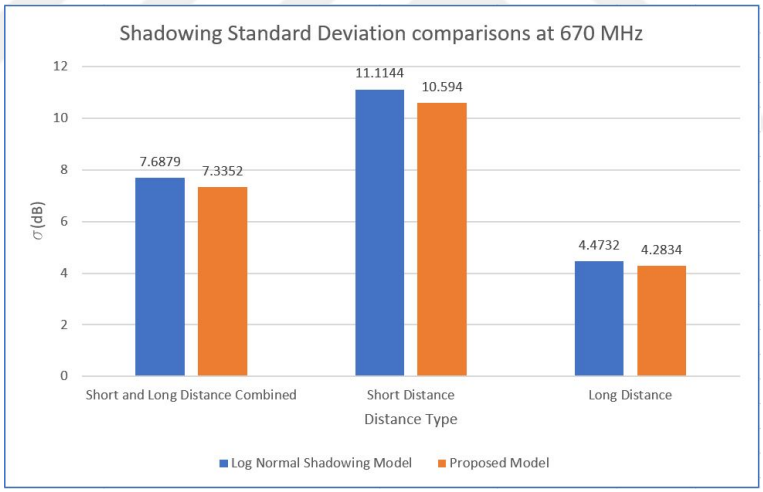

Figure 4.24: Shadowing comparison chart at 670 MHz

The comparison between short distance models show that, there is a considerable difference in path loss and shadowing. Proposed model indicates that the path loss coefficient should be higher than the coefficient of the log normal model for all frequencies. By increasing the path loss, proposed model decreases the shadowing standard deviation. On the other hand, for long distance measurements, calculated path loss is lower in proposed model and it reduces the shadowing standard deviation.

Chapter 5

Air to Ground Wireless Channel Modeling

In this section, wireless channel modeling for air to ground channels in TVWS band is discussed. Generally, channel parameter estimations are performed using results from extensive measurements in the environment [28] [29]. Alternative method employs outcomes from ray tracing simulations which provides acceptable performance compared to the real measurements [30]. Ray tracing simulations require 3D models of the environment which is tedious to design. Alternative and a novel approach is to extract these 3D models of a real outdoor environment from CAD tools.

In this particular work, channel parameters are estimated in a systematic manner first by using ray tracing simulations in Wireless InSite to measure path loss at multiple locations on a 3D model which is identical to the aerial/satellite image and then estimating channel parameters (n and σ) with Log Normal Shadowing Model (LNSM) from path loss measurements using Matlab.

5.1 Channel parameter estimation

There are multiple studies in literature regarding air to ground channel parameter estimation using ray tracing simulations [31] [32]. Here, Log Normal Shadowing Model was selected to perform channel parameter estimation which is defined by the following equation:

$$PL_{dB} = PL(d_0) + 10n \log_{10}\left(\frac{d}{d_0}\right) + X_\sigma \tag{5.1}$$

Where, $PL(d_0)$ is the path loss in dB at a reference distance d_0, d is the direct distance between transmitter and receiver, n is the path loss exponent and X_σ is a random variable with zero mean and standard deviation of σ which is generally refers to the shadowing in the environment.

Path loss measurements were taken using ray tracing simulations in Wireless InSite software. In this work, we selected New York city covering multiple scenarios and environments. This was used due to unavailability of the data for Istanbul. Table 5.1 shows the measurement setup parameters.

Table 5.1: Measurement setup parameters (Wireless InSite)

Transmission frequencies	470, 580 and 670 MHz
Transmit Power	+60 dBm
Antenna polarization	Vertical
Antenna radiation pattern	Omni-directional
Transmitter antenna height	300 m
Receiver antenna height	1.5 m
Transmitted signal	Sinusoid
Bandwidth	8 MHz
d_0	57.28 m
$PL(d_0)$	63.44 dB

Figure 5.1 shows the block diagram of the work flow to generate channel parameters and aerial/satellite images.

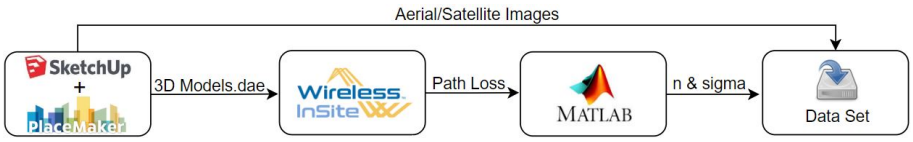

Figure 5.1: Channel parameters generation work flow

From Figure 5.1 and starting from the first block (left), the Google SketchUp software with Placemaker plugin is used to acquire aerial images and 3D models (1.8x1.8 km area each) of New York city from two multiple sources.

After that, 3D model is imported and merged with a flat terrain in Wireless InSite. Ray tracing simulation environment is created by placing squared XY grid of 12,100 receivers and a transmitter at the center in the 3D model. Transmit power of +60 dBm and omni-directional antennas are selected in order to achieve a good coverage area. The material of terrain is dry earth while the buildings are concrete. Transmitter antenna is positioned at 300 meter height from the terrain in order to replicate the scenario of air to ground channel. Receiver antenna height of 1.5 meter is selected to model the average holding height of a cellular phone. Further, ray tracing simulations are performed to generate path loss values at each receiver. Examples of ray tracing simulation environment is presented in Figure 5.2 while corresponding aerial image is given in Figure 5.3. In Figure 5.2 green area shows the terrain profile, red points on terrain show the receiver positions and orange point (radiation pattern) in the center employs transmitter position.

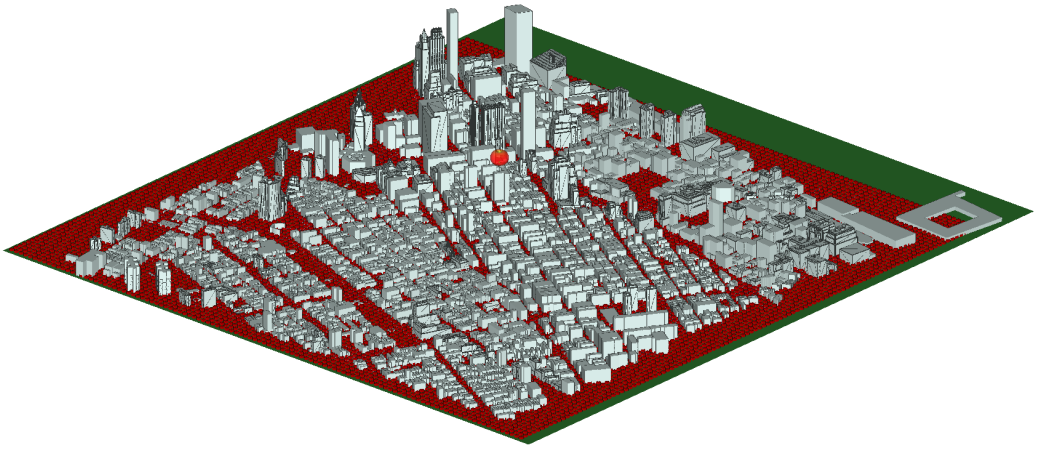

Figure 5.2: Ray tracing simulation in Wireless InSite

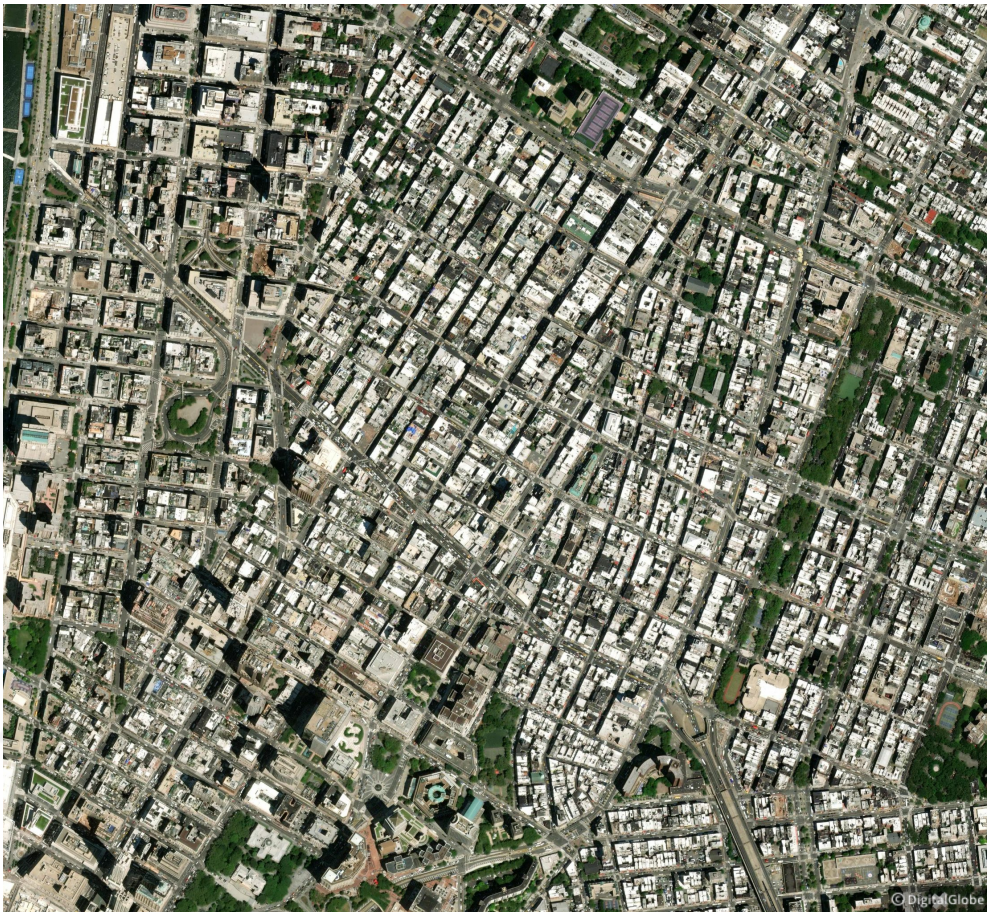

Figure 5.3: Corresponding aerial image

Moreover, generated path losses are used to calculate air to ground wireless channel parameters (n and σ) using custom Matlab function and script. Finally, the calculated channel parameters and respective aerial image are saved in the disk.

5.2 Simulation Results

In order to analyze air to ground wireless channel characteristics, path loss measurements were taken in high rise buildings and sub urban scenarios using ray tracing simulations at TVWS frequencies. In this section, path loss coefficient (n) and shadowing parameter (σ) calculated for multiple scenarios are presented.

5.2.1 High Rise Building Scenario

The maximum height of the building in this scenario is 417 meters (world trade center) which is also included in the measurement results. Similarly, there are multiple high rise buildings which can cause interference in transmission and transmitted signals more likely to undergo multi-path reflections. For the measurements, total 3 locations of area 1.8x1.8 km were chosen. Results at 580, 470, and 670 MHz frequencies are presented as follows:

5.2.1.1 Results at 580 MHz

For the first location, Figures 5.4(a) and 5.4(b) show the color map of received power and corresponding aerial image while Figures 5.5(a) and 5.5(b) show measured/estimated log normal shadowing model path loss and measured/fitted Gaussian PDF of X_σ, respectively. The calculated channel parameters are found to be $n = 3.9742$, $\sigma = 45.0224$ dB and, Gaussian PDF with $\mu = 1.27055$ dB and $\sigma = 45.0063$ dB. We fitted Gaussian PDF on my measured results and found μ and σ by using Log likelihood method in Matlab's distribution fitter tool.

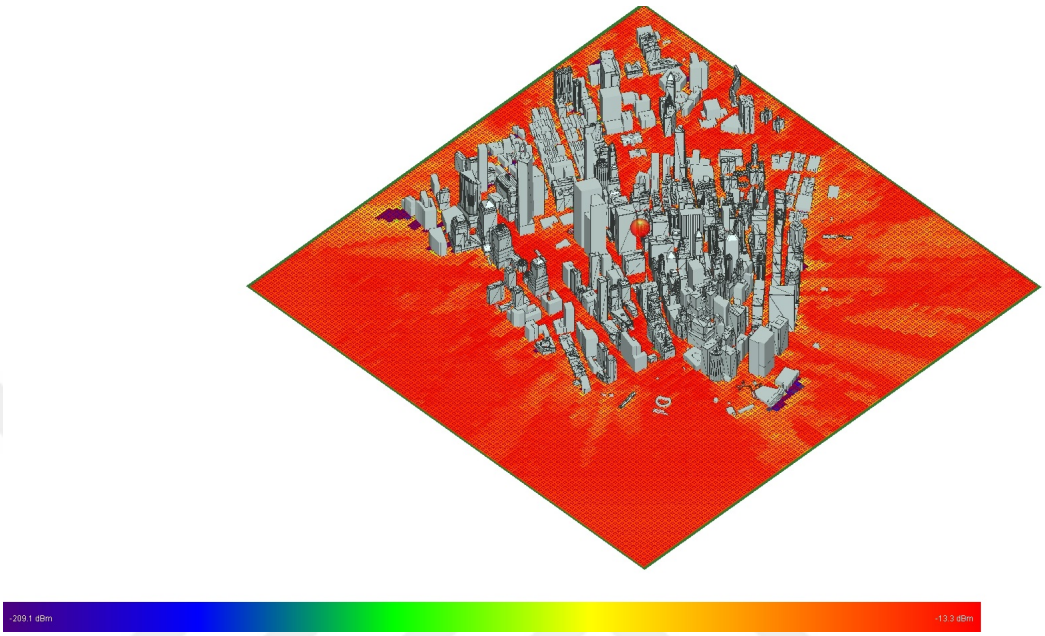

(a)

(b)

Figure 5.4: Received power color map at 580 MHz and corresponding aerial image(1^{st} Location)

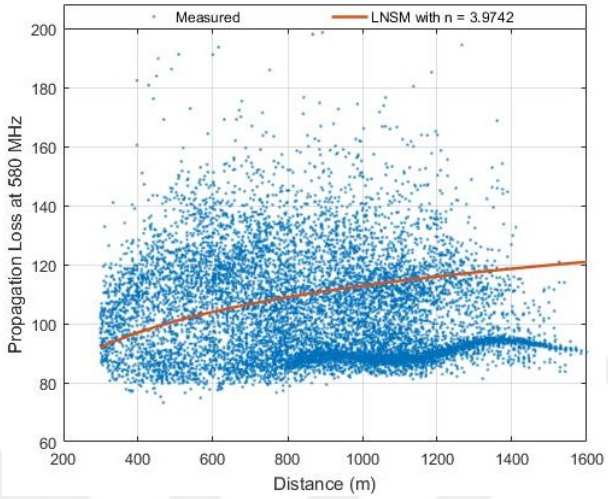

(a)

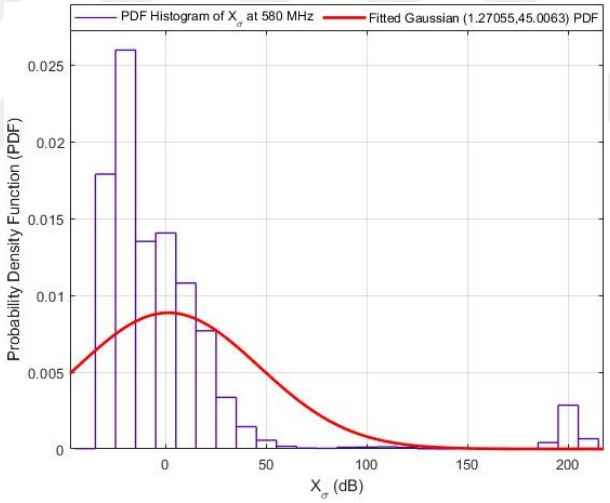

(b)

Figure 5.5: Measured/estimated path loss and measured/ fitted Gaussian PDF of X_σ at 580 MHz (1^{st} Location)

Similarly, for the second location, Figures 5.6(a) and 5.6(b) show the color map of received power and corresponding aerial image while Figures 5.7(a) and 5.7(b) show measured/estimated log normal shadowing model path loss and measured/fitted Gaussian PDF of X_σ, respectively. The calculated channel parameters are found to be $n = 3.4956$, $\sigma = 24.8912$ dB and, Gaussian PDF with $\mu =$ -0.23866 dB and $\sigma = 24.8911$ dB.

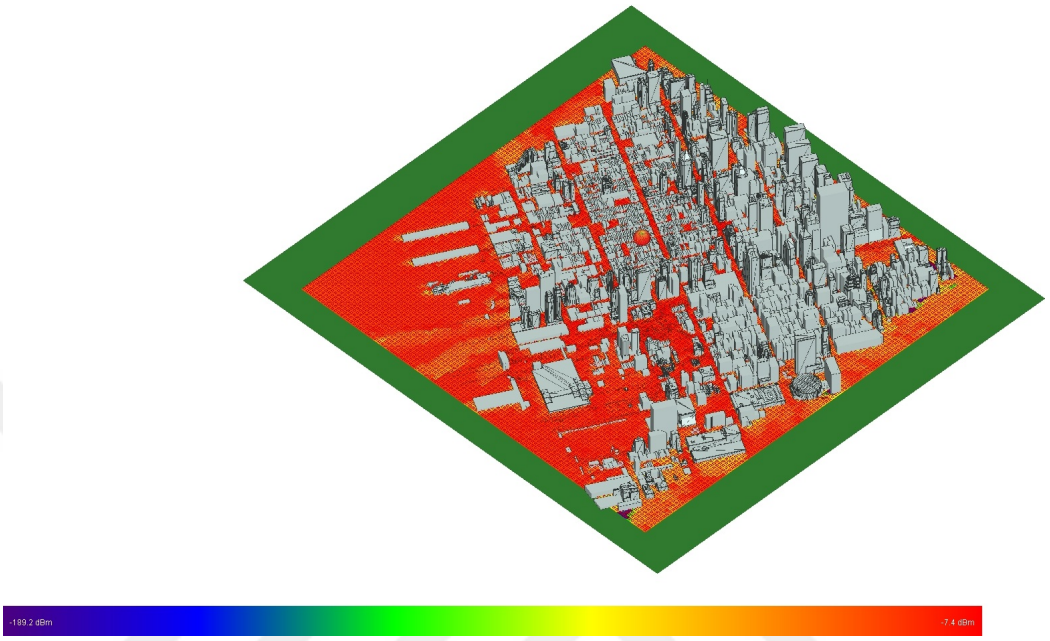

(a)

(b)

Figure 5.6: Received power color map at 580 MHz and corresponding aerial image (2^{nd} Location)

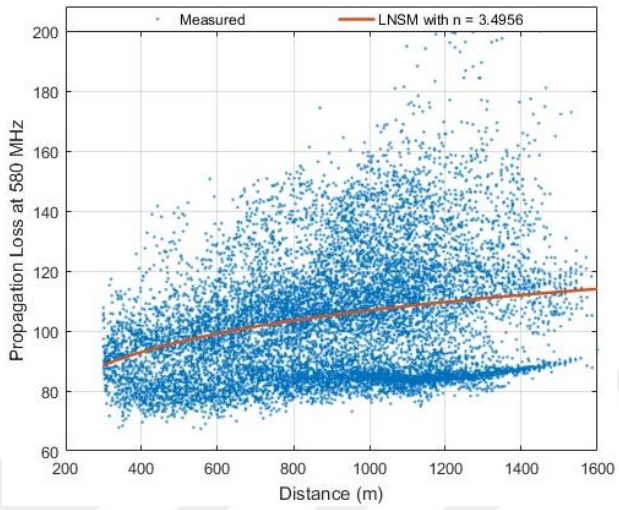

(a)

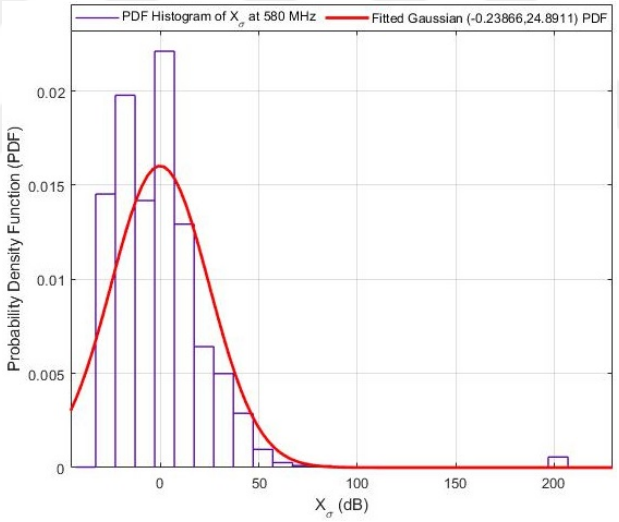

(b)

Figure 5.7: Measured/estimated path loss and measured/ fitted Gaussian PDF of X_σ at 580 MHz (2^{nd} Location)

For the third location, Figures 5.8(a) and 5.8(b) show the color map of received power and corresponding aerial image while Figures 5.9(a) and 5.9(b) show measured/estimated log normal shadowing model path loss and measured/fitted Gaussian PDF of X_σ, respectively. The calculated channel parameters are found to be $n = 3.2945$, $\sigma = 24.0181$ dB and, Gaussian PDF with $\mu = 0.29775$ dB and $\sigma = 24.0173$ dB.

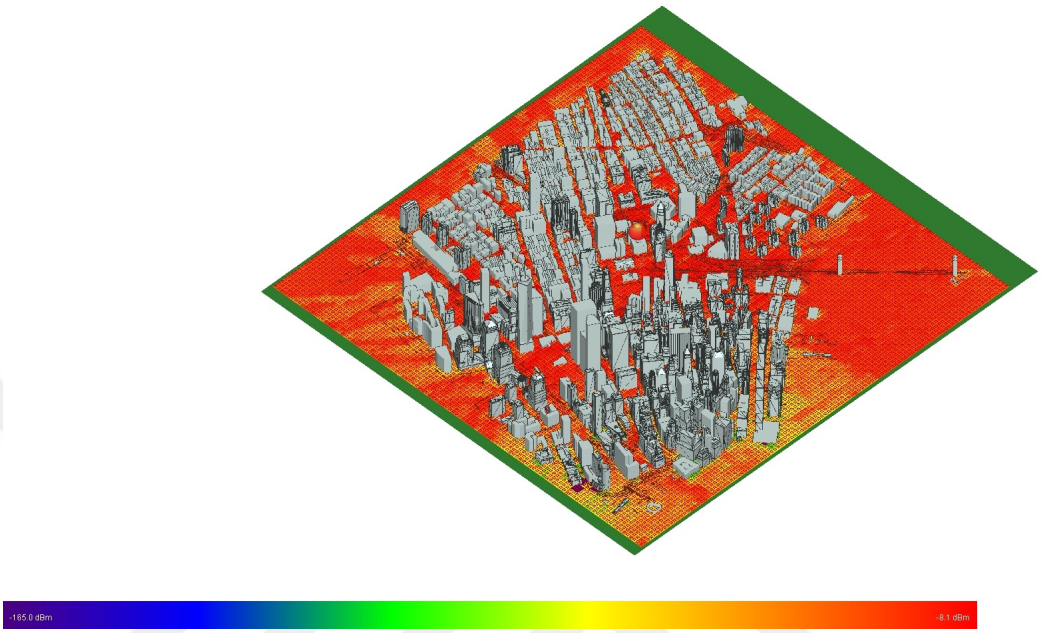

(a)

(b)

Figure 5.8: Received power color map at 580 MHz and corresponding aerial image (3^{rd} Location)

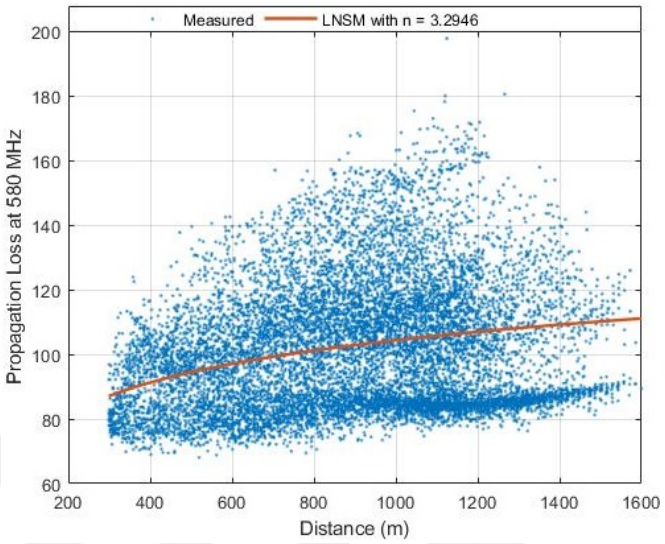

(a)

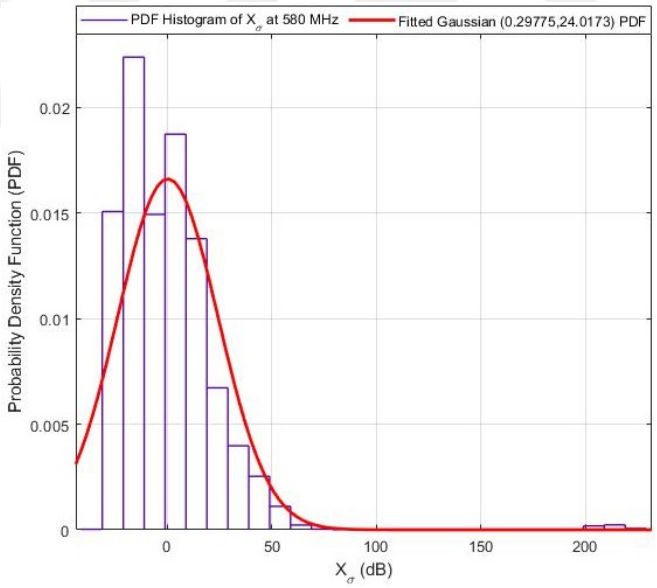

(b)

Figure 5.9: Measured/estimated path loss and measured/ fitted Gaussian PDF of X_σ at 580 MHz (3^{rd} Location)

5.2.1.2 Results at 470 MHz

For the first location, Figures 5.10(a) and 5.10(b) show measured/estimated log normal shadowing model path loss and measured/fitted Gaussian PDF of X_σ,

respectively. The calculated channel parameters are found to be $n = 3.2333$, $\sigma = 45.4536$ dB and, Gaussian PDF with $\mu = 0.8600$ dB and $\sigma = 45.4474$ dB.

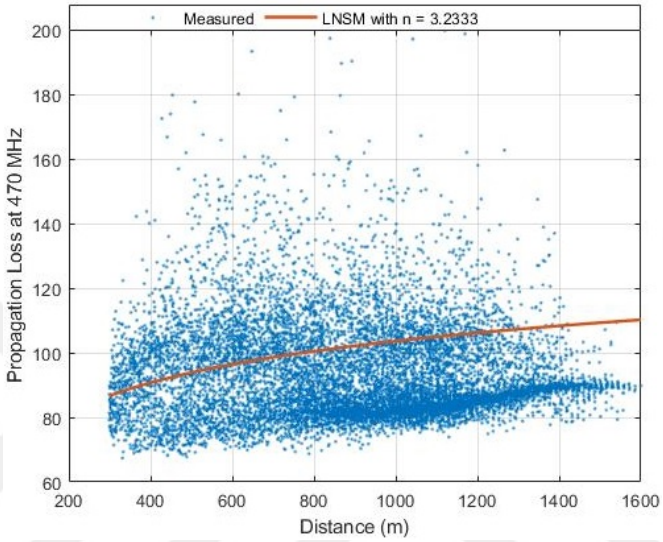

(a)

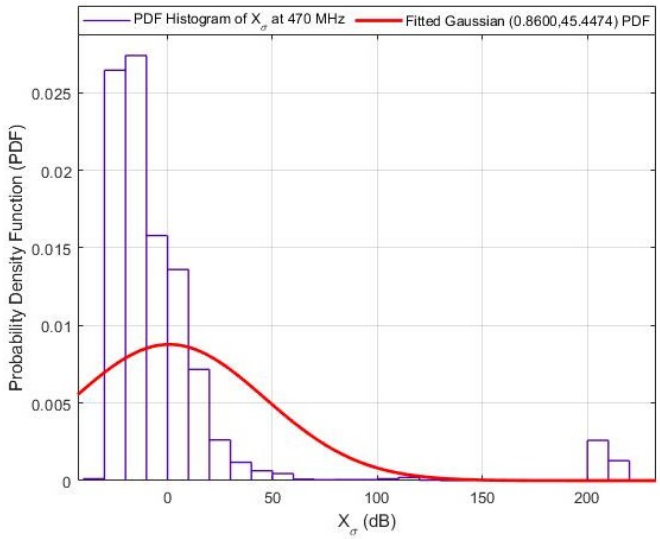

(b)

Figure 5.10: Measured/estimated path loss and measured/ fitted Gaussian PDF of X_σ at 470 MHz (1^{st} Location)

Similarly, for the second location, Figures 5.11(a) and 5.11(b) show measured/estimated log normal shadowing model path loss and measured/fitted Gaussian PDF of X_σ, respectively. The calculated channel parameters are found

to be $n = 3.3045$, $\sigma = 24.4956$ dB and, Gaussian PDF with μ = -0.28227 dB and $\sigma = 24.4951$ dB.

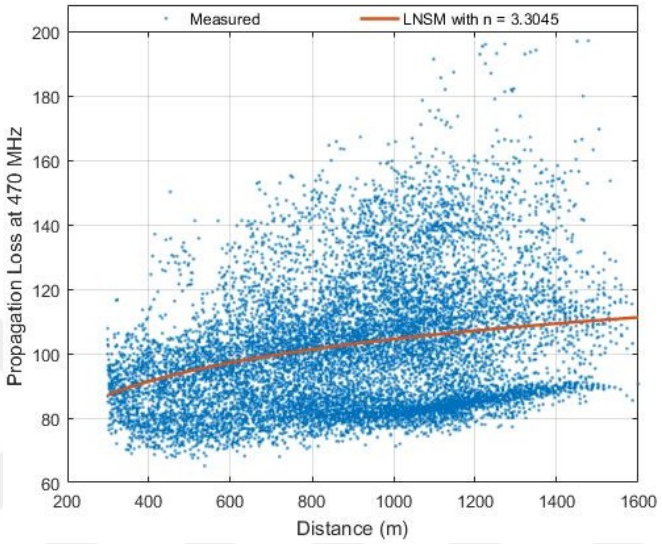

(a)

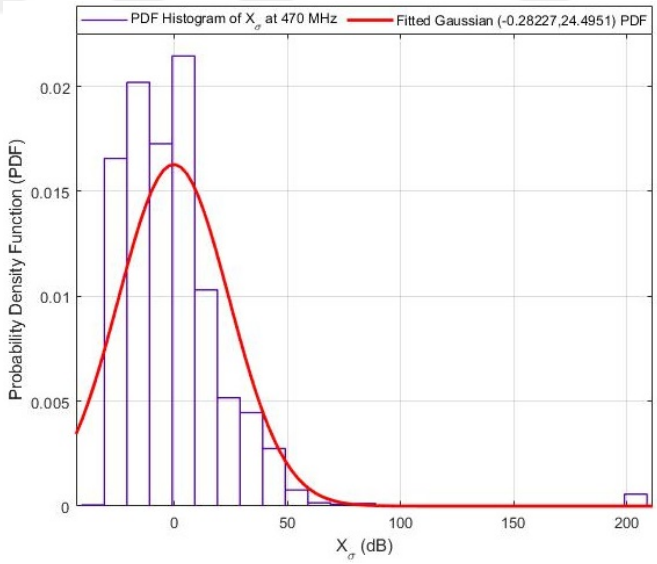

(b)

Figure 5.11: Measured/estimated path loss and measured/ fitted Gaussian PDF of X_σ at 470 MHz (2^{nd} Location)

For the third location, Figures 5.12(a) and 5.12(b) show measured/estimated log normal shadowing model path loss and measured/fitted Gaussian PDF of X_σ, respectively. The calculated channel parameters are found to be $n = 3.0822$, σ

= 22.1880 dB and, Gaussian PDF with $\mu = 0.16679$ dB and $\sigma = 22.1884$ dB.

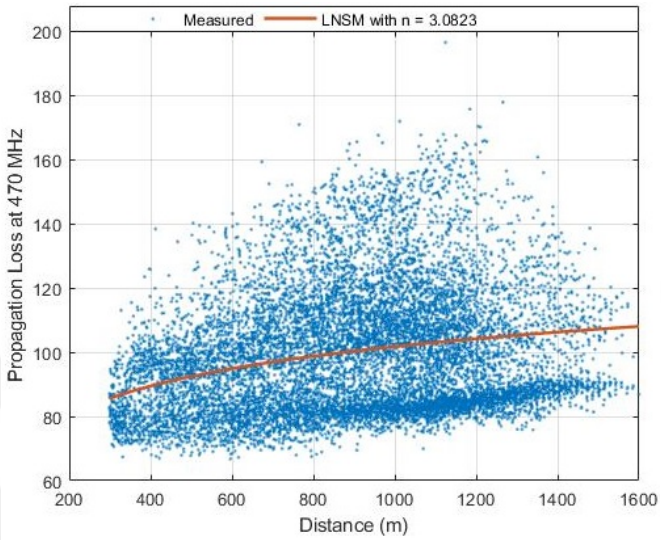

(a)

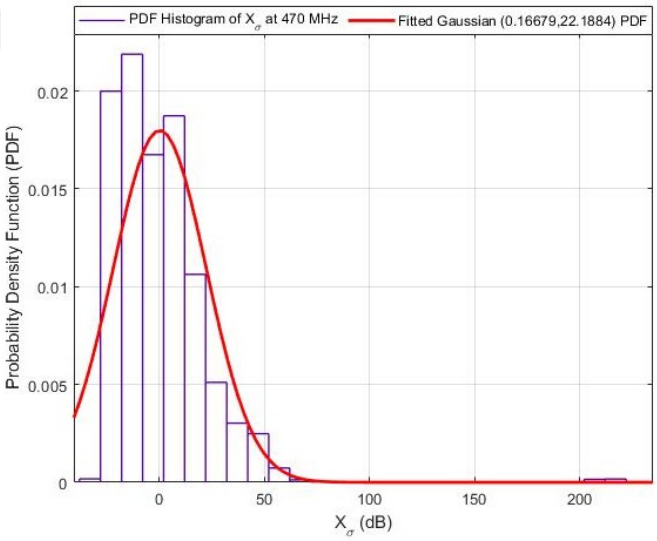

(b)

Figure 5.12: Measured/estimated path loss and measured/ fitted Gaussian PDF of X_σ at 470 MHz (3^{rd} Location)

5.2.1.3 Results at 670 MHz

For the first location, Figures 5.13(a) and 5.13(b) show measured/estimated log normal shadowing model path loss and measured/fitted Gaussian PDF of X_σ, respectively. The calculated channel parameters are found to be $n = 3.7656$, $\sigma = 45.5193$ dB and, Gaussian PDF with $\mu = 1.30627$ dB and $\sigma = 45.5025$ dB.

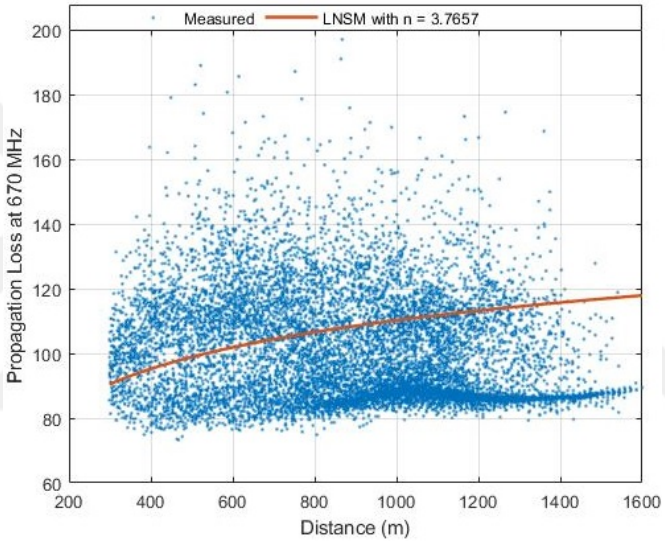

(a)

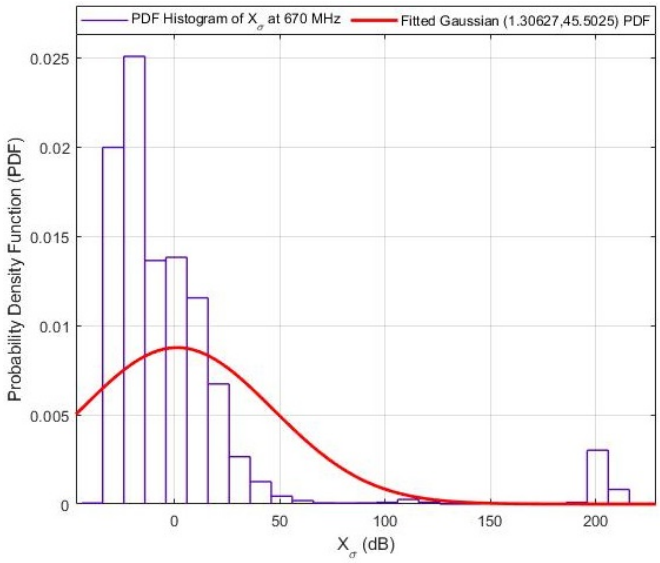

(b)

Figure 5.13: Measured/estimated path loss and measured/ fitted Gaussian PDF of X_σ at 670 MHz (1^{st} Location)

Similarly, for the second location, Figures 5.14(a) and 5.14(b) show measured/estimated log normal shadowing model path loss and measured/fitted Gaussian PDF of X_σ, respectively. The calculated channel parameters are found to be $n = 3.8873$, $\sigma = 25.2994$ dB and, Gaussian PDF with μ = -0.09183 dB and $\sigma = 25.3004$ dB.

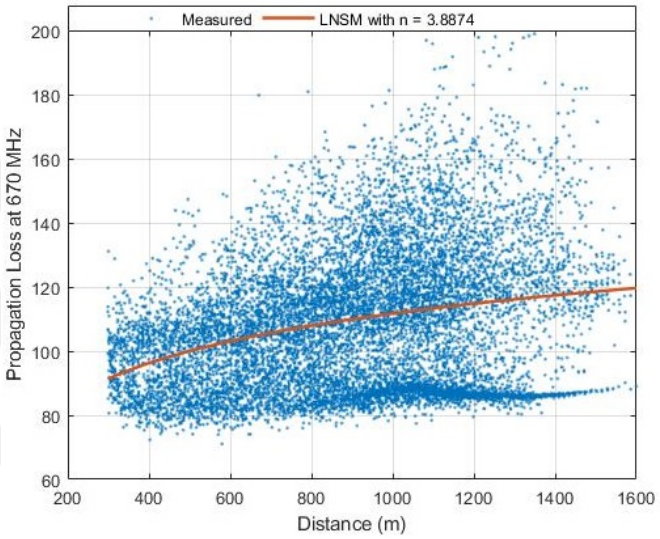

(a)

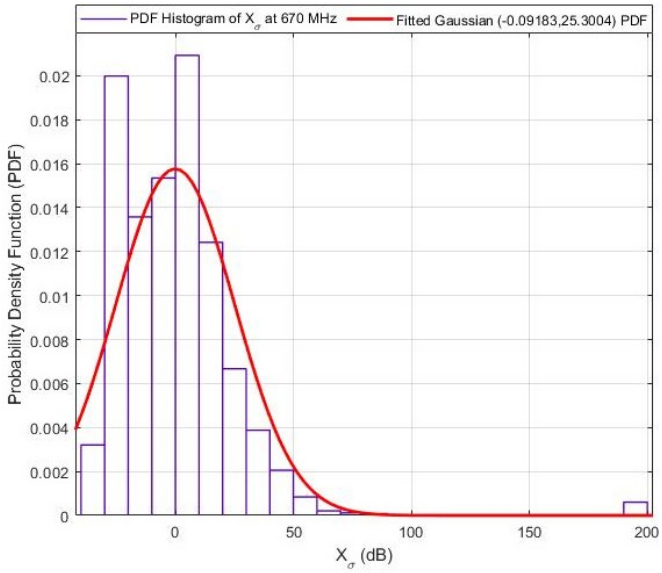

(b)

Figure 5.14: Measured/estimated path loss and measured/ fitted Gaussian PDF of X_σ at 670 MHz (2^{nd} Location)

For the third location, Figures 5.15(a) and 5.15(b) show measured/estimated log normal shadowing model path loss and measured/fitted Gaussian PDF of X_σ, respectively. The calculated channel parameters are found to be $n = 3.6725$, $\sigma = 23.5762$ dB and, Gaussian PDF with $\mu = 0.4495$ dB and $\sigma = 23.5730$ dB.

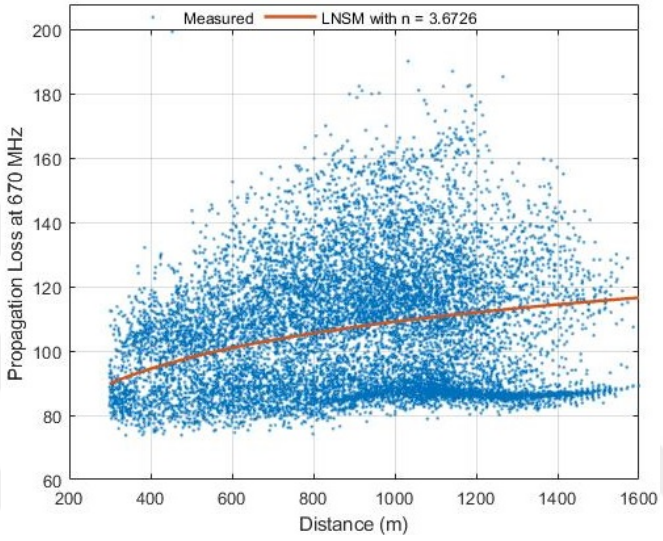

(a)

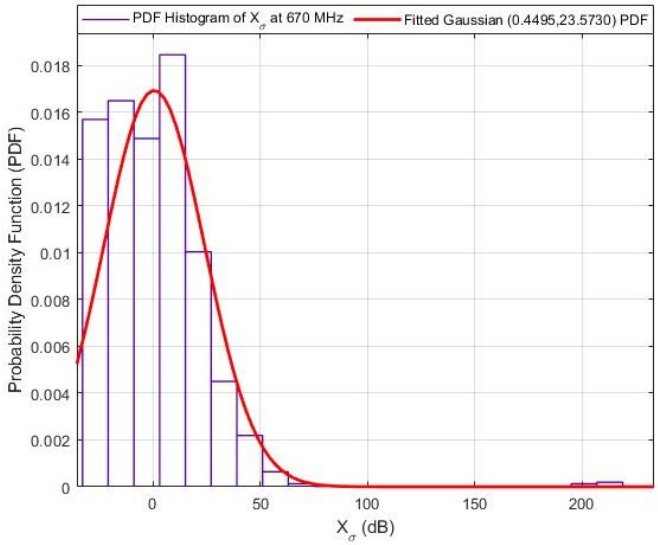

(b)

Figure 5.15: Measured/estimated path loss and measured/ fitted Gaussian PDF of X_σ at 670 MHz (3^{rd} Location)

5.2.2 Sub-urban scenario

In this section, path loss measurements using ray tracing simulations were taken on the Manhattan side of the New York city and similar to the previous section, three different sub-urban locations were selected and processed in Wireless InSite. Results at 580, 470 and 670 MHz frequencies are presented as follows:

5.2.2.1 Results at 580 MHz

For the first location, Figures 5.16(a) and 5.16(b) show the color map of received power and corresponding aerial image while Figures 5.17(a) and 5.17(b) show measured/estimated log normal shadowing model path loss and measured/fitted Gaussian PDF of X_σ, respectively. The calculated channel parameters are found to be $n = 2.5540$, $\sigma = 16.2012$ dB and, Gaussian PDF with $\mu = 0.5677$ dB and $\sigma = 16.1920$ dB.

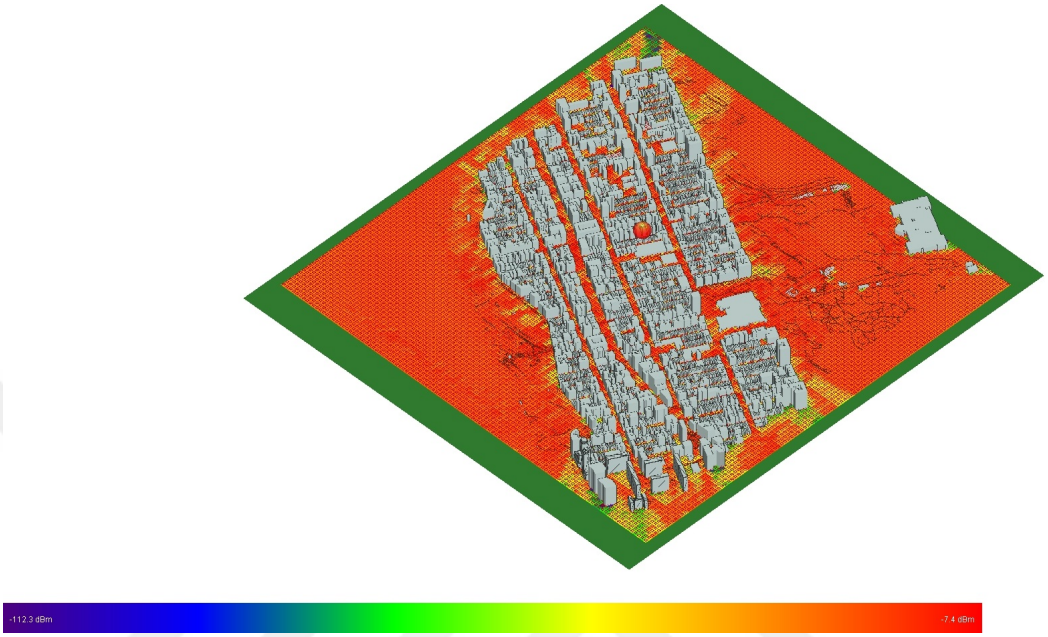

(a)

(b)

Figure 5.16: Received power color map at 580 MHz and corresponding aerial image(1^{st} Location)

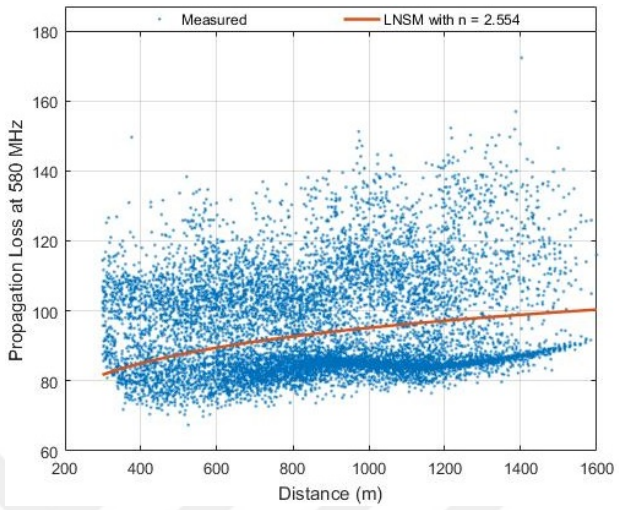

(a)

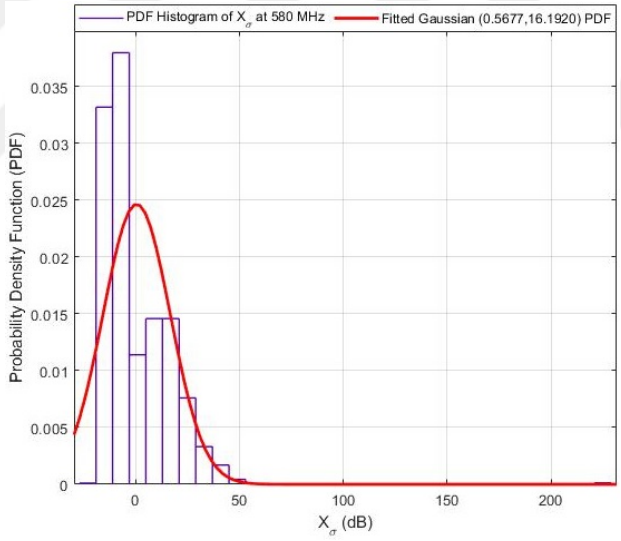

(b)

Figure 5.17: Measured/estimated path loss and measured/ fitted Gaussian PDF of X_σ at 580 MHz (1^{st} Location)

Similarly, for the second location, Figures 5.18(a) and 5.18(b) show the color map of received power and corresponding aerial image while Figures 5.19(a) and 5.19(b) show measured/estimated log normal shadowing model path loss and measured/fitted Gaussian PDF of X_σ, respectively. The calculated channel parameters are found to be $n = 2.7361$, $\sigma = 15.3332$ dB and, Gaussian PDF with $\mu = 0.1181$ dB and $\sigma = 15.3334$ dB.

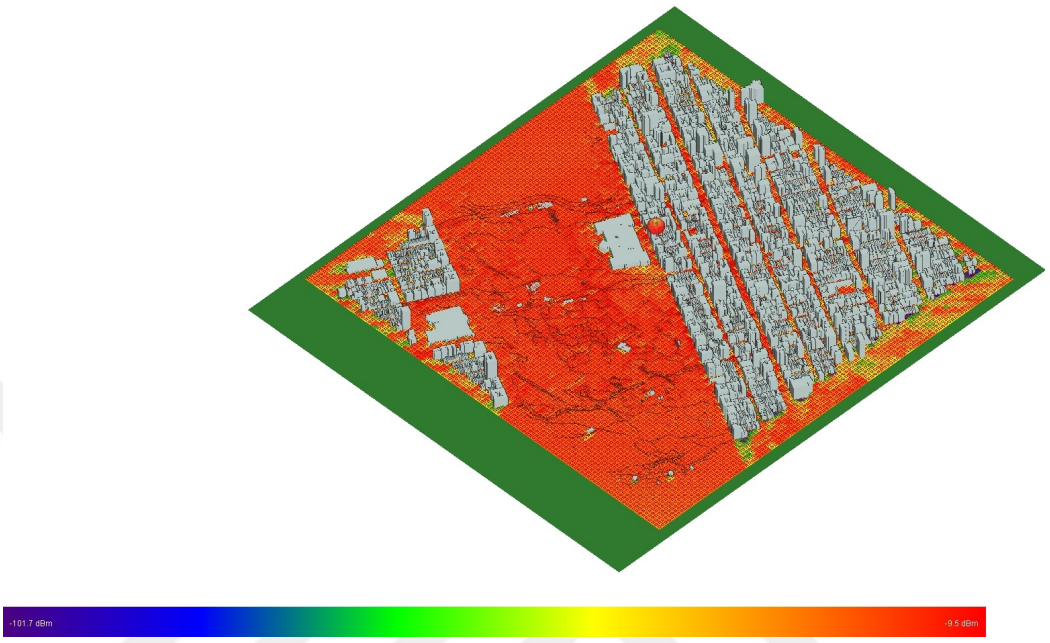

(a)

(b)

Figure 5.18: Received power color map at 580 MHz and corresponding aerial image (2^{nd} Location)

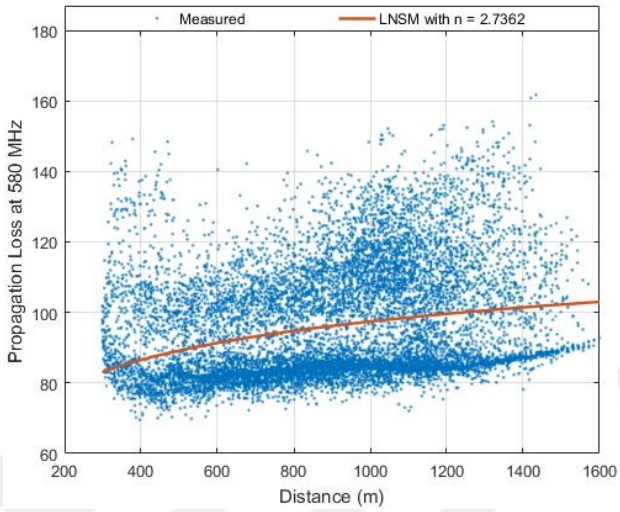

(a)

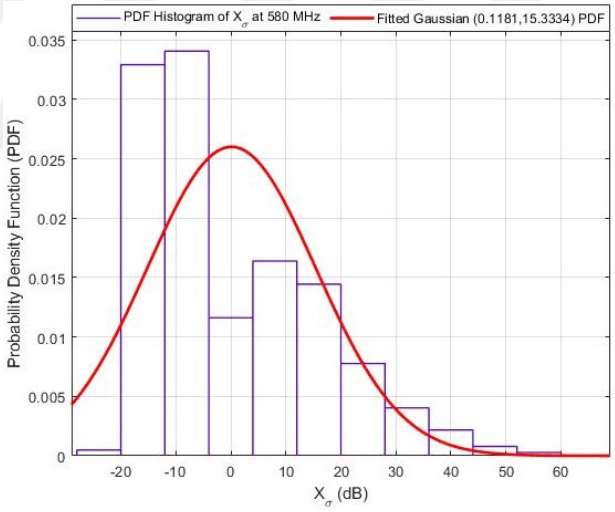

(b)

Figure 5.19: Measured/estimated path loss and measured/ fitted Gaussian PDF of X_σ at 580 MHz (2^{nd} Location)

For the third location, Figures 5.20(a) and 5.20(b) show the color map of received power and corresponding aerial image while Figures 5.21(a) and 5.21(b) show measured/estimated log normal shadowing model path loss and measured/fitted Gaussian PDF of X_σ, respectively. The calculated channel parameters are found to be $n = 2.5437$, $\sigma = 19.3865$ dB and, Gaussian PDF with $\mu = 0.4801$ dB and $\sigma = 19.3814$ dB.

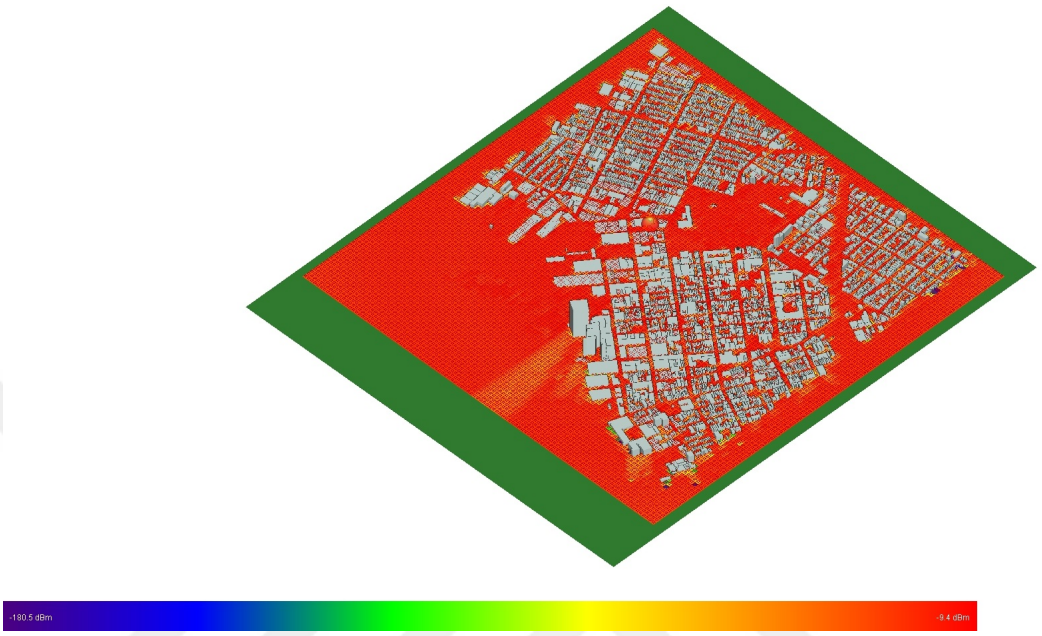

(a)

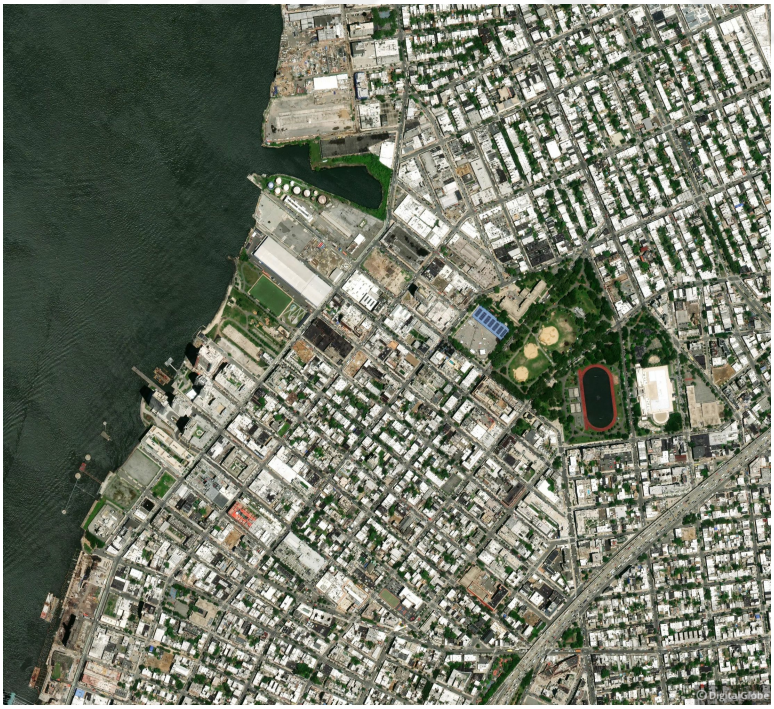

(b)

Figure 5.20: Received power color map at 580 MHz and corresponding aerial image (3^{rd} Location)

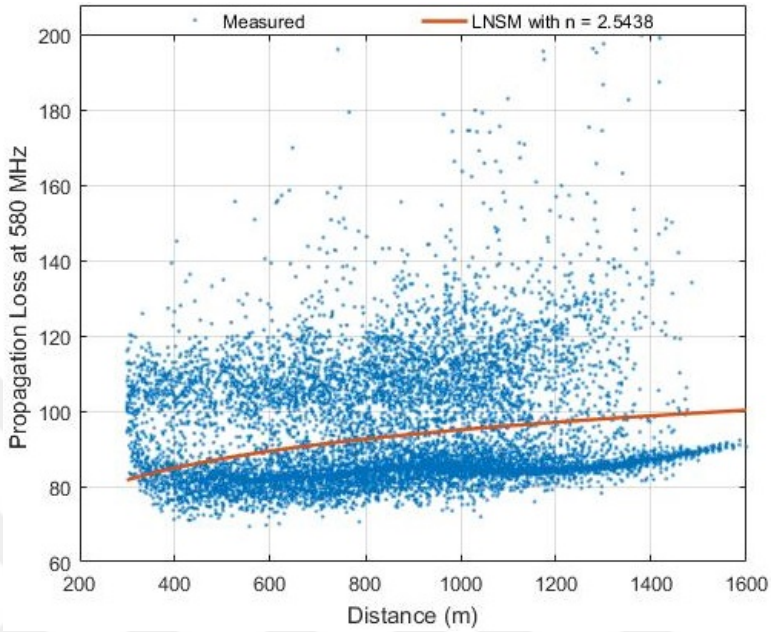

(a)

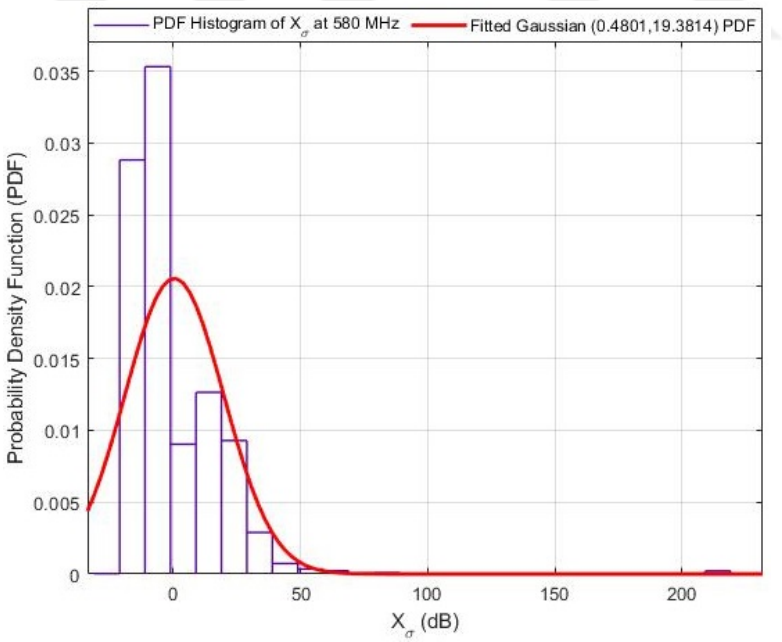

(b)

Figure 5.21: Measured/estimated path loss and measured/ fitted Gaussian PDF of X_σ at 580 MHz (3^{rd} Location)

5.2.2.2 Results at 470 MHz

For the first location, Figures 5.22(a) and 5.22(b) show measured/estimated log normal shadowing model path loss and measured/fitted Gaussian PDF of X_σ, respectively. The calculated channel parameters are found to be $n = 2.4135$, $\sigma = 15.9891$ dB and, Gaussian PDF with $\mu = 0.4538$ dB and $\sigma = 15.9833$ dB.

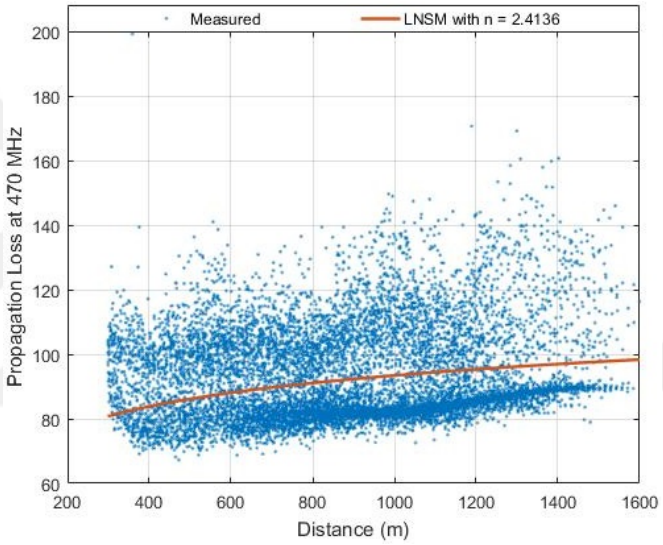

(a)

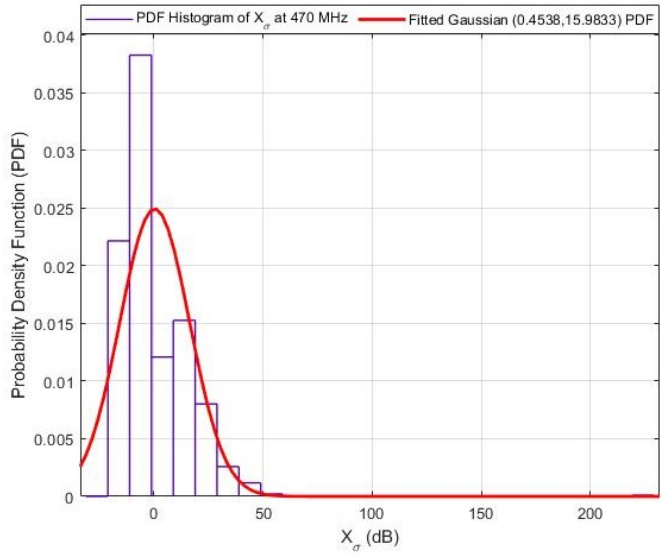

(b)

Figure 5.22: Measured/estimated path loss and measured/ fitted Gaussian PDF of X_σ at 470 MHz (1^{st} Location)

Similarly, for the second location, Figures 5.23(a) and 5.23(b) show measured/estimated log normal shadowing model path loss and measured/fitted Gaussian PDF of X_σ, respectively. The calculated channel parameters are found to be $n = 2.5711$, $\sigma = 15.1126$ dB and, Gaussian PDF with $\mu = 0.0650$ dB and $\sigma = 15.1131$ dB.

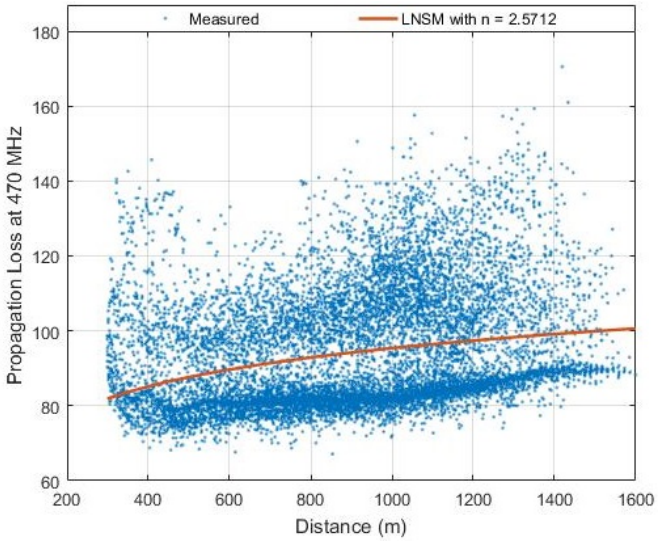

(a)

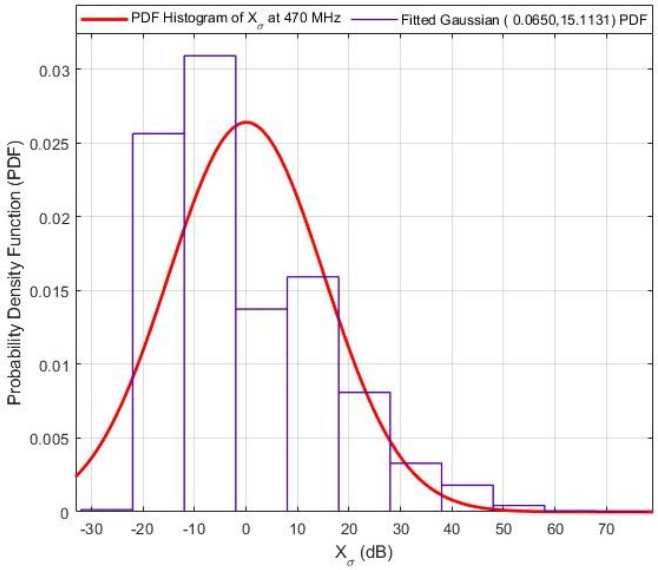

(b)

Figure 5.23: Measured/estimated path loss and measured/ fitted Gaussian PDF of X_σ at 470 MHz (2^{nd} Location)

For the third location, Figures 5.24(a) and 5.24(b) show measured/estimated log normal shadowing model path loss and measured/fitted Gaussian PDF of X_σ, respectively. The calculated channel parameters are found to be $n = 2.4178$, $\sigma = 18.9974$ dB and, Gaussian PDF with $\mu = 0.3610$ dB and $\sigma = 18.9948$ dB.

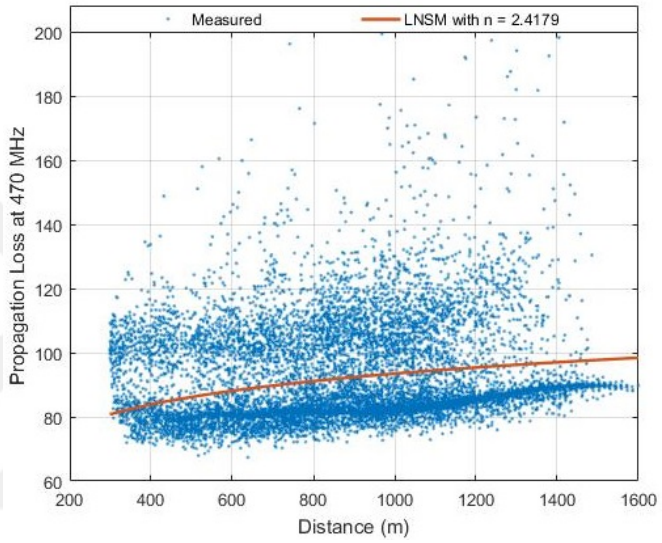

(a)

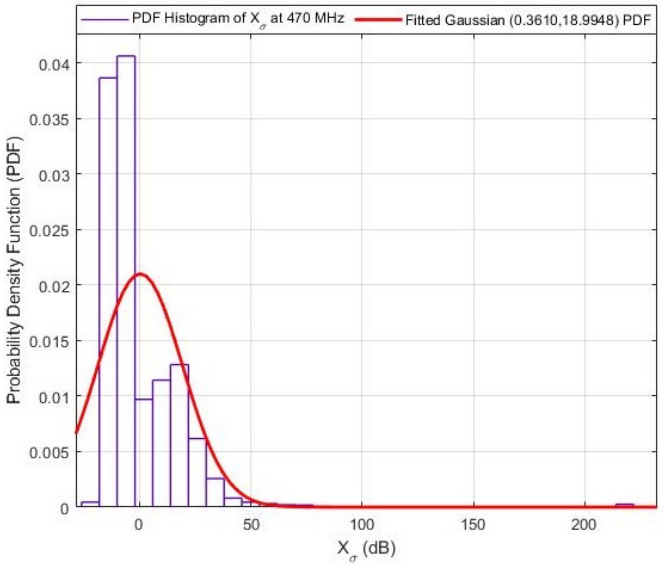

(b)

Figure 5.24: Measured/estimated path loss and measured/ fitted Gaussian PDF of X_σ at 470 MHz (3^{rd} Location)

5.2.2.3 Results at 670 MHz

For the first location, Figures 5.25(a) and 5.25(b) show measured/estimated log normal shadowing model path loss and measured/fitted Gaussian PDF of X_σ, respectively. The calculated channel parameters are found to be $n = 2.8764$, $\sigma = 16.9760$ dB and, Gaussian PDF with $\mu = 0.7026$ dB and $\sigma = 16.9622$ dB.

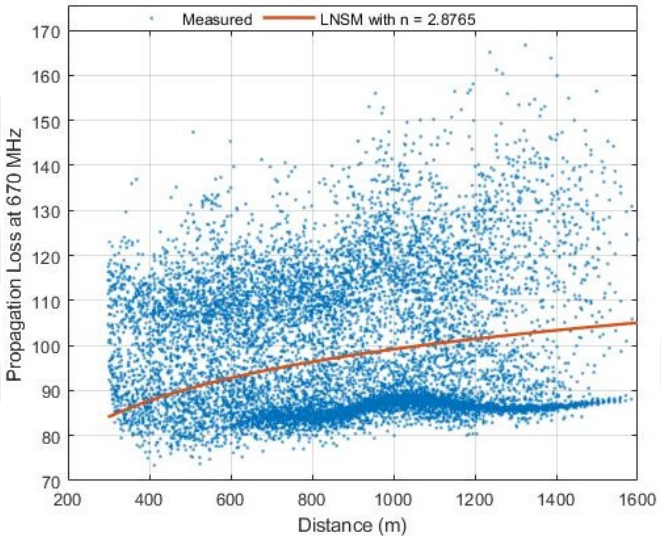

(a)

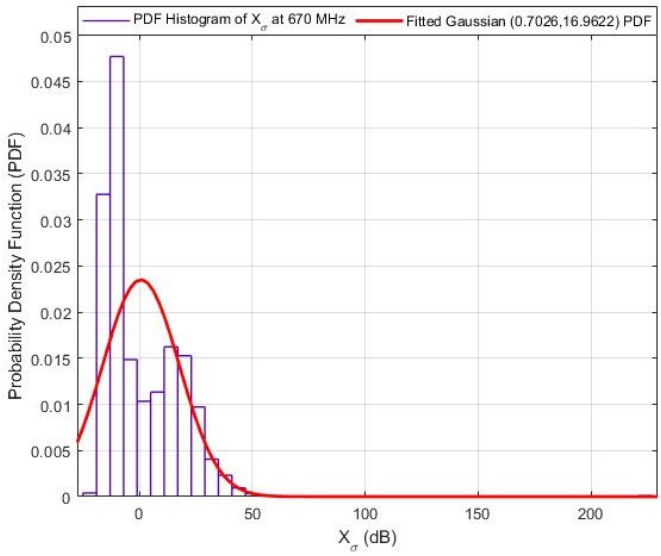

(b)

Figure 5.25: Measured/estimated path loss and measured/ fitted Gaussian PDF of X_σ at 670 MHz (1^{st} Location)

Similarly, for the second location, Figures 5.26(a) and 5.26(b) show measured/estimated log normal shadowing model path loss and measured/fitted Gaussian PDF of X_σ, respectively. The calculated channel parameters are found to be $n = 3.0581$, $\sigma = 16.6198$ dB and, Gaussian PDF with $\mu = 0.2113$ dB and $\sigma = 16.6192$ dB.

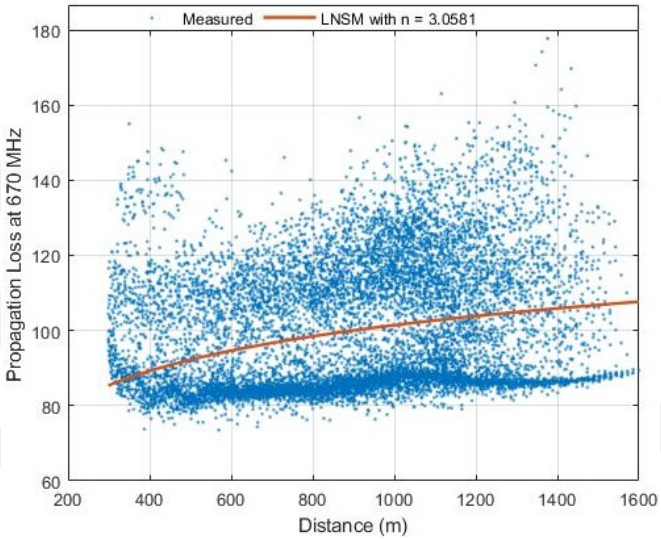

(a)

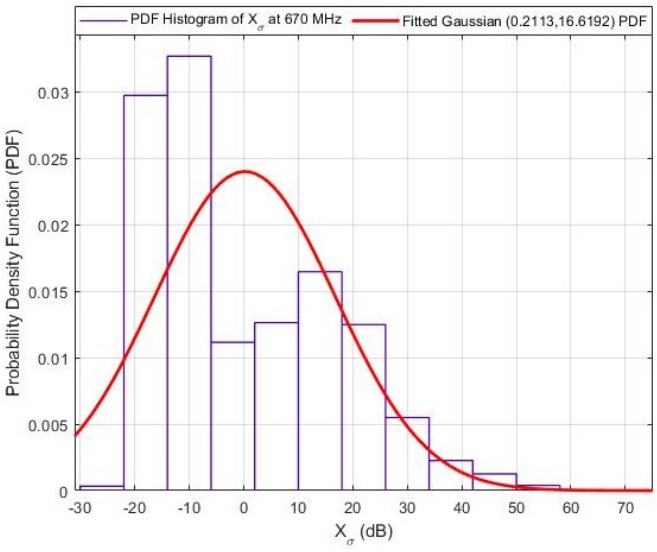

(b)

Figure 5.26: Measured/estimated path loss and measured/ fitted Gaussian PDF of X_σ at 670 MHz (2^{nd} Location)

For the third location, Figures 5.27(a) and 5.27(b) show measured/estimated log normal shadowing model path loss and measured/fitted Gaussian PDF of X_σ, respectively. The calculated channel parameters are found to be $n = 2.8364$, $\sigma = 20.4334$ dB and, Gaussian PDF with $\mu = 0.5804$ dB and $\sigma = 20.4261$ dB.

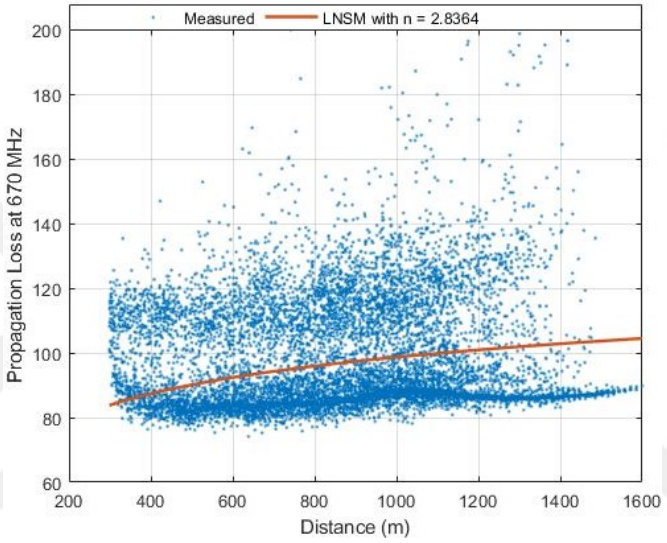

(a)

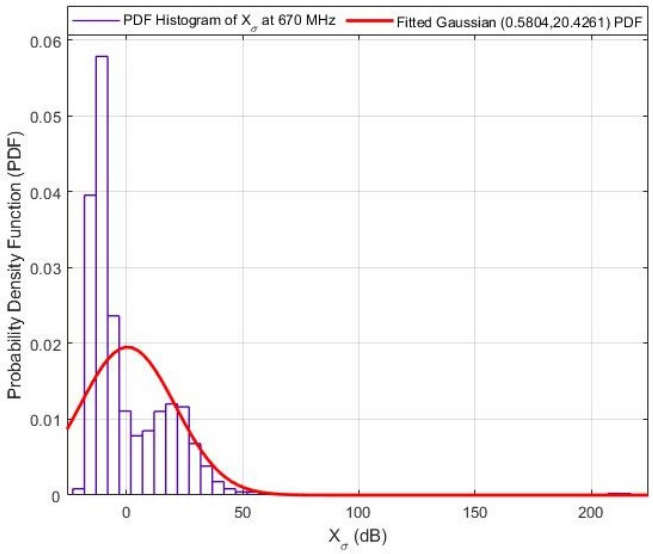

(b)

Figure 5.27: Measured/estimated path loss and measured/ fitted Gaussian PDF of X_σ at 670 MHz (3^{rd} Location)

5.2.3 Modeling Shadowing with Gaussian Mixture Distribution

From the results of previous section, it can be easily said that Gaussian distribution of shadowing does not hold for air to ground channels in TVWS bands. Thus, an efficient model is required for shadowing. In this part, we are proposing Gaussian Mixture Model (GMM) for shadowing which is more compliant with the actual shadowing and can reduce the inaccuracies in modeling found with single Gaussian distribution. GMM PDF is defined by the following equation.

$$f_X(x) = \sum_{k=1}^{\infty} \pi_k \mathcal{N}(\mu,\, \sigma^2), \quad k = 1, ..., N \tag{5.2}$$

where π_k are the mixing proportions (which are positive and sum up to one), where the Gaussian (pdf) is defined as follows:

$$P(x) = \frac{1}{\sigma\sqrt{2\pi}} e^{-(x-\mu)^2/2\sigma^2} \tag{5.3}$$

To obtain mixture model parameters, we have used Expectation-Maximization (EM) method in parameter estimation to model shadowing. Mathematical description of the method is available in [33] [34].

Measured and estimated results at 580 MHz frequency are presented here because other frequencies have nearly similar channel characteristics. GMM PDF is fitted to the measured shadowing in high rise building and sub-urban scenarios. Additionally, GMM CDF are also shown for better comparisons. We started to fit the GMM distribution sequentially from N=1 till that value where the average CDF difference between measured and fitted GMM become stable. It was found that total of five Gaussian mixtures i.e. N=5 best describes the shadowing for air to ground channel in two different types of scenarios. Other statistical parameters (including mean, variance and mixing proportions of each Gaussian in

GMM) will be provided in the comparison and discussion section.

5.2.3.1 Results in High Rise Building Scenario

Figure 5.28(a) and 5.28(b) show the measured/GMM fitted PDF and CDF at the first location.

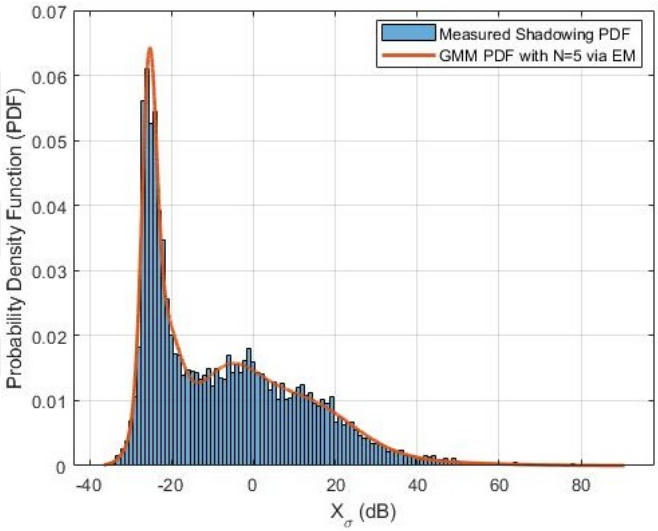

(a)

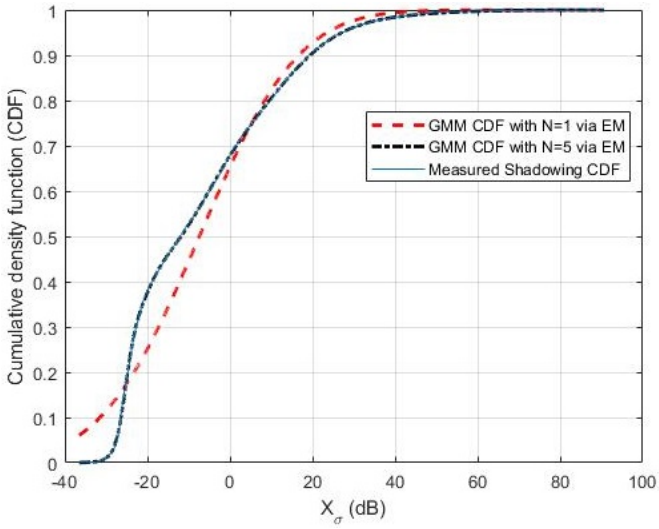

(b)

Figure 5.28: Measured/ fitted GMM PDF and CDF of X_σ at 580 MHz (1^{st} Location)

Similarly, Figure 5.29(a) and 5.29(b) show the measured/GMM fitted PDF and CDF at the second location.

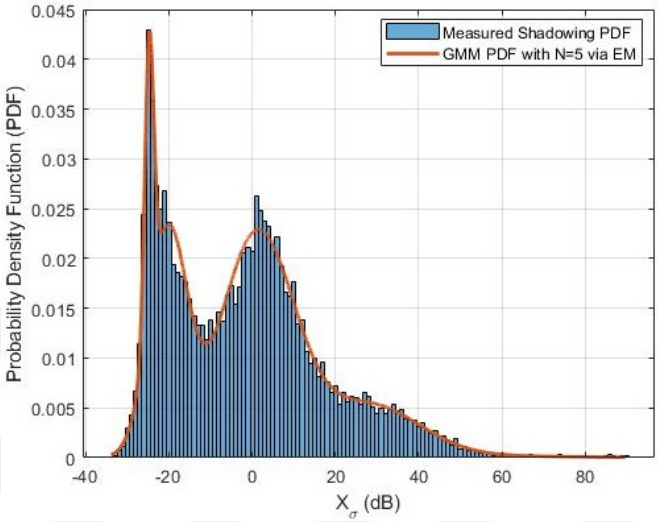

(a)

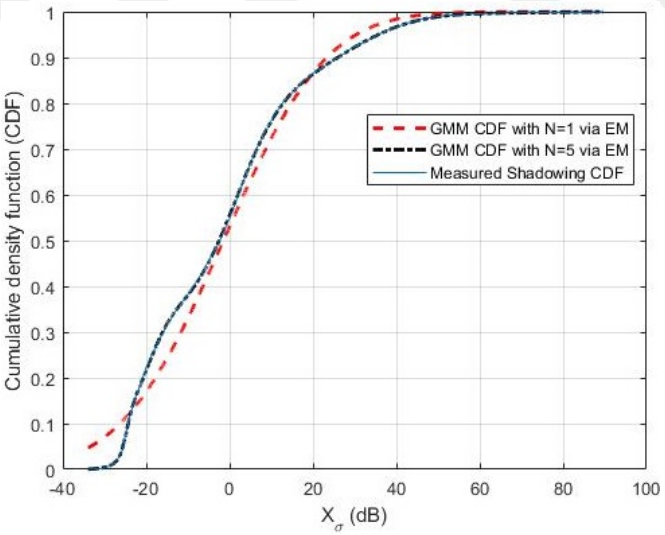

(b)

Figure 5.29: Measured/ fitted GMM PDF and CDF of X_σ at 580 MHz (2^{nd} Location)

Figure 5.30(a) and 5.30(b) show the measured/GMM fitted PDF and CDF at the third location.

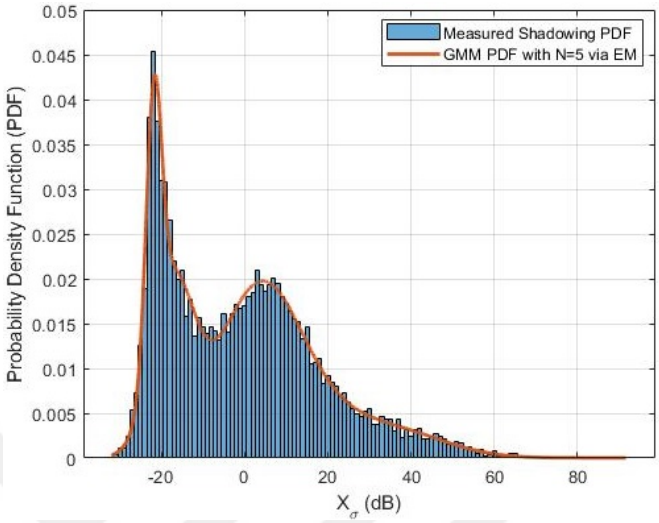

(a)

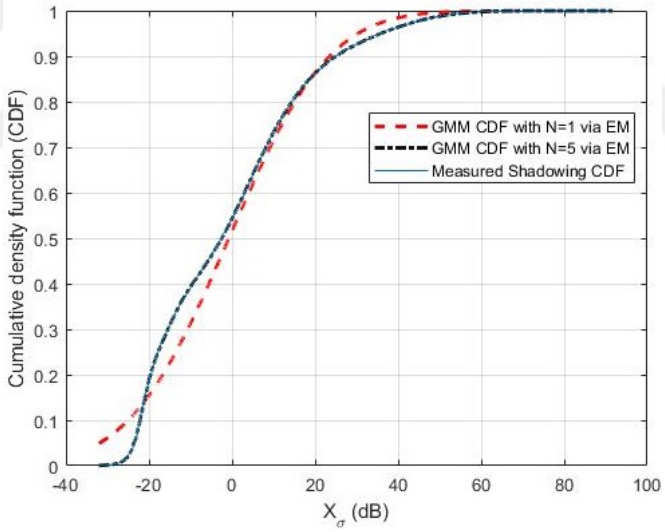

(b)

Figure 5.30: Measured/ fitted GMM PDF and CDF of X_σ at 580 MHz (3^{rd} Location)

Overall results in high rise building scenario show the validity of GMM model for air to ground channel in TVWS band and it turned out to be an acceptable model compared to simple Gaussian.

5.2.3.2 Results in Sub-Urban Scenario

Figure 5.31(a) and 5.31(b) show the measured/GMM fitted PDF and CDF at the first location.

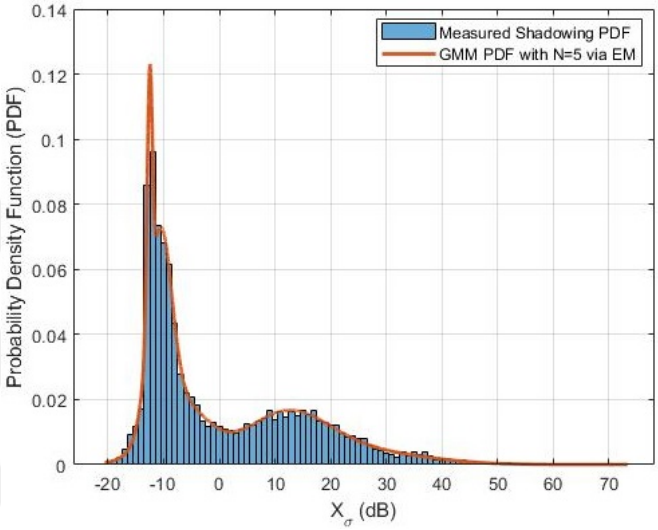

(a)

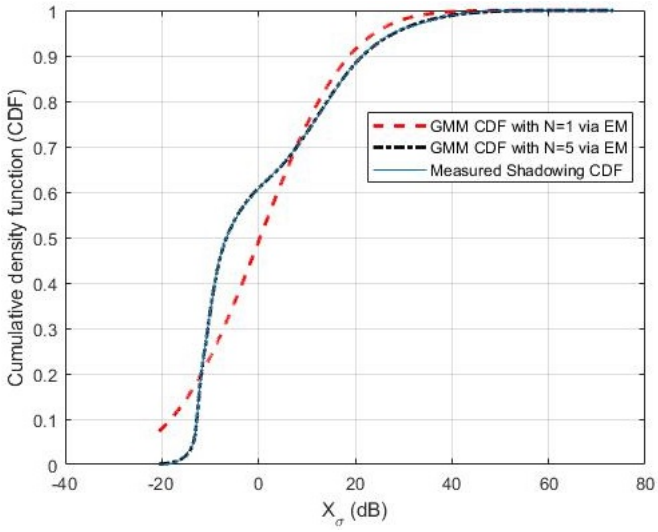

(b)

Figure 5.31: Measured/ fitted GMM PDF and CDF of X_σ at 580 MHz (1^{st} Location)

Similarly, Figure 5.32(a) and 5.32(b) show the measured/GMM fitted PDF

and CDF at the second location.

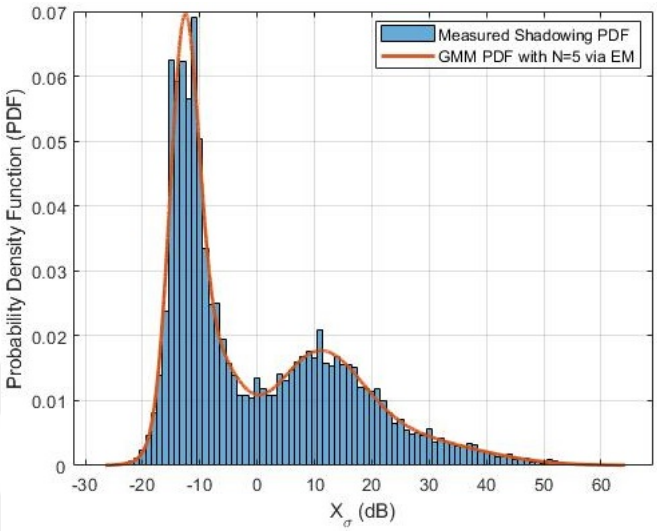

(a)

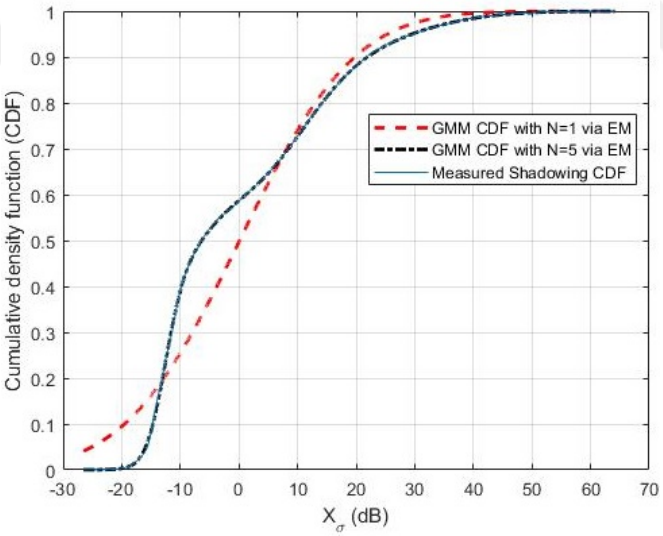

(b)

Figure 5.32: Measured/ fitted GMM PDF and CDF of X_σ at 580 MHz (2^{nd} Location)

Figure 5.33(a) and 5.33(b) show the measured/GMM fitted PDF and CDF at the third location.

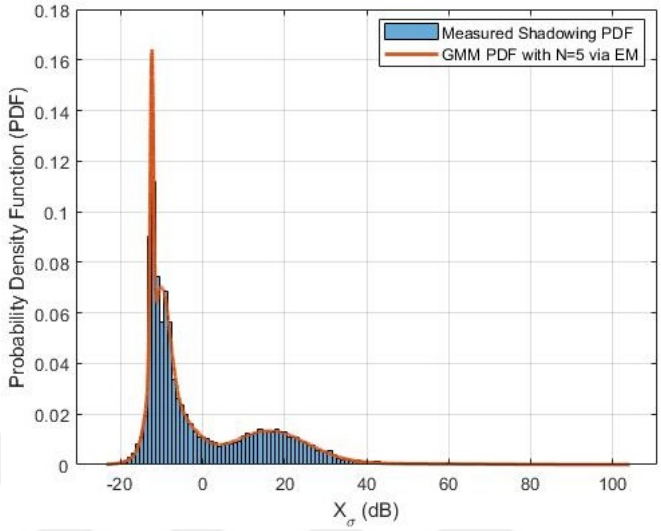

(a)

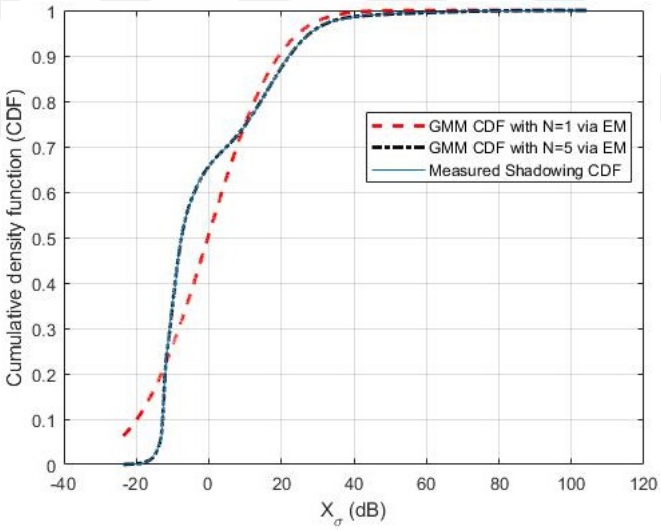

(b)

Figure 5.33: Measured/ fitted GMM PDF and CDF of X_σ at 580 MHz (3^{rd} Location)

Similar to the high rise building scenario, results of sub urban scenario show that GMM with N=5 holds for air to ground channel in TVWS bands.

5.3 Comparisons and Discussion

In this section, results and channel parameters for high rise building and sub-urban scenarios are compared by using statistical parameters. Table 5.2 and Figure 5.34 show the comparison of results at all frequencies.

Table 5.2: Comparison of Results

Frequency (MHz)	**Scenario**	**Location**	n	$\sigma(dB)$	**Fitted Gaussian**	
					$\mu(dB)$	$\sigma(dB)$
470	**High Rise**	1^{st}	3.2333	45.4536	0.6242	6.9895
		2^{nd}	3.3045	24.4956	1.3698	8.3341
		3^{rd}	3.0822	22.1880	1.1715	7.6185
	Sub-Urban	1^{st}	2.4135	15.9891	0.6242	6.9895
		2^{nd}	2.5711	15.1126	1.3698	8.3341
		3^{rd}	2.4178	18.9974	1.1715	7.6185
580	**High Rise**	1^{st}	3.9742	45.0224	0.6242	6.9895
		2^{nd}	3.4956	24.8912	1.3698	8.3341
		3^{rd}	3.2945	24.0181	1.1715	7.6185
	Sub-Urban	1^{st}	2.5540	16.2012	0.6242	6.9895
		2^{nd}	2.7361	15.3332	1.3698	8.3341
		3^{rd}	2.5437	19.3865	1.1715	7.6185
670	**High Rise**	1^{st}	3.7656	45.5193	0.6242	6.9895
		2^{nd}	3.8873	25.2994	1.3698	8.3341
		3^{rd}	3.6725	23.5762	1.1715	7.6185
	Sub-Urban	1^{st}	2.8764	16.9760	0.6242	6.9895
		2^{nd}	3.0581	16.6198	1.3698	8.3341
		3^{rd}	2.8364	20.4334	1.1715	7.6185

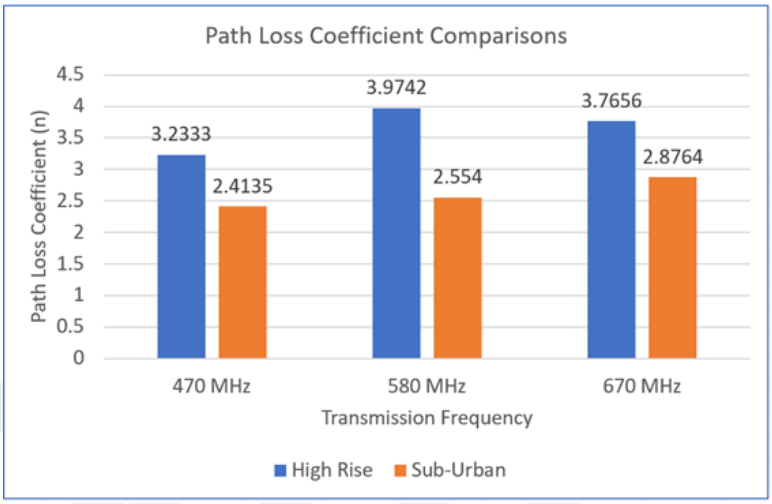

(a)

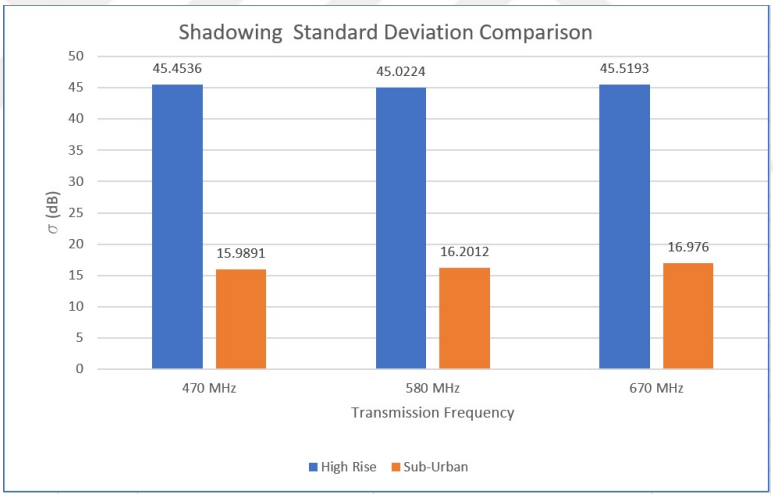

(b)

Figure 5.34: Comparison of results in high rise and sub-urban scenarios (1^{st} location)

GMM estimated parameters at 580 MHz for high rise building and sub-urban scenarios are given in Table 5.3. From the result of previous section, it seems that the measured and GMM fitted shadowing CDF has similar distribution function. Here, Kolmogorov-Smirnov (K-S) test is used as goodness of fit with the confidence level p=0.01 (corresponding to null hypothesis rejection level of 1%) to determine the suitability of proposed shadowing GMM for the measured shadowing histogram. Additionally, mean relative difference (MRD) is used as error

vector to quantify the difference between measured and estimated CDF. All the comparisons and results are presented in Table 5.3.

Table 5.3: GMM estimated parameters and error metrics

Scenario	**Location**	**Gaussian Mixture Model Parameters**					**MRD Error**	**K-S (p=0.01)**
		π_{k1}, μ_1, σ_1^2	π_{k2}, μ_2, σ_2^2	π_{k3}, μ_3, σ_3^2	π_{k4}, μ_4, σ_4^2	π_{k5}, μ_5, σ_5^2		
High Rise	**1**	0.2523, -7.6205, 65.9316	0.2654, 11.0010, 131.3629	0.2173, -22.6031, 17.8490	0.1992, -25.4295, 2.9271	0.0658, 23.7330, 437.0285	0.0025	Passed
	2	0.0805, -24.7468, 1.2685	0.1844, 26.7005, 187.6821	0.4760, 1.1201, 74.4606	0.2564, -20.1768, 21.4831	0.0026, 77.9493, 82.8843	0.0018	Passed
	3	0.2382, -17.3596, 25.6137	0.0959, 35.8905, 152.2273	0.3771, 1.7384, 82.8142	0.1346, -21.8231, 3.3543	0.1541, 14.3665, 90.8035	0.0013	Passed
Sub-Urban	**1**	0.0446, 22.0697, 200.5914	0.1095, -12.3799, 0.3242	0.4140, 10.5046, 117.2615	0.4182, -10.0037, 8.3556	0.0137, 38.5997, 18.9466	0.0051	Passed
	2	0.0858, 29.1089, 135.1237	0.2093, -8.5186, 25.6716	0.2269, 10.1966, 52.9556	0.1221, 13.2437, 110.9409	0.3560, -12.7139, 6.1243	0.0028	Passed
	3	0.1149, -12.4438, 0.1481	0.3053, -10.2807, 4.9919	0.0226, 41.8918, 553.0756	0.2424, -6.9826, 26.5606	0.3148, 16.0950, 91.6854	0.0023	Passed

Results comparisons show that high rise building scenario has more shadowing at all frequencies which ranges from σ = 22.1880 dB to 45.5193 dB, compared to the sub-urban shadowing which ranges from σ = 15.1126 to 20.4334 dB. Sub-urban scenario has low path loss coefficient in a range of n = 2.4135 to 3.0581, compared to high rise buildings which ranges from n = 3.0822 to 3.9742. Results show that the log normal model is only suitable for path loss coefficient (n) estimations whereas proposed GMM can be used to model shadowing (σ) for air to ground channel in TVWS frequency band. Ray tracing simulations presented in this section can be extended to find channel parameters in multiple frequency bands. The methodology to calculate channel parameter from a simple aerial image/3D model (c.f.Figure 5.1) can be used to generate extensive training and testing data set for machine learning algorithms to find channel parameters which

is an important topic among most of the researchers.

Chapter 6

Conclusion

Spectrum sharing is the utmost requirement to tackle the issues of increasing data traffic and demand of high speed communications. Extensive research has been done for spectrum sharing in TVWS and that shows the great possibility of providing high performance for next generation systems. To analyze these systems, an effective channel modeling is necessary. In this work, TVWS wireless channel characteristics have been studied based on a measurement campaign in indoor-indoor, indoor-outdoor and air-ground channel environments.

For indoor-indoor environment, several existing models have been analyzed and their modeling accuracy is assessed by comparing with measurement results. Considering that the effect of glass windows and doors is neglected in previous models, a new model is proposed that not only models the effect of distance and walls on propagation loss but also models the effect of floors, doors and windows in the environment. Results indicate that the proposed model has better estimation accuracy in terms of standard deviation of estimation error compared to previous models.

For indoor-outdoor, propagation characteristics have been studied. After determining parameters for log normal shadowing model, it is observed that there are low and high shadowing zones. A distance threshold is determined to separate

zones and new model is created. New channel model with multiple zones reduced the RMSE for all distances and transmission frequencies.

For air-ground, measurements based on ray tracing simulations were taken on three different TVWS frequencies. Two different types of scenarios were analyzed which includes high rise buildings and sub-urban. Wireless channel parameters were calculated using log normal shadowing model. Results indicate that high shadowing zones was found in high rise buildings scenarios while sub-urban scenario has low path coefficient. Results shows that log normal model (for path loss coefficient) and proposed GMM (for shadowing) turned out to be an acceptable model to analyze air-ground channels in TVWS frequency bands.

Conclusively, the new models can be used to improve link budget, interference, and cell design analysis of TVWS communication systems.

Bibliography

[1] "Cisco Visual Networking Index: Global mobile data traffic forecast update, 2012-2017," Feb. 2013.

[2] T. Baykas, C. S. Sum, Z. Lan, J. Wang, M. A. Rahman, H. Harada, and S. Kato, "IEEE 802.15.3c: The first IEEE wireless standard for data rates over 1 Gb/s," *IEEE Communications Magazine*, vol. 49, pp. 114–121, July 2011.

[3] T. Kürner and S. Priebe, "Towards THz communications-status in research, standardization and regulation," *Journal of Infrared, Millimeter, and Terahertz Waves*, vol. 35, no. 1, pp. 53–62, 2014.

[4] R. Q. Hu, Y. Qian, S. Kota, and G. Giambene, "Hetnets - A new paradigm for increasing cellular capacity and coverage," *IEEE Wireless Communications*, vol. 18, pp. 8–9, June 2011.

[5] F. Zou, Y. Shi, and F. Wang, "NGB-E: Cable, wireless and satellite convergence network," in *2015 IEEE International Symposium on Broadband Multimedia Systems and Broadcasting*, (Ghent), pp. 1–6, 2015.

[6] S. Filin, T. Baykas, H. Harada, F. Kojima, and H. Yano, "IEEE standard 802.19.1 for TV White Space coexistence," *IEEE Communications Magazine*, vol. 54, pp. 22–26, March 2016.

[7] C. S. Sum *et al.*, "Cognitive communication in TV White Spaces: An overview of regulations, standards, and technology," *IEEE Communications Magazine*, vol. 51, pp. 138–145, July 2013.

[8] T. Baykas, M. Muck, S. Filin, M. Kasslin, P. Ruuska, and J. Wang, "Standardization Activities related to TV White Space: Coexistence and Dynamic Spectrum Access Standards," *TV White Space Spectrum Technologies: Regulations, Standards, and Applications*, p. 173, 2011.

[9] M. Hata, "Empirical formula for propagation loss in land mobile radio services," *IEEE Transactions on Vehicular Technology*, vol. 29, pp. 317–325, Aug 1980.

[10] Longley, A. G, and P. L. Rice, "Prediction of tropospheric radio transmission loss over irregular terrain. A computer method," tech. rep., Institute for Telecommunication Sciences Boulder Co, 1968.

[11] T. S. Rappaport *et al.*, *Wireless communications: principles and practice*, vol. 2. Prentice hall PTR New Jersey, 1996.

[12] E. Damosso *et al.*, "Digital mobile radio: COST 231 view on the evolution towards 3rd generation systems," in *European Commission*, 1998.

[13] P. Series, "Propagation data and prediction methods for the planning of indoor radio communication systems and radio local area networks in the frequency range 900 MHz to 100 GHz," *Recommendation ITU-R*, pp. 1238–7, 2012.

[14] M. Lott and I. Forkel, "A multi-wall-and-floor model for indoor radio propagation," in *IEEE VTS 53rd Vehicular Technology Conference, Spring 2001. Proceedings (Cat. No.01CH37202)*, (Rhodes, 2001, pp. 464-468 vol.1).

[15] A. Valcarce and J. Zhang, "Empirical indoor-to-outdoor propagation model for residential areas at 0.9–3.5 ghz," *IEEE Antennas and Wireless Propagation Letters*, vol. 9, pp. 682–685, 2010.

[16] A. Valcarce, D. López-Pérez, G. De La Roche, and J. Zhang, "Predicting small-scale fading distributions with Finite-Difference methods in Indoor-to-Outdoor scenarios," in *Vehicular Technology Conference, 2009. VTC Spring 2009. IEEE 69th*, pp. 1–5, IEEE, 2009.

[17] A. Seville, S. Cirstea, and J. Taylor, "Effects of propagation between the indoor and outdoor environment," 2003.

[18] Z. Zhang, R. K. Sorensen, Z. Yun, M. F. Iskander, and J. Harvey, "A ray-tracing approach for indoor/outdoor propagation through window structures," *IEEE Transactions on Antennas and Propagation*, vol. 50, no. 5, pp. 742–749, 2002.

[19] M. Ho, S. Berber, and K. Sowerby, "Building leakage propagation measurements for indoor cognitive radio systems," *Electronics letters*, vol. 48, no. 23, pp. 1508–1510, 2012.

[20] S. Celik, Y. E. Yoruk, M. Bitirgan, O. Kurnaz, B. Basyigit, S. Helhel, and S. Ozen, "Indoor to outdoor propagation model improvement for gsm900/gsm1800/cdma-2100," in *General Assembly and Scientific Symposium, 2011 XXXth URSI*, pp. 1–4, IEEE, 2011.

[21] Y. Corre, J. Stephan, and Y. Lostanlen, "Indoor-to-outdoor path-loss models for femtocell predictions," in *Personal Indoor and Mobile Radio Communications (PIMRC), 2011 IEEE 22nd International Symposium on*, pp. 824–828, IEEE, 2011.

[22] M. Ettus, "Universal Software Radio Peripheral (USRP). Ettus Research LLC," 2008.

[23] R. Nilsson and J. van de Beek, "Channel measurements in an open-pit mine using USRPs: 5G — Expect the unexpected," in *2016 IEEE Wireless Communications and Networking Conference*, pp. 1–6, April 2016.

[24] M. Ettus *et al.*, "Ettus research, LLC," *Online information on USRP board). http://www. ettus. com*, 2008.

[25] M. Release, "The MathWorks," *Inc., Natick, Massachusetts, United States*, vol. 488, 2013.

[26] L. U. Manual, "National Instruments," *Austin, TX*, 1998.

[27] W. Yamada *et al.*, "Indoor propagation model for TV White Space," in *2014 9th International Conference on Cognitive Radio Oriented Wireless Networks and Communications (CROWNCOM)*, pp. 209–214, Oulu, 2014.

[28] T. S. Rappaport, G. R. MacCartney, M. K. Samimi, and S. Sun, "Wideband millimeter-wave propagation measurements and channel models for future wireless communication system design," *IEEE Transactions on Communications*, vol. 63, no. 9, pp. 3029–3056, 2015.

[29] S. Sangodoyin, S. Niranjayan, and A. F. Molisch, "A measurement-based model for outdoor near-ground ultrawideband channels," *IEEE Transactions on Antennas and Propagation*, vol. 64, no. 2, pp. 740–751, 2016.

[30] B. Ai, K. Guan, R. He, J. Li, G. Li, D. He, Z. Zhong, and K. M. S. Huq, "On Indoor Millimeter Wave Massive MIMO Channels: Measurement and Simulation," *IEEE Journal on Selected Areas in Communications*, vol. 35, pp. 1678–1690, July 2017.

[31] W. Khawaja, O. Ozdemir, and I. Guvenc, "UAV Air-to-Ground Channel Characterization for mmwave systems," in *2017 IEEE 86th Vehicular Technology Conference (VTC-Fall)*, pp. 1–5, Sept 2017.

[32] E. Greenberg and P. Levy, "Channel characteristics of UAV to ground links over multipath urban environments," in *2017 IEEE International Conference on Microwaves, Antennas, Communications and Electronic Systems (COMCAS)*, pp. 1–4, Nov 2017.

[33] G. McLachlan and T. Krishnan, "The EM Algorithm and Extensions. Whiley Series in Probability and Statistics," *John Wiley & Sons, New York, USA, second edition. Moon, TK (1996). The expectation-maximization algorithm. IEEE Signal Processing Magazine*, vol. 13, no. 6, pp. 47–60, 2008.

[34] J. A. Bilmes *et al.*, "A gentle tutorial of the EM algorithm and its application to parameter estimation for Gaussian mixture and hidden Markov models," *International Computer Science Institute*, vol. 4, no. 510, p. 126, 1998.

WIRELESS CHANNEL MODELING IN THE TVWS BAND BASED ON MEASUREMENTS

ORIGINALITY REPORT

8%	5%	5%	4%
SIMILARITY INDEX	INTERNET SOURCES	PUBLICATIONS	STUDENT PAPERS

PRIMARY SOURCES

1	Submitted to Nashville State Community College Student Paper	1%
2	Submitted to Higher Education Commission Pakistan Student Paper	<1%
3	Ahmed M. Al-Samman, Tharek A. Rahman, Marwan H. Azmi, Nor R. Zulkefly, Abdallah M.S. Mataria. "Path loss model for outdoor environment at 17 GHz mm-wave band", 2016 IEEE 12th International Colloquium on Signal Processing & Its Applications (CSPA), 2016 Publication	<1%
4	www.nsf.gov Internet Source	<1%
5	R, Mardeni., and T. Siva Priya. "Optimised COST-231 Hata Models for WiMAX Path Loss Prediction in Suburban and Open Urban Environments", Modern Applied Science, 2010. Publication	<1%